Bioelectrical and Biophysical Interactions Across Spatio-Temporal Domains: Identifying the Conduit for the Emergence of Material from the Immaterial

by

Trevor N. Carniello

A Manuscript submitted in partial fulfillment of the requirements for the degree of
Master of Science (M.Sc) in Biology

The Faculty of Graduate Studies
Laurentian University
Sudbury, Ontario, Canada

THESIS DEFENCE COMMITTEE/COMITÉ DE SOUTENANCE DE THÈSE
Laurentian Université/Université Laurentienne
Faculty of Graduate Studies/Faculté des études supérieures

Title of Thesis Titre de la thèse	Bioelectrical and Biophysical Interactions Across Spatio-Temporal Domains: Identifying the Conduit for the Emergence of Material from the Immaterial
Name of Candidate Nom du candidat	Carniello, Trevor
Degree Diplôme	Master of Science
Department/Program Département/Programme	Biology
Date of Defence Date de la soutenance	January 15, 2016

APPROVED/APPROUVÉ

Thesis Examiners/Examinateurs de thèse:

Dr. Michael Persinger
(Supervisor/Directeur(trice) de thèse)

Dr. Rob Lafrenie
(Committee member/Membre du comité)

Dr. Peter Ryser
(Committee member/Membre du comité)

Approved for the Faculty of Graduate Studies
Approuvé pour la Faculté des études supérieures
Dr. David Lesbarrères
Monsieur David Lesbarrères

Dr. Michel Cifra Acting Dean, Faculty of Graduate Studies
(External Examiner/Examinateur externe)

Doyen intérimaire, Faculté des études supérieures

ACCESSIBILITY CLAUSE AND PERMISSION TO USE

Abstract

The emergence of biophysical and bioelectrical dynamics at the level of the organism are explored in an attempt to identify the physiological correlates of the onset of senescence in plants. Furthermore, the ability of phylogenically disparate entities to demonstrate the potential to simultaneously display correlated electro-dynamic processes akin to sharing the "same space" or spatial parameters is investigated. The underlying, aforementioned electrophysiological changes associated with senescence and the potential for phylogenically disparate systems to display markedly correlated processes may share water as a common source of variance. The imperative investigations on the physical nature of water and its interactions with applied electromagnetic fields with respect to enhanced latency of the onset of deviations in pH and enhanced electro-dynamic correlations are experimentally explored. A hypothesis, supplemented by marked quantitative convergence, suggests that water is the central conduit necessary for the emergence of material from the immaterial.

Keywords

Excess correlation, immortality, material, energy, electrodynamics, electric fields, magnetic fields, bacteria, plants, electrical potential.

Acknowledgements

I wish to acknowledge, in this section, four individuals whose influence were instrumental for the development of this particular dissertation. First and foremost, I wish to thank, although his influence could not be directly appreciated, Michael Faraday. His ingenuity and practical exploratory nature, along with his remarkable ability to experimentally demonstrate the geometric nature of electromagnetic phenomenon has greatly inspired this author. To a most imaginative and brilliant individual, much gratitude. Secondly, I wish to acknowledge Hermann Minkowski for his contribution to the physical understanding of space and time. For your geometrical interpretation of 4 dimensional coordinates systems, the basis of which time is introduced as the 4th parameter, has provided the necessary contingencies for the quantification of most of this document. My penultimate acknowledgement is directed towards a much under-appreciated scientist, Sir Arthur Stanley Eddington. In memoriam of this great individual I have dedicated the contents of the 6th chapter. For a man who verified Einstein's hypothesis that large masses distort the physical construct of space-time, whose mathematical interpretation of the limits of the Universal set, as described as Eddignton's number whose value approaches the approximate number of atoms in the Universe, and whose insight to the nature of the physical is unparalleled, my deepest admiration. Finally I wish to thank, and cannot thank enough, my mentor Dr. Michael A. Persinger. For your most patience, insight, guidance and appropriate differential reinforcement of my abilities, I am indebted to you. My perpetual continuation and fruitful futuristic contributions to all matters, personal and scientific, I attribute to the skills that I have acquired under your mentorship. I am looking forward to my continued work under your supervision, acquiring and refining new found skill that will propel me to achieve my potential.

I would also like to acknowledge my committee members Dr. Peter Ryser and Dr. Robert Lafrenie for your assistance and participation in this journey.

Table of Contents

List of Tables

List of Figures

Chapter 1

1 Introduction to the Blueprint for Immortality

Immortality, at least from the human perspective, cannot seemingly be obtained. This idea has pervaded the themes of many novels, forever etched in the concepts of the unattainable fountain of youth. Furthermore, the application of the ability to exist in a suspended state, roaming the lands feasting on living flesh has been the apocalyptic finale of existence on the big screen. Although fantasized, to obtain a solution capable of reversing the causal nature of time and extend our existence to an era which surpasses the limits of the human boundary would be quite advantageous. However, the concept of immortality is merely a White Whale created to divert us from the inevitably of death; the complete dissolution of our being. Although the abstract concept of immortality may demonstrate juvenile intentions, perhaps one may be able to reify the idea.

Fantasy aside, immortality is nothing more than the continued propagation of a set of parameters across an unbounded magnitude of time. The central dogma associated with the reverie of a non-realistic immortal existence suggests that a singular unit can exist for eternity. Yet we, as an aggregate of individuals, fail to acknowledge the persistence of many such units that adhere to the aforementioned definition of immortality. Take for instance the biological aspects for the inheritance of genetic information. Genes, the unit of inheritance, are passed from both a maternal and paternal biological source in order to form a subsidiary being, the offspring, the entity that is you. Now postulate on the origins of your immediate relatives, your biological sources, and posit the notion of their existence. Where did they come from? They are nothing more than the combination and recombination of the genetic information (or the re-structuring of

the genetic units) of their biological sources. Reiterate this process any number of times over successive generations and you may begin to realize that regardless of the number of permutations, you are comprised of successively less genetic information of your ancestors. Alternatively, your ancestors comprise a relatively small proportion of your genetic constituents. Thus one may argue that, in a sense, a part of them has survived indefinitely, far exceeding the limits of a single life, and has obtained a form of immortality. Even if we acknowledge the rules of inheritance small portions of your genetic code still resemble past and distant relatives (Tyler, 2005). Thus, we have identified a singular aspect of immortality, a component if you will, that is based solely upon the continuity of a given structure of a material nature.

The *material* can be defined as the structural analog of energy occupying both space and time and composed of discrete units of matter. Matter is said to change very slowly over time and maintain a consistent level of organization (Stachel and Toretti, 2002). Organization is an emergent property of discrete units that coalesce into remarkably complex geometries. The biological equivalent of the emergence of complex geometries derived from discrete units is the structure of DNA. The composition and order of paired DNA bases are the foundations of genes, the representative units of inheritance. There is a limit to the influence of the structure of a solitary unit, and as the number of permutations increases over the course of successive generations so too does the complex assemblages of geometries resulting in a decrease in the influence of initially inherited information. The re-organization and recombination of initial assembled geometries (i.e. distant genetic inheritance) can have unique interactions resulting in highly variable final arrangements (individuals). In this discussion we have neglected an important aspect of material, its ability to maintain structure and retain a process. In the aforementioned sense, even if we received equal contributions of genetic material from our

biological sources, the combinatorial interactions that result from the initial genetic donors produce completely new (individual) genetic structures. Our ideation of true immortality as conceived by the propagation of a single unit (referred to as the self) cannot be obtained based upon structure. An alternative property to structure (matter) is that it is finite, it persists over long periods of time and it has the unique ability to represent a process.

Consider for a moment the concept of a cable wire conducting electricity. The example of how electricity is conducted in said wire is often approached as the flow or movement of electrons passing from one end of the wire to the other (Nitzan and Ratner, 2003). The metaphor is erroneous as the material that makes up the wire, primarily a metal or metal-alloy, contains a series of electrons that extend the entire length of the wire. In this case the electrons are bound to adjacent atoms whilst some remain free-floating or unencumbered by the adhesion forces of atoms. The application of an electromotive force then pushes one free electron off of the distal end of the wire while simultaneously another enters the proximal end. The unencumbered electrons then bounce into another free floating electron in a Grötthus-type mechanism and allows for the generation of electricity. Still this example operates under an erroneous pretence. Electrons in a material do interact in a Grötthus-type mechanism however the calculated velocity at which these electrons travel, their drift velocity, is extremely small and would not account for the immediacy in which one receives electrical power after inserting a device into an outlet. What then can explain this phenomenon?

Consider for an instant the effect of applying a voltage over a given distance. The resultant physical representation of said force can then be described as an *electric field*. The concepts and behaviours of such emergent phenomenon have been extensively examined by Faraday and modeled by Maxwell in his mathematical derivations (Maxwell, 1904; Maxwell,

1865). An electric field can be defined as a unit force acting on a unit charge and can have either static (non-moving) or time-varying (dynamic) parameters. For our analogy, the current (flow of electrons generated by their drift velocity) generates a movement of charge, a process which assumes a temporal dimension occurring over finite increments. Returning to our cable metaphor, the addition of a time-varying electromotive force generates a level of dynamism. In turn the resultant application of a dynamic electromotive force produces a time-varying electric field allowing for the immediate extraction of the necessary power from the overhead-wire, to the breaker of your home, to the outlet and finally to the desk lamp that you have conveniently turned on. Thus, it is the result of the electric field and its vector that allows for the necessary properties associated with electrical conductivity in this example.

What, pray tell, does the cable do then if it is not directly involved with the conduction and propagation of electricity in the common sense? The answer: cables provide structure to the electric field. Any electric field, generated from a single charge, will radiate outwards isotropically in all spatial directions producing a net equilibrium state (Plimpton and Lawton, 1936; McLaughlin, 1989). When we structure a series of charges in a bounded system (the wire) and we apply a current in a single direction, we structure the resultant electric field such that its vector lies parallel to the vector of the applied current. Thus the structure of the material adds structure to the field, and the field functions in this case to supply a given target with a form of energy. The aforementioned dichotomy has been immortalized in the concept that structure dictates function.

We return now to our genetic structure and its unit of the DNA double-helix. The structural result of the combination of these base chemicals allows for the delocalization of electrons, similar to the unencumbered electrons in our wire. The net effect of the delocalized

electrons is the generation of static and dynamic electric fields. Similarly, DNA itself is not static and undergoes structural changes such as compression, rotation, stretching, amongst others (Bustamente *et al.*, 2003; Kosikov, 1999). These conformational activities are the result of the dynamic nature of the cell and its associated cytoskeleton leading to mechanical forces in the picoNewton range that thus change the nature and movement of the delocalized electrons (Kubar *et al.*, 2008; Walert and Zakrzewski, 2005). The net electric flux associated with the structure of DNA helps amplify the electric field associated with the static organization and distribution of free electrons along its backbone, resulting in the production of a dynamic, time-varying electric field. Complimentary to this aspect, any other physical changes to the structure of the DNA, either during transcription, translation, gene regulation, expression, DNA damage *etc*., will change the nature of the resultant electric field. Thus far, all the presented information has an underlying theme – the importance of structure defining the nature of the emergence of function. This pre-supposition has ushered in an era examining the importance of structure and material but has discounted the reverse hypothesis. What if function also influenced structure? What then would the influence of structure have on function?

Contemplate the question: What is a human? No more than the composition of calcium based salts, bounded by a semi-permeable membrane in a colloidal suspension. However, one cannot take the components of a human being in their respective proportions put them in a beaker and generate a whole human as the alchemists would believe. In presenting this solution I have not violated the idea that structure is an important factor in generating life. Yet the result of the *Gedanken* experiment is still the same, it does not result in the manifestation of a human in the beaker. What merely is left is approximately 70 kg of a solution containing a mixture of salts

and proteinaceous material in suspension. Perhaps a functional process is a necessity for the generation of structure and is a requirement for the genesis and protracted assemblage of life.

Under the assumption that a process is required in order to initiate the appropriate assemblage of subunits required to generate prototypal life, Miller and Urey conducted a series of investigations examining the potential of electrical discharges affecting the composition of gases akin to the constituents present on primordial Earth (Miller *et al*., 1976). What was determined was that under the right conditions the discharges resulted in the synthesis of a number of the essential amino acids, the basic building blocks of life. The generation of biological subunits from inorganic material was coined *abiogenesis* and successfully demonstrated the potential need of a process to organize the structure of matter (Huxley, 1870; Hudgson and Baker, 1967).

In this manner structure can arise from a process, but what is the process of an electrical discharge? Much like the lightning present during the abiogenic events of the primordial Earth, electrical discharges result when the magnitude of spatially separated charges and the generated electric field exceeds the dielectric constant of the material in which it is generated (Rakov and Uman, 2003). This discharge occurs over a relatively short period of time, again resulting in the generation of dynamic electric fields. One could postulate the necessity of a process as being equally important to maintaining and generating the structure as is the structure in maintaining the order of the process. This raises an interesting concept, that the electric fields or electrodynamic processes of organized material are essential to the proper functioning of the unit and may even precede the material organization in terms of necessity for the formation of the unit.

Such a theory was proposed in the 1930's by Harold Saxton Burr and further studied by Leonard J. Ravitz, Jr. into the 1960's. The proposed theory suggested that the characteristics of the electric fields generated by a multitude of organisms were a pre-requisite for the nature of the organism to be maintained (Burr and Northrop, 1935; Burr and Northrop, 1939; Burr, 1932; Northrop and Burr, 1937; Burr, 1944). This proposal was coined the *electrodynamic theory of life* and postulated that changes in the electric field of the organism, measured as slow shifts of electrical potential, maintained the structure of the material. That is the emergent force, the electric force from the electric field, acted as a binding agent and proverbial glue necessary to bind and maintain the functional aspects of the material. Furthermore, any change in the background quasi-stable nature of the intrinsic electrodynamic profiles of different organisms could be used to assess aberrancies in the normal, operational parameters of the organism (Burr, 1941; Burr and Hovland, 1937; Burr, 1940; Burr, 1952; Ravitz, 1959; Ravitz, 1953; Ravitz, 1955; Ravitz, 1962). Burr and Ravitz also postulated that changes in electrodynamics preceded the restructuring of the material with respect to wound healing and associated these measures with the differential stages of embryological development (Burr and Hovland, 1937; Burr, 1941; Ravitz, 1959). Furthermore, depending on the stage of development, the embryo would demonstrate conspicuous alterations in the polarity (direction) of the electrodynamic vector. Recent studies corroborate these findings and even suggest a role of polarity in the migration and orientation of neuronal populations undergoing development (Yao *et al.*, 2008, Yao *et al*., 2009).

Levin and colleagues examined the nature of electrodynamic correlates in directing planarian regeneration (Oviedo *et al*., 2010; Nogi and Levin, 2005; Beane *et al.*, 2011; Lobo *et al*., 2012). The concept employed is based around the essentials of polarity, or the orientation of charges in a specific direction. The net result of all charges produces a polar separation of

charges creating a net positive and net negative segregation. The separation and maintenance of these polar regions can be accommodated by the generation and temporally bounded effects of electric fields and thus can be inferred as the causal agents of electrodynamic field effects. The fact is the labels might change, the metaphors might evolve and the tools may become more refined, but the underlying ideas do not differ from their original conception.

What might this have to do with the concept of immortality in the context which we have described? We return to the man that started it all, Burr. Burr (1972) released a book entitled: *Blueprint for Immortality: The Electric Patterns of Life* which chronicled his works and those of others in the field of electrodynamics. The crux of the dissertation examined the slow changing nature of plants, primarily trees, as they demonstrated an extended life beyond that of a human life. In his book Burr suggested that the very nature of the electric fields generated the necessary parameters in order to maintain life or coalesce the structures necessary to maintain life. An inference of the work suggests the possibility of super-imposing distinct patterns of electric fields from one organism to another which is composed of the same material. One must be cautious at the notion that the same structures produce the same fields – they do not. Even though organisms may be structurally homologous with each other they do not demonstrate homologous electrical patterns. That is to say that the electric field patterns of a given organism can be described as a fingerprint for that organism distinct from all that rest (Ravitz, 1955; Ravitz, 1951). Unfortunately many of Burr's hypotheses could not be tested as the technology at the time was limited in its scope.

Burr's theory postulates that material interacts by way of an arbitrary boson, a unit of information transfer. However, consider the alternative hypothesis which incorporates Burr's postulate, of the effect of an appropriate applied magnetic field interacting with a structures'

electric field and ultimately influence/direct any underlying processes. Such a magnetic field can interact with distant material in two ways: 1) propagations through a medium, or 2) through an entanglement-like phenomenon. The first method, that of propagation, assumes that the intensity of the magnetic field decreases as the square of the distance increases and is said to follow the Inverse Square Law. This requires the materials to be within a proximal distance to each other for any exchange to possibly occur. The second method, that which obeys the notion of entanglement (a simultaneous alteration in the properties of isolated materials that cannot be described by classical methods), is not limited by the reduction in intensity of the field in any manner. We have considered that the magnetic and electric fields act as a carrier wave projecting units of information. In the propagation method the information that is being transmitted is reduced in its effectiveness (akin to magnitude) due to the depression of the amplitude associated with this classical transmission technique (Inverse Square Law). In stark contrast, the phenomenon of entanglement does not affect the clarity of the signal and its efficacy of being transferred from one location to the next.

A field is a continuum of discrete tangible potentials that interact with the components constituting space and time. This can be likened to a diffuse array of varying potentials producing a background flux allowing for complex interactions. We have identified fields in this context as either being magnetic or electric in nature. The effects of the application of these fields are generally described as a wave. A wave can have two properties with regard to information theory; it is either it is a *carrier wave* or a *signal wave* which exist as a complimentary unit. A carrier wave is generally large in amplitude and low in complexity whilst the signal wave is generally very low in amplitude with marked complexity. Here the purpose of the carrier wave is to have a signal of a more complex nature (primarily temporally modulated or

phase shifted) embedded within it. It acts as a shuttle or package that accompanies the message from sender to receiver. Conversely, the signal wave generally carries the necessary information from the sender to the receiver. We have presented an idea that the resultant electrodynamic field patterns (signal) subsequently generate magnetic field equivalents containing both the properties of carrier and signal. This allows the magnetic field to act as both an initiator of entanglement (i.e. displays the appropriate parameters necessary to induce the correlates of entanglement) or participate as a carrier wave through propagation and classical transmission mechanisms. The activities of these fields are not limited by our functional definitions and can demonstrate multiple properties simultaneously.

The phenomenon of entanglement has been explored in relativistic and quantum mechanical means and can be rationalized such that if you have two particles (e.g. electrons, protons) that are entangled any change in one unit will result in a proportional and inverse change in the other unit even though the two systems are isolated and separated by vast distances (Hill and Wootters, 1997; Bell, 1964; Polchinski, 1991). Given that this scenario is possible, the alteration in the information (field dynamics) of one material may indeed affect the same material simultaneously regardless of the degree of separation. From our previously identified equations, as derived by Maxwell, the application of a magnetic field can alter the electrodynamic properties (time-varying electric field component) through a Faraday induction effect and thus alter the characteristics, the electric pattern, of a given substance. This indirect application of Burr's hypothesis may substantiate the claims of super-position of electrodynamic patterns between similar materials. What is required, however, is not simply the sceptical application of theory but the direct observation and measurement of serial manipulation. Thus we propose a series of experiments examining the nature of immortality, and the possible application

parameters necessary to alter the structural arrangement of the organism and a potential investigation into the super-position of electrodynamic states between similar and dissimilar material and the limits of this application.

If one wishes to identify the origins of the *Blueprint for Immortality* one must understand the nature of how the primary building blocks of our existence interact. The physical perspective of the genesis of living material commenced at the initiation of the Big Bang. From this moment the energy of the Universe expanded outwardly forming pockets of plasma (Copi *et al*., 1995). These high energy areas gradually cooled and amalgamated into the fundamental building blocks of our Universe, the various atomic elements. Classically, this explanation is proposed to accommodate how atoms are formed and from that our inevitable genesis. However, consider an alternative, one where matter is strictly the necessary constituent to bind energy and contain it over larger temporal spans. Energy itself can interact with material. It can be transformed from one form to the next but ultimately it is insubstantial. Matter, in contrast, has permanence to it. Matter allowed the exchange of energies to occur across space time and to become stored. In order for any process to evolve, matter must have been formed from energy. It is suggested that energy itself is the Blueprint, or at least holds the Blueprint, for Immortality. It is the transition of energy (insubstantial) to matter (substantial) which denotes the initial genesis of prototypical life. Studying the nature of matter in its fundamental forms should then provide insight to the Immortal nature of energy.

It is important to determine the nature of the fundamental constituents of our Universe and this endeavour is well underway. Similarly, in order to understand the origins of our Blueprint and examine the Immortal potential that we may possess, we must begin with our

genesis. I have discussed the origin of our genesis with regards to the Miller-Urey studies however we have neglected a key constituent of the experiment: water.

The properties of water are suggestive of a complex nature of activity reflecting the necessary parameters to encourage the directed genesis of life. We generalize the term *life* to include all forms that contain a cell membrane. The potential for a primordial precursory membrane has been hypothesized and its origins traced to the structure of water. Trevors and Pollack (2011) hypothesized that radiant energy in the infrared portion of the spectrum results in a charge differential of 100 to 200 mV and is associated with the genesis of pre-biotic cells. The hypothesis presented in the current document was based upon the observations of Chai and Pollack (2010) which demonstrated a maximum expansion of the exclusion zone (EZ) of water when exposed to incident radiation of 3.4 μm wavelength. The exceptional property of water to generate EZ's (i.e. solute free zones) around a surface supports the hypotheses of water having the potential to generate impermeable or semi-permeable regions akin to membranes. The idea of water as the precursor to the formation of biological membranes is predicated on the generation of these solute free zones. Magnitudes of electrical potential of the exclusion zone is well within the range of the depolarization of neurons (Kandel and Spencer, 1961) and reflects the magnitude of the resting membrane potential of some bacterial and animal cell types (Hodgkin and Huxley, 1952; Hille, 2001).

Further evidence supporting the hypothesis of water being a precursor cell membrane is provided by Murugan and colleagues (2013). When samples of spring water were stored in a dark environment (18 d) and exposed, for the same duration, to 1 μT physiologically patterned electromagnetic fields which were complimented by complex frequency modulations, a reliable shift in peak fluorescent wavelength of 10 nm was observed. These results demonstrate the

potential for appropriately patterned magnetic fields to displace the energetic equivalents by about the size or thickness of a cell membrane. Furthermore, Zheng and colleagues (2006) measured T_2 relaxation times of bulk and interfacial water using MRI imaging techniques. It was determined that a value of 27.2 ± 0.4 msec and 25.4 ± 0.1 msec were identified for both bulk and interfacial water respectively. The latter value corresponds to findings determined by Murugan *et al*. (2014) and reflects a level homogeneity associated with the rostral-caudal depolarization time most commonly correlated to consciousness.

In this dissertation we outline a series of experiments that honour the electrodynamic postulates originating with Burr and to extend the breadth of knowledge using more refined equipment. In our first experiment we examine the electrodynamic changes in plants as they undergo transition into their senesced state. Generally, senescence is a state of quiescence that annual plants undergo upon transition into the winter months. This particular investigation serially examines transitional phases over short periods of time in order to identify the electrodynamic correlates associated with maintaining the necessary structure to extend the life of the organism. Our second approach examines the possibility that dissimilar materials sharing a process can in fact demonstrate similar electrodynamic properties. This latter investigation, if possible, eliminates the constraints applied by Burr in his original hypothesis. It may usher in the opportunity to store electrodynamic patterns in a vessel not necessarily effected to the same extent of a human shell to the progressive nature of time. In this context we operate under the assumption that if plants and bacteria share a potential candidate for the *Blueprint of Immortality* then they should interact in a meaningful way even though they may not possess the same genetic or structural organizations. Our penultimate experiment examines the possible application of entanglement-like phenomena as a means to exert a change in the electrodynamic

characteristics of similar material. In this context we examine the passive exchange of electrical patterns in an attempt to synthesize Burr's far-reaching ideas and explore the important role water may play in it. Our final experiment examines the interaction of temperature variations and electromagnetic fields on the unique properties of water in order to understand the dynamic nature of the initiator of our existence.

1.1 References

Beane, W. S., Morokuma, J., Adams, D. S., & Levin, M. (2011). A chemical genetics approach reveals H, K-ATPase-mediated membrane voltage is required for planarian head regeneration. *Chemistry & biology*, 18(1), 77-89.

Bell, J. S. (1964). On the einstein-podolsky-rosen paradox. *Physics*, 1(3), 195-200.

Burr, H. S. (1972). Blueprint for immortality: electric patterns of life discovered in scientific breakthrough. CW Daniel Co. Ltd.

Burr, H. S., & Northrop, F. S. C. (1935). The electro-dynamic theory of life. *The Quarterly Review of Biology*, 10(3), 322-333.

Burr, H. S. (1941). Field properties of the developing frog's egg. *Proceedings of the National Academy of Sciences of the United States of America*, 27(6), 276.

Burr, H. S., & Hovland, C. I. (1937). Bio-electric potential gradients in the chick. *The Yale journal of biology and medicine*, 9(3), 247.

Burr, H. S., & Hovland, C. I. (1937). Bio-electric correlates of development in Amblystoma. *The Yale journal of biology and medicine*, 9(6), 540.

Burr, H. S. (1944). The meaning of bio-electric potentials. *The Yale journal of biology and medicine*, 16(4), 353.

Burr, H. S. (1952). Electrometrics of atypical growth. *The Yale journal of biology and medicine*, 25(1), 67.

Burr, H. S. (1940). Biologic organization and the cancer problem. *The Yale journal of biology and medicine*, 12(3), 277.

Burr, H. S. (1943). Electrical correlates of pure and hybrid strains of sweet corn. *Proceedings of the National Academy of Sciences of the United States of America*, 29(6), 163.

Burr, H. S., & Northrop, F. S. C. (1939). Evidence for the existence of an electro-dynamic field in living organisms. *Proceedings of the National Academy of Sciences of the United States of America*, 25(6), 284.

Burr, H. S. (1932). An electro-dynamic theory of development suggested by studies of proliferation rates in the brain of Amblystoma. *Journal of Comparative Neurology*, 56(2), 347-371.

Bustamante, C., Bryant, Z., & Smith, S. B. (2003). Ten years of tension: single-molecule DNA mechanics. *Nature*, 421(6921), 423-427.

Chai, B., & Pollack, G.H. (2010). Solute-free interfacial zones in polar liquids. *The journal of Physical Chemsitry B*, 114(16),5371-3575.

Copi, C. J., Schramm, D. N., & Turner, M. S. (1995). Big-bang nucleosynthesis and the baryon density of the universe. *Science*, 267(5195), 192-199.

Hill, S., & Wootters, W. K. (1997). Entanglement of a pair of quantum bits. *Physical review letters*, 78(26), 5022.

Hille, B. (2001). Ion channels of excitable membranes (Vol. 507). Sunderland, MA: Sinauer.

Hodgkin, A. L., & Huxley, A. F. (1952). The dual effect of membrane potential on sodium conductance in the giant axon of Loligo. *The Journal of physiology*, 116(4), 497-506.

Hodgson, G. W., & Baker, B. L. (1967). Porphyrin abiogenesis from pyrrole and formaldehyde under simulated geochemical conditions. *Nature*, 216, 29-32.

Huxley, T. H. (1870). Biogenesis and abiogenesis. Collected Essays of Thomas H. Huxley, 8, 256.

Kandel, E. R., & Spencer, W. A. (1961). Electrophysiology of hippocampal neurons: II. After-potentials and repetitive firing. *Journal of Neurophysiology*, 24(3), 243-259.

Kosikov, K. M., Gorin, A. A., Zhurkin, V. B., & Olson, W. K. (1999). DNA stretching and compression: large-scale simulations of double helical structures. *Journal of molecular biology*, 289(5), 1301-1326.

Kubar, T., Woiczikowski, P. B., Cuniberti, G., & Elstner, M. (2008). Efficient calculation of charge-transfer matrix elements for hole transfer in DNA. *The Journal of Physical Chemistry B*, 112(26), 7937-7947.

Lobo, D., Beane, W. S., & Levin, M. (2012). Modeling planarian regeneration: a primer for reverse-engineering the worm. *PLoS Comput Biol*, 8(4), e1002481-e1002481.

James Clerk Maxwell, "A Dynamical Theory of the Electromagnetic Field", *Philosophical Transactions of the Royal Society of London* 155, 459-512 (1865).

Maxwell, James Clerk (1904), A Treatise on Electricity and Magnetism, Vol. II, Third Edition. Oxford University Press.

McLaughlin, S. (1989). The electrostatic properties of membranes. *Annual review of biophysics and biophysical chemistry*, 18(1), 113-136.

Miller, S. L., Urey, H. C., & Oro, J. (1976). Origin of organic compounds on the primitive earth and in meteorites. *Journal of molecular evolution*, 9(1), 59-72.

Murugan, N.J., Karbowski, L.M., & Persinger, M.A. (2014). Serial pH increments (~20 to 40 milliseconds) in water during exposrues to weak, physiologically patterned magnetic fields: implications for consciousness. *Water*,6,45-60.

Murugan, N.J., Karbowski, L.M., Dotta, B.T., & Persinger, M.A.(2015). Delayed shifts in pH responses to weak acids in spring water exposed to circular rotating magnetic fields: A narrow band intensity-dependence. *International research Journal of Pure and Applied Chemistry*, 5 (2), 131.

Nitzan, A., & Ratner, M. A. (2003). Electron transport in molecular wire junctions. *Science*, 300(5624), 1384-1389.

Nogi, T., & Levin, M. (2005). Characterization of innexin gene expression and functional roles of gap-junctional communication in planarian regeneration. *Developmental biology*, 287(2), 314-335.

Northrop, F. S. C., & Burr, H. S. (1937). Experimental findings concerning the electro-dynamic theory of life and an analysis of their physical meaning. *Growth*, 1, 78-88.

Oviedo, N. J., Morokuma, J., Walentek, P., Kema, I. P., Gu, M. B., Ahn, J. M., & Levin, M. (2010). Long-range neural and gap junction protein-mediated cues control polarity during planarian regeneration. *Developmental biology*, 339(1), 188-199.

Pollack, G.H., Figueroa, X., & Zhao, Q. (2009). Molecules, water and radiant energy; new clues for the origin of life. *International journal of molecular sciences*, 10(4), 1419-1429.

Polchinski, J. (1991). Weinberg's nonlinear quantum mechanics and the Einstein-Podolsky-Rosen paradox. *Physical Review Letters*, 66(4), 397.

Plimpton, S. J., & Lawton, W. E. (1936). A very accurate test of Coulomb's law of force between charges. *Physical Review*, 50(11), 1066.

Rakov, V. A., & Uman, M. A. (2003). Lightning: physics and effects. Cambridge University Press.Ravitz, L. J. (1959). Application of the Electrodynamic Field Theory in Biology, Psychiatry, Medicine, and Hypnosis: I. General Survey. *American Journal of Clinical Hypnosis*, 1(4), 135-150.

Ravitz, L. J. (1953). Electrodynamic field theory in psychiatry. *Southern medical journal*, 46(7), 650-660.

Ravitz, L. J. (1951). Standing potential correlates of hypnosis and narcosis. *AMA Archives of Neurology & Psychiatry*, 65(4), 413-436.

Ravitz, L. J. (1955). Comparative clinical and electrocyclic observations on twin brothers concordant as to schizophrenia: With Periodic Manifestations of Folie a Deux Phenomena. *The Journal of nervous and mental disease*, 121(1), 72-87.

Ravitz, L. J. (1962). History, measurement, and applicability of periodic changes in the electromagnetic field in health and disease. *Annals of the New York Academy of Sciences*, 98(4), 1144-1201.

Ravitz, L. J. (1951). Daily variations of standing potential differences in human subjects: preliminary report. *The Yale journal of biology and medicine*, 24(1), 22.

Stachel, J., & Torretti, R. (2002). Einstein's first derivation of mass-energy equivalence. *Einstein from" B" to" Z"*, 9, 215.

Trevors, J.T.,& Pollack, G.H. (2012). Origin of microbial life hypothesis: A gel cytoplasm lacking a bilayer membrane, with infrared radiation producing exclusion zone (EZ) water, hydrogen as an energy source and theromsynthesis for bioenergetics. *Biochimie*, 94(1), 258-262.

Tyler, K. (2005). The genealogical imagination: the inheritance of interracial identities. *The Sociological Review*, 53(3), 476-494.

Walet, N. R., & Zakrzewski, W. J. (2005). A simple model of the charge transfer in DNA-like substances. *Nonlinearity*, 18(6), 2615.

Yao, L., McCaig, C. D., & Zhao, M. (2009). Electrical signals polarize neuronal organelles, direct neuron migration, and orient cell division. *Hippocampus*, 19(9), 855-868.

Yao, L., Shanley, L., Mccaig, C., & Zhao, M. (2008). Small applied electric fields guide migration of hippocampal neurons. *Journal of cellular physiology*, 216(2), 527-535.

Zheng, J.M., Chin, W.C., Khijniak, E., & Pollack, G.H. (2006) Surfaces and interfacial water: evidence that hydrophilic surfaces have long-range impact. *Advances in colloid and interface science*, 127(1), 19-27.

Chapter 2

2 Electrophysiology of the Dynamic Profiles of Plants Undergoing Senescence

2.1 Abstract:

DC voltage changes of whole sedge plants (*Carex stricta*) demonstrate conspicuous alterations in recorded electrophysiological profiles whilst undergoing senescence. We demonstrate time-dependent changes contingent upon the seasonal variations of environmental variables as measured by whole plant electrodynamics. Furthermore, plants responding to applied light demonstrate three peak intensities capable of eliciting significantly different changes in voltage between plants. Quantitative support for threshold of light stimulation converges at the level of the cell and demonstrates a quantum-cell equivalent. The implications of water and charge for maintaining membrane dynamics are also explored.

2.2 Introduction:

2.2.1 Physiological Perspectives of Senescence

Senescence is a complex biochemical and physiological process as the final stage of the plant life cycle (Lim *et al.*, 2007). Although the result of the transition from one stage of development to another is associated with an intricate variation in the total organism, senescence has been limited to the examination of physiological changes and their associated alterations in protein production or degradation (Gan and Amasino, 1997). The study of senescence has been categorized into two groups of observation reflecting the distinct structural components which are intended to be examined. The first approach to understanding senescence is accomplished by examining the change in leaf structure and chlorophyll composition and other biochemical

alterations over time. Subsequent to the analysis of leaf dynamics, changes associated with the progression and alterations in the apical meristem constitute the second categorical observation of senescence (Hensel *et al.*, 1994). The respective investigations of leaf and meristematic associated senescence are considered post-mitotic and mitotic senescence, respectively (Gan, 2003).

In this particular instance, the examination of both mitotic and post-mitotic senescence can be translated into whole plant changes. For instance, degradation in leaf chlorophyll composition alters the efficacy of photosynthetic processes (Dickinson *et al.*, 1991; Bing *et al*., 1993) which can affect other processes that are dependent upon the products of the photosynthetic cascade. The reduction in photosynthesis initiates for the mobilization of macromolecules to storage areas situated in appropriate tissues of the plant (Thomas and Donnison, 2000; Zavaleta-Mancera *et al*., 1999; Buchanan *et al*., 2003).

Alterations occurring at the meristematic region, an area which is associated with high growth rates, slow in order to accommodate such a large scale change (Rolland *et al*., 2006). The slowing and eventual cessation of meristematic area activity reduces the overall energy consumed by the plant or a redistribution of said energy. Reduction and cessation of growth results in two phenomena: an increase in available energy and cellular arrest. In the latter case cells arrest their differentiation and maintain a prolonged state of inactivity (Havel and Durzan, 1996). Cell cycle arrest allows for the structural equivalent of the cell to be maintained until the environment contains the appropriate variables to re-initiate and sustain prolonged regular cellular activity (Bleecker and Patterson, 1997; Lim *et al*., 2007).

Plants demonstrate the ability to undergo both post-mitotic and mitotic senescence (Gan, 2003) which may in turn impact the electrical potential of the plant proper which is supported by

the changes in the electrochemical properties of the plant as recognized by Davies (2004). From a leaf senescence perspective, physical changes in the plant result in the marked degradation of available chlorophyll in a reliable manner (Lim *et al*., 2007). It is suspected that changes in electrochemical potential can be translated into alterations in the electrical potential of the entire plant (Fromm and Lautner, 2007; Fensom, 1957; Zimmerman *et al*., 2009).

2.2.2 Electrophysiological Perspectives: The possibility of using light-mediated alterations to affect electrophysiological responses in plants in order to assess differential stages of senescence

Ultrastructural alterations within the complex cellular matrix of plant biology provide valuable information with respect to the structural alterations that accompany senescence. However, the method of ultrastructural, cellular investigation into senescence does not provide dynamic information throughout the progression of senescence to its termination. Primarily, these investigative techniques rely on measuring static, completed changes and reveal no information into the time-course of the process. Furthermore, despite the specificity of genetic and histological analyses, they do not produce a full picture of the sum of the changes that occur with the entire plant. In light of such limitations, the possibility of employing a dynamic measurement to assess the transient alterations within the entire plant as it undergoes structural alterations associated with senescence may provide alternative insights.

One potential candidate which can accommodate such dynamic measures would be the use of direct current (DC) potential differences over a given distance. DC potential is an emergent property of the aggregate organization of electrogenic plant tissue, orienting the flow of current within the plant ultimately generating an electric field around the organism (Nuccitelli, 1984). Physically, if an electric field is applied over a given distance (i.e. the distance between two sensors of a voltmeter) a potential difference results. Masi *et al*. (2009) utilized a 60

microelectrode array to study the spatiotemporal electrical activity at the root apex and found a pattern in which spikes of electrical activity developed spontaneously. These spontaneous electrical spikes formed synchronous, transient episodes that were followed by epochs of no activity which lasted many seconds. This demonstration of electrical spike activity may lend credence to the hypothesis that plant action potentials generated in electrically excitable cells may be linked to processes such as photosynthesis and respiration (Fromm and Lautner, 2007; Lautner *et al*., 2005).

Supplementary support for the use of electrical measures in plant research were provided by Gurovich and Hermosilla (2009) who used continuous measures of electrical potential in plants to identify changes in responses associated with alterations in local environmental variables (temperature, humidity, moisture, water availability, light and dark exposure, *etc*.). The determination of a complex relationship between local variables and electrical potential difference was identified aiding the notion of whole plant electrical alterations as an effective means of assessing information on the responses of the organism. Specifically, changes associated with light and dark conditions displayed alterations in profiles of potential difference (Gurovich and Hermosilla, 2009) whose activity may be related to membrane depolarizations linked to photosynthetic processes (Whitmarsh, 2004). Szechyńska-Hebda and colleagues (2010) corroborated these ideas by demonstrating that photoelectrophysiological signals could be generated by altering the amount and duration of light exposure. They concluded that plant action potentials (ranging from 15 to 50 mV in intensity) occurred within seconds of the initial stimulus and could be related to many physiological processes (Szechyńska-Hebda *et al*., 2010). The time domain, in the order of seconds, may correspond to slow conduction velocities or may represent an optimal spatial relationship. Felle and Zimmerman (2007) concluded that biphasic

potential differences in barley samples corresponded to a conduction velocity of 20-30 $cm \cdot min^{-1}$ whilst Masi *et al*. (2009) demonstrated conduction velocities in the order of 20 $cm \cdot s^{-1}$ in maize. Thus, in order for measures of potential difference to be effectively assessed, times frames of seconds to minutes and distances in the order of tens of centimeters are required.

Examining electrophysiological measures over tens of centimeters and temporal durations of seconds to minutes is corroborated and can indeed be used to assess whole plant alterations. However, the question of the efficacy of such a technique to assess the degree of senescence arises. Szechyńska-Hebda and Karpiński (2013) demonstrated the ability of plants to acclimate to alternating light intensities and linked said alterations to photo-electrochemical potential (a form of induced voltage change) mediated by chloroplast signalling. Relating potential difference to senescence, the onset of leaf senescence is related to a decline in available photosynthetic proteins and associated activities (Szechyńska-Hebda and Karpiński, 2013). Furthermore, the initiation of senescence is contingent upon the intensity of available light rather than quality (Szechyńska-Hebda and Karpiński, 2013) and involves the degradation of chloroplasts (Pogson *et al*., 2008; Pfannschmidt, 2010). Thus a change in the integrity of the chloroplasts alters the electrochemical gradient resulting in changes in the potential difference of the plant that can be transmitted along the bundle sheath throughout the organism (Szechyńska-Hebda and Karpiński, 2013). Any compromise to the chloroplasts or photosynthesis-associated proteins will change the degree of response to, and the efficacy of the incident light's ability to activate, the appropriate pathways which in turn will affect the generated potential difference across the plant. Is it then possible to assess the degree of senescence of a plant based upon the electrical responses to cyclic presentations of light and dark?

2.3 Methods:

2.3.1 Measurement devices

Measurements were conducted using two independent Victor 70C direct current (DC) digital multimeters, two independent laptop computers and associated recording software. The laptop monitoring systems remained paired with their associated DC multimeters for the duration of the experiment. There was no experimental measurement error associated with the port time of the computer as the monitoring systems (digital multimeters) had matched sampling frequencies and port time delays. Sampling rate was set at 10 sec increments.

2.3.2 Specimen

Plants of *Carex stricta* (tussock sedge; Cyperaceae, three replicates), originating from a Sudbury area wetland were vegetatively propagated and grown in 10 L plastic containers that were perforated at the base. These plants were grown for two years in an experimental garden 25 km north of the Laurentian University campus and were standing in 10 cm deep pools of ground water. In the latter part of September 2014, these plants were moved to smaller pools of water located on the grounds of Laurentian University where measurements were conducted between the 8th of October 2014 and the 7th of November 2014. During this time leaves of this species senesce as nutrients are mobilised into storage organs before the onset of winter (Ryser and Kamminga, 2009; Figure 2A). Individual plants were tested once a week on the same night each week for four weeks. On the day of testing, the selected plants were removed from their water basin and placed in another basin containing 10 to 15 cm of water in the testing location. The temperature in the test location was consistently held at 23℃ with ample light. All plants were allowed to acclimatize to the testing room for at least 12 h prior to testing. Testing began between the hours of 22:00 and 02:00 local time (EST). The duration of direct light exposure

ranged from 11 h 21 min (October 8th 2014) to 9 h 49 min (November 7th, 2015) during all conditions and acclimation periods.

2.3.3 Sensor placement

Sensors, anodes and cathodes, were attached to the root and leaves of each specimen. The anode (reference) was placed approximately 10 cm below the potting soil surface and was attached by a silver-chloride flat disc sensor to a single root. The distal end of the flat disc sensor was affixed upon the carrying handle to which each individual plant was housed. Both DC multimeters were referenced to the distal end of the flat disc sensor. The cathodes (measuring sensors) were attached to twodifferent samples of leaves on the plant. The criteria for selection will be addressed in the following section. The two leaf samples were attached to their respective monitoring devices by use of an alligator clip. The linear equivalent distance from the surface of the potting soil to the alligator clip was approximately 10 cm, resulting in a total linear separation between the sensors of 20 cm.

2.3.4 Leaf selection

Two leaf samples were selected in order to discern the differential progression of senescence within an individual plant as measured by electrophysiological parameters. Leaves were selected based upon their progressive loss of chlorophyll before the commencement of this experiment. Here green leaves (S1 measures) were leaves that retained a bright green colour along their entire length. If, however, there were no fully identifiable green leaves then the criteria such that at least 80 % of the leaf retained its bright green colour was employed. All plants met at least one of these two criteria for the S1 samples. Conversely, senescing leaves (S2 samples) had to meet the following criteria: complete absence of green pigmentation and/or wilting with the presence of a discolouration (along the continuum between yellow and brown)

along the apical surface of the leaf. All S2 measures met these criteria before the initial testing phase began.

2.3.5 Electrophysiological manipulation

Testing was conducted on individual plants once a week whose DC electrical potentials were sampled once per 10 sec for the duration of the measurement period and repeated for the four weeks of observation. Plants were monitored for changes in electrical potential (DC voltage) along a concentration of light intensity (lux). The exposure paradigm consisted of a photo-stimulus (light-on), photo-absence (light-off) cycle following a 2-min cycle length in an A-B-A-B-A format. Gradient alterations in stimulus intensity were modulated by moving the source of photo-stimulation away from the plant. The photo-stimulus source was a 40-W incandescent light-bulb in a conical lamp positioned along a continuum between 20 and 200 cm. Each new intensity was modulated by consecutive 20 cm linear displacements in the light source until a distance of 200 cm was obtained. Raw values for the gradient of light intensity have been included in Table 2.1. In this particular environment, the dissipation of heat from the stimulus apparatus was negligible. All values for DC potential were recorded using the appropriate software and raw recordings were imported into IBM SPSS 17 for statistical analyses and accompanied data transformations.

Table 2.1: Raw intensity measures intensity along the various distances of stimulation. Converted values from intensity in lux to power density have also been provided.

Distance (cm)	Intensity (Lux)	Power Density ($W \cdot m^{-2}$)
20	1686	2.47
40	560	$8.20 \cdot 10^{-1}$
60	255	$3.73 \cdot 10^{-1}$
80	152	$2.23 \cdot 10^{-1}$
100	95	$1.39 \cdot 10^{-1}$
120	73	$1.07 \cdot 10^{-1}$
140	49	$7.17 \cdot 10^{-2}$
160	38	$5.56 \cdot 10^{-2}$
180	29	$4.25 \cdot 10^{-2}$
200	25	$3.66 \cdot 10^{-2}$

2.4 Results:

2.4.1 The effects of intensity and photoperiodicity

The mean of the instantaneous change in voltage (the change in voltage per measurement interval) was calculated across individual plants from either S1 or S2 leaves referenced to the root and entered into a 4-way photoperiod by intensity by leaf age by week repeated measures multivariate analysis of variance (MANOVA) and revealed a significant within subjects interaction [$F_{(27,693)} = 3.64$, $p<.001$, $p\eta^2 = 0.12$]. The resultant 4-way interaction is presented in Figures 2.1 A thru D. Multiple *post-hoc* one-way analyses of variance (ANOVAs) were conducted in order to identify the origin of the interaction and determined that the source of the interaction was due to the discreteness of the intensity of light that the specimen received. Differential effects associated with the application of a light stimulus demonstrated a necessary threshold of intensity for the effective alteration in the voltage of the whole plant. Results from the *post-hoc* analyses determined a trifurcation of intensity (three peaks along the gradient of light intensity) corresponding to linear equivalents of 20 to 40 cm (P1), 120 to 140 cm (P2) and 180 to 200 cm (P3). Figures 2.2A) thru 2D) represent the threshold phenomenon for these

particular specimen under this paradigm. These results are suggestive of essential peak intensities that are necessary for the appropriate response of the plant. Furthermore, *Carex stricta* undergoing changes in response to variable alterations in the local environment do not respond in an intensity dependent manner.

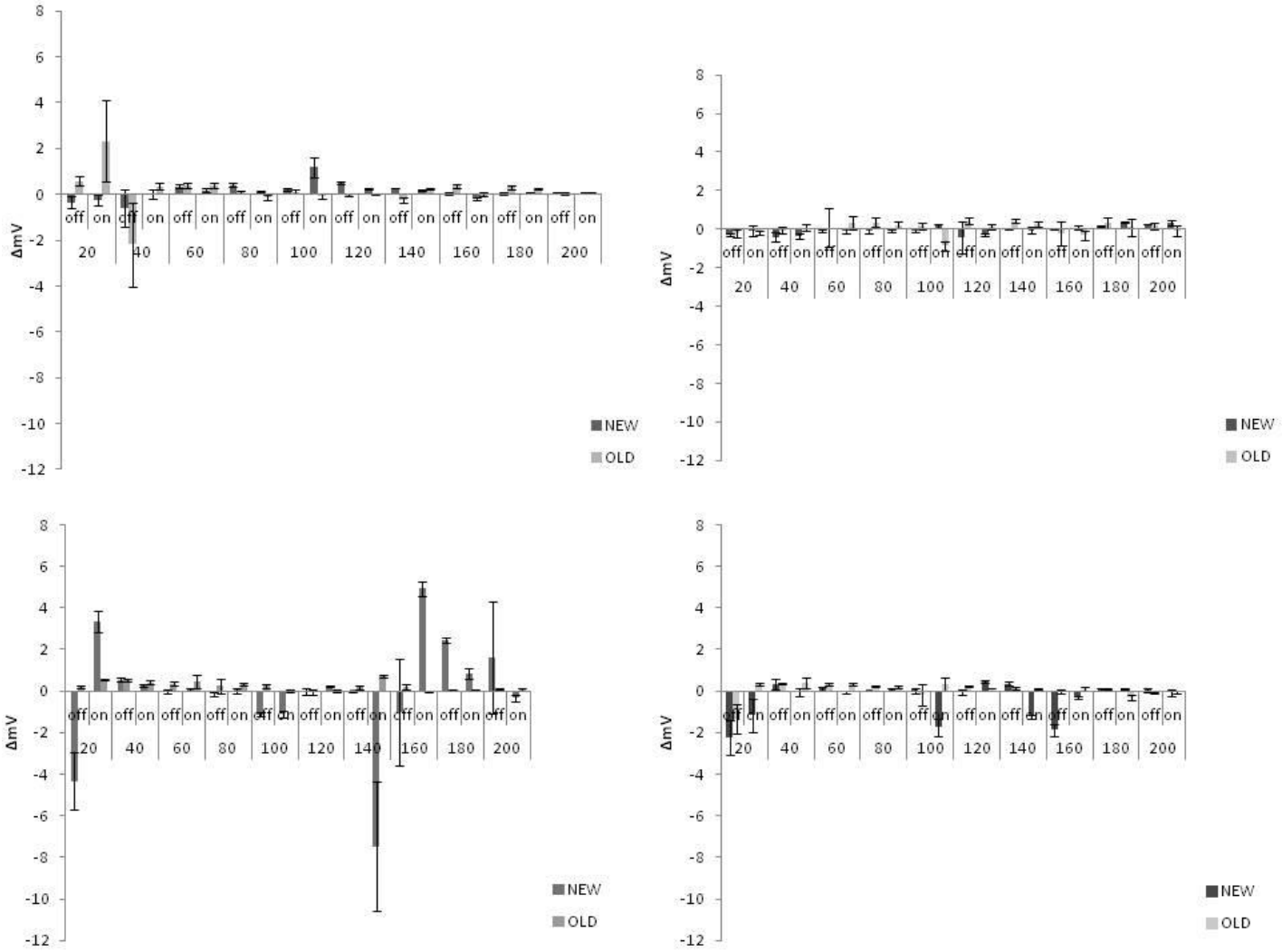

Figure 2.1a) – d) left to right and top to bottom display the serial organization of the days of testing ranging from weeks 1 to 4. The data presented in the graphs represent the 4-way photoperiod, by intensity, by leaf type by week interaction. Bars represent the mean of the change in voltage of all the plants measured during their respective weeks of observation. Error bars are representative of the standard error of the mean. The x-axis represents the distance (in cm) away from the light source. Conversions for the appropriate intensity are located in Table 2.1.

2.4.2 Weekly variations in electrodynamic responses to peak intensities:

Further examination of the now defined peaks for each of the green leaves were conducted to assess differences in the mean change in voltage of all plants corresponding to the identified three peak intensities over time. Here the results of serial ANOVAs suggest that 6 out of the 8 computed variables were different between the three peak intensities. Primary differences in peak intensities during Week 1 for the green leaves were being driven by the mean changes in voltage of all specimen associated with the first peak (P1, -0.29 mV) and the second peak (P2, 0.30 mV) peaks. The mean change in voltage of the green leaves during Week 2 of the paradigm for the second peak (P2) and the first peak (P1) intensities (-0.28 mV and -0.17 mV, respectively) were significantly different from the third peak (P3) intensity (0.27 mV) [$F_{(2,154)}$ = 6.60, $p<.01$, Ω^2-est = 0.08]. Week 3 differences were generated by the differences in mean change in voltage of all specimen between intensities at the second peak (P2, -1.97 mV) and the third peak (P3, 1.18 mV) intensities [$F_{(2,154)}$= 3.31, $p<.05$, Ω^2-est = 0.04]. Finally, for the green leaves on Week 4, the driving force behind the interaction was the result of the difference in mean voltage changes between the primary peak (P1, -0.77 mV) and both third (P3, -0.14mV) and second peak (P2, 0.04mV) intensities [$F_{(2,154)}$ = 5.22, $p<.01$, Ω^2-est = 0.06].

Senesced leaves did not demonstrate significant differences between the mean change in voltage at the three peak intensities during Weeks 1 and 4. However, for Week 2 significant differences were determined to be between the mean change in voltage of senesced leaves during the first peak (P1, -0.10 mV) and the second peak (P2, 0.30 mV) intensities [$F_{(2,154)}$ = 3.10, $p<.05$, Ω^2-est = 0.04]. Lastly, Week 3 differences in the mean change in voltage of senesced leaves at the third peak (P3, 0.08 mV) and the second peak (P2, 0.23 mV) intensities were

significantly different from each other and from the primary peak (P1, 0.43 mV) values [$F_{(2,154)}$ = 19.12, $p<.001$, Ω^2-est = 0.20].

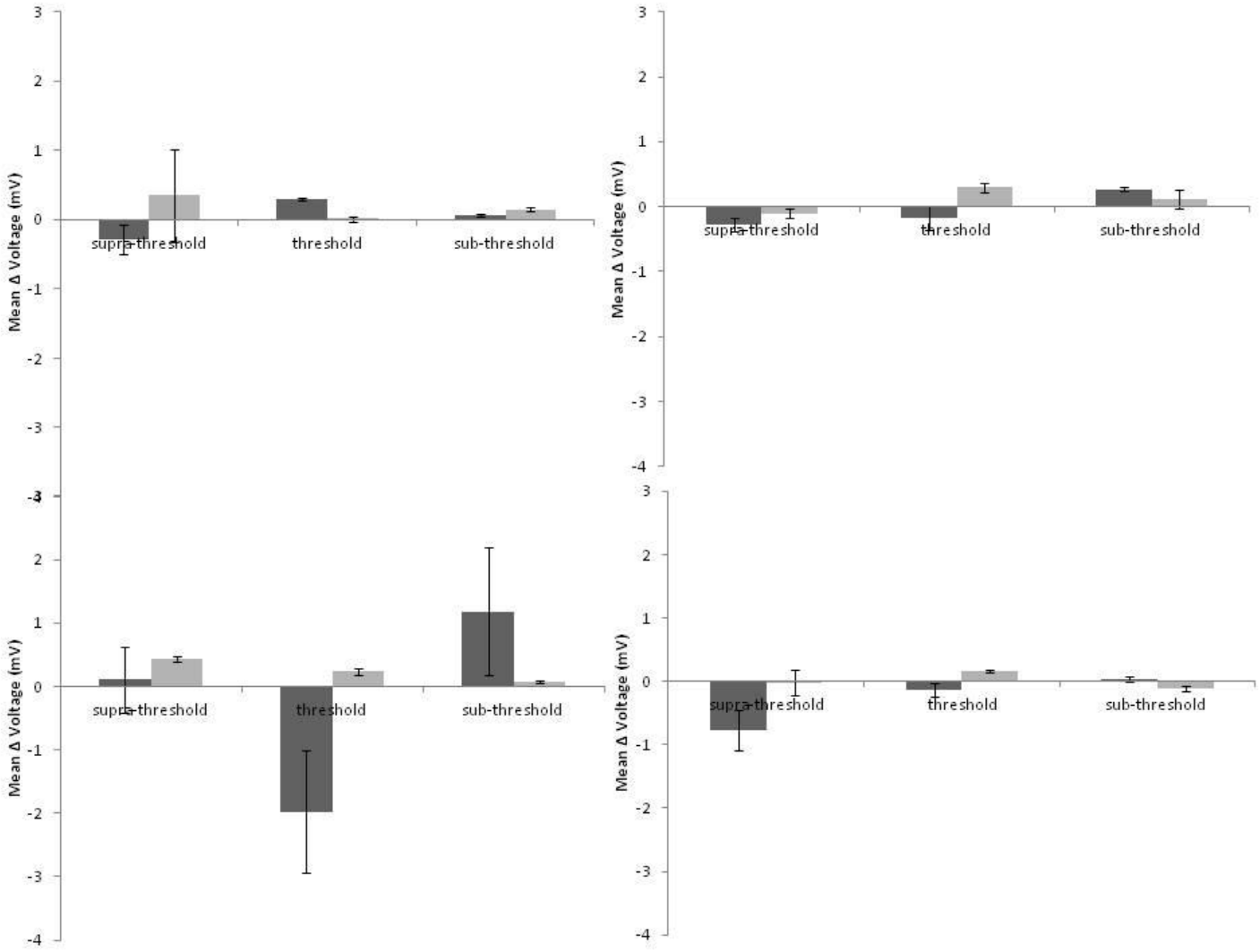

Figure 2.2 a - d left to right and top to bottom representing the threshold phenomenon representing weeks 1 thru 4 respectively. Dark grey bars represent green leaves while light grey bars represent the senesced leaves. Values displayed include the overall mean of the change in the potential difference between specimens. The values of the threshold have been discussed in the previous section. Error bars signify standard error of the mean.

Supplementary two-way analyses of variance with time as a covariate (ANCOVAs) were conducted on the mean change in voltage and its associated standard deviation across specimens for the appropriate stage of senescence (week of measurement) in order to discern the degree of

interaction between the photoperiod and intensity as a between subjects effect. A summary of these results are presented in Table 2.2.

Table 2.2: The combined results of a series of analyses of covariance (ANCOVAs) for presented variables with photoperiod (on-off cycle) and intensity as between subject's measures with time of observation as a covariate. Here S1 and S2 represent the relative age of the leaves green and senesced leaves respectively. SD is the standard deviation of the change in potential difference between S1 and S2 leaves. All other measures constitute the mean of the change in potential difference. Only the significance of the two-way interaction is presented.

Leaf type	**Week**	**Sig.**	**F-value**	**ΔF**	**Ω^2-est.**	**$\Delta\Omega^2$**
S1	1	----------	1.79	----------	0.057	----------
S1	2	----------	.087	-1.70	0.003	-0.054
S1	3	<.001	3.92	3.83	0.122	0.119
S1	4	<.001	6.12	2.2	0.149	0.027
S2	1	----------	1.38	----------	0.046	----------
S2	2	----------	.56	-0.82	0.021	-0.025
S2	3	----------	1.75	1.19	0.055	0.034
S2	4	<.01	2.35	0.60	0.087	0.032
SD	1	----------	1.14	----------	0.039	----------
SD	2	<.05	2.07	0.93	0.072	0.033
SD	3	<.05	2.42	0.35	0.070	-0.002
SD	4	<.001	4.92	2.5	0.105	0.035

2.4.3 Common sources of variance:

To further the understanding of the effects observed in the electrophysiological changes, the mean change in voltage for each leaf age (senesced and green) and associated stage of senescence (Weeks 1 thru 4) were entered into a factor analysis. The primary reason for this analysis was to examine potential shared sources of variance that may be associated with the temporal (age of leaf) characteristics of electrophysiological parameters associated with the now defined peak intensities. The mean change in voltage between specimens for the age of the leaf and the intensity of the photo-stimulus were the variables that were used in this particular analysis. The analyses generated 8 factors that contributed to a total variance explained of ~ 65% with respect to age of leaf and intensity dependence. The results of the varimax rotated component matrix (with a loading coefficient of 0.40 or greater) are presented in Table 2.3 along with the individual contribution to the total explained variance of each factor.

Table 2.3: Results of the factor analysis demonstrating the combined sources of shared variance. Here S1 and S2 refer to sample leaf type either green or senesced leaves respectively.

Factor	% Variance explained	Component Variables	Loading Coefficients
1	11.4	S1 at 80 cm	.638
		S1 at 120 cm	.708
		S2 at 160 cm	.842
2	9.7	S1 at 40 cm	.940
		S2 at 40 cm	.910
3	9.2	S1 at 200 cm	.603
		S2 at 100 cm	-.661
4	8.7	S1 at 20 cm	.466
		S2 at 140 cm	.690
5	7.0	S2 at 60 cm	.786
		S2 at 200 cm	.814
6	7.0	S1 at 20 cm	-.541
		S1 at 140 cm	.549
		S1 at 180 cm	.694
		S1 at 200 cm	.493
7	6.3	S2 at 80 cm	.512
		S2 at 120 cm	.807
8	5.5	S1 at 60 cm	.633

2.4.4 Classification of distinct stages of senescence

A discriminant analysis was conducted on computed raw variables (with intact number of cases) in order to identify the possibility of differential stages of senescence. Here max-steps were set to five, and the variables that entered into the discriminant equation were the between samples standard deviation of the relative change in voltage (SDREL), the root mean square of the relative change in voltage (RMSREL), the squared relative voltage of both the green and the senesced leaves (RELSQ1 & RELSQ2), and the relative change in voltage of the senesced leaves (RELS2). The classification success of the discriminant analysis approached 74% accuracy based on a cross-validated method [X^2 (15) = 4054.406, p <.001, 1-λ = 0.77] (Figure 2.3).

Equation 2.1: Discriminant Function Equation 1 = -0.013·(RELS2)+0.059·(SDREL) - $7.2\cdot10^{-5}$ · (RELSQ1) + $3.3\cdot10^{-4}$ · (RELSQ2) - 0.025·(RMSREL) -1.590

Equation 2.2: Discriminant Function Equation 2 = 0.016·(RELS2)+0.027·(SDREL) + $4.1 \cdot 10^{-5}$ · (RELSQ1) + $8.9 \cdot 10^{-4}$ · (RELSQ2) - 0.070·(RMSREL) +1.789

Highest scores for the discriminant function equation were obtained for Week 4 (1.98) whilst the lowest scores were obtained for Week 1 (-1.06). Weeks 2 and 3 demonstrated remarkably similar discriminate function equation values for group centroids of -.56 and -.71 respectively. Upon examining the resultant classification statistics for each group membership a divergence in the classification accuracy arises. Here the appropriate classification for Week 1 and Week 4 group memberships were 99.6% and 86.1%, respectively, however both Week 2 and 3 values were not as precise at separating measured electrophysiological parameters into distinct group memberships. The overlap and reduced discrimination of Weeks 2 and 3 may suggest a temporal evolution to the onset of senescence which can be approximated using electrophysiological measures.

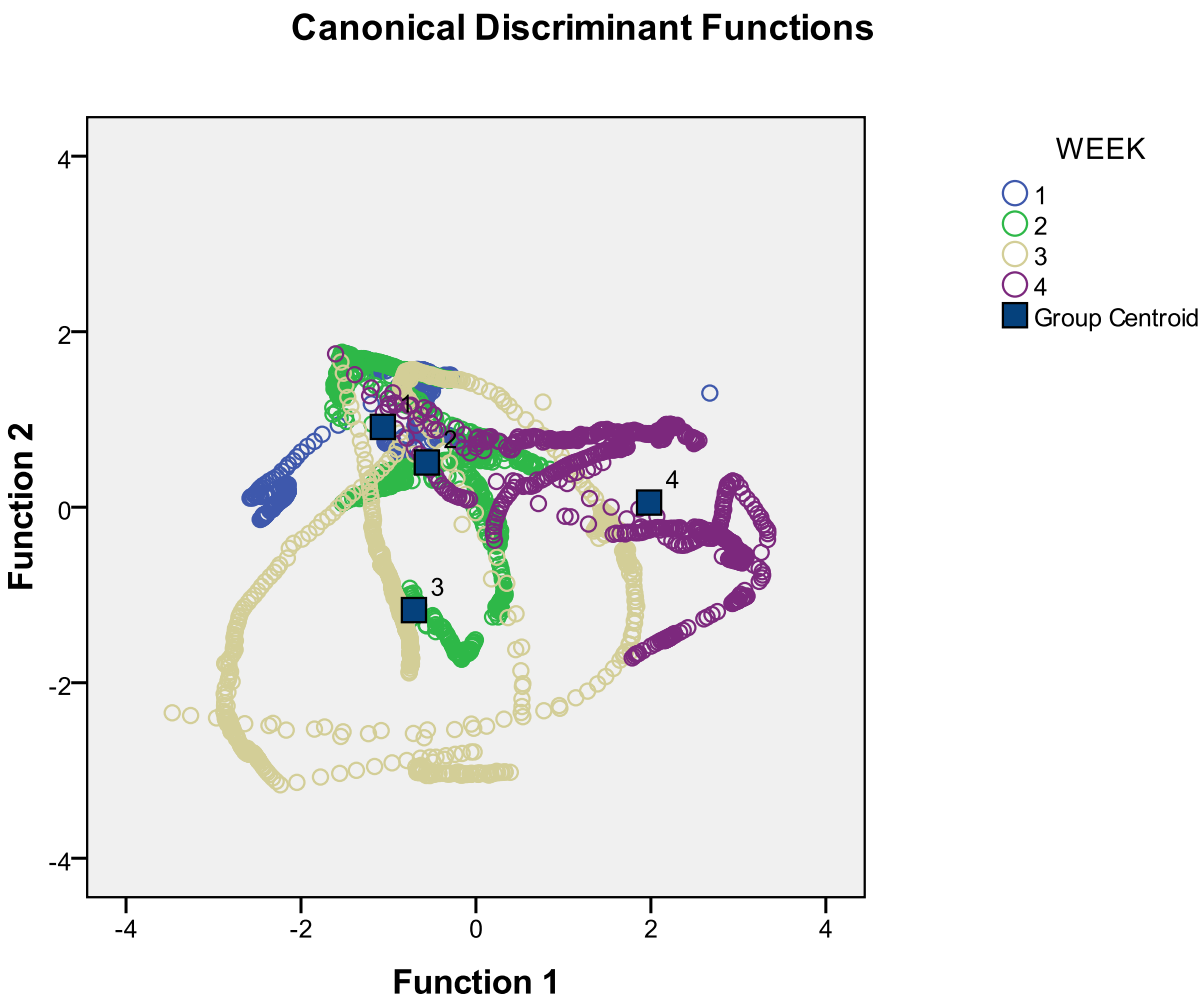

Figure 2.3: Distribution of discriminant function group centroids for classification accuracy. Each function along the x and y axes represent the combination of distinct variables that contribute to the overall discrimination of the appropriate weeks of testing. In this case the linear combination of discrete variables, defined in equation 2.1 and 2.2, the overall contribution to the appropriate differentiation of the weeks of testing is apparent. The overlap between the computed centroid functions (representative of the mean of the computed discriminant function equations) demonstrate a conspicuous sharing of variance that does not fully distinguish between independent stages of senescence. Here centroid functions demonstrate the geometrical combination of computed function variables and the associated triangulation of the arithmetic mean of the combination of group classification values.

2.4.5 Temporal Dynamics

Using the results obtained from our discriminant function a model of the temporal evolution of senescence can be approached. Here the predictive model for the onset of senescence was conducted using only the mean change in voltage between specimens and their

associated standard deviations of this measure across successive trials in a multiple regression analysis. The results of the successive multiple regression analyses (Table 2.4) suggest, and corroborate, that a temporal phenomenon associated with senescence exists.

Table 2.4: Multiple regression analysis results. Here the variables that are trying to be predicted are the mean of the change in potential difference (DEL) for each sample, green and senesced (S1 and S2 respectively) with their temporal equivalents of testing. Variables entered that are represented of an SD followed by a number are the standard deviation of the change in potential difference between samples along the temporal continuum. All significant values are reported such that p<.001.

Dependent Variable	Variables Entered	F-value	Adj. R^2	Predictive Equation
DELS1T1	SD1, DELS2T1, DELS2T4	45.65	.349	-.328·SD1 +.200·DELS2T1 + 199·DELS2T4 +.227
DELS1T2	SD2 DELS2T2	21.98	.144	-.385·SD2 -.084·DELS2T2 +.196
DELS1T3	----------	----------	----------	----------
DELS1T4	SD4 SD3 SD1 DELS1T3	69.25	.522	-.975·SD4 -.057·SD3 -.258·SD1 +.020·DES1T3 +.373
DELS2T1	SD1 DELS1T1 DELS1T4	48.72	.364	.743·SD1 + 1.253·DELS1T1 - .258·DELS1T4 -.410
DELS2T2	SD2 DELS1T4 DELS1T2	11.02	.107	-.513·SD2 +.120·DELS1T4 - .216·DELS1T2 +.380
DELS2T3	----------	----------	----------	----------
DELS2T4	SD4 SD3 DELS1T3	6.47	.062	-.179·SD4 -.032·SD3 +.018·DELS1T3 +.222

2.5 Discussion:

2.5.1 Electrophysiological Correlates of Senescence

We have demonstrated that complex bio-electrophysiological changes in response to alterations in periodic light application occur during the transition into a state of senescence. First and foremost, *Carex stricta* plants, at least in regards to this particular paradigm, do not respond to light in an intensity dependent manner. However appropriate peaks in intensity that

sufficiently alter the voltage of the plant can be observed. These peak intensities demonstrate variable responses depending on the time of experimentation (i.e. the associated stage of senescence). The time-dependent activity associated with responses in voltage to peak intensities may reflect the necessary alterations in the distribution of potential and free energy within the system (plant). The potential redistribution of energy may be inherently linked to the function of light sensitive channels or other cellular processes (Krol and Trebacz, 2000). Identifying distinct wavelengths of light along the spectrum can be used as an inference of the particular biochemical changes in the plant.

Synthesizing the results from the factor analysis as well as the discriminant analysis supports a unifying notion of a residual plant electrodynamic profile that shares discrete sources of variance across a temporal duration. Classification of different stages of senescence did not yield successful 100% classification accuracy. The reduced classification accuracy (to 74% of cases) of electrophysiological variables suggests a common source of variance that remains even though the plants may be undergoing marked changes in physiology. The notion that a functional residual activity, one that is shared or which can be elicited during the appropriate application of varying peaks of light, primarily associated with electrodynamic properties, is corroborated by the results of our factor analysis. They suggest a shared source of variance between green and senesced leaves and their associated stages of senescence when presented with varying intensities of photo-stimulation. These results indicate that even though the senesced leaves had qualitatively less chlorophyll at the beginning of the experiment, the resultant responses to different intensities of light remained the same. Responses of the plants to light at different temporal frames, which may be correlates of different stages of senescence, demonstrate a similar trend with respect to electrophysiological changes.

Furthermore, the lack of discriminative capabilities between the photo-stimulus and the photo-absent periods (data not presented) of this paradigm suggests that regardless of the degree of chlorophyllic degradation, the activity of both the senesced leaves and green leaves share an underlying mechanism. An alternative hypothesis suggests that there seems to be a conservation in activity of the electrodynamic responses of leaves over a discrete period of time, regardless of their integrity, to some exogenous stimuli. The residual activity present in plants undergoing senescence reveals a hidden characteristic suggesting that plants that have marked degradation in chlorophyll composition still undergo responses to light. We do not suggest that plants demonstrate an alternative means of photosynthesis. We do suggest however that plants possess an alternative means of collecting information, in the form of light, which may be contributing to observed changes in electrical potential.

An additional hypothesis as to the mechanism by which light may be interacting with the plant in a significant manner with respect to changes in electrical potential is through the interaction of phytochromes. Newman and Briggs (1971) demonstrated that potential differences of varying intensities could be elicited when plants were exposed to incident light within the red and far red spectrums and whose action was mediated through phytochrome activity. Furthermore, Yanovsky *et al*. (1997) and Kircher *et al*. (2012) observed differential responses in the phytochrome subunits when exposed to low intensities of red and far-red incident light. We suggest this as a possible mechanism of interaction as the applied light intensity is remarkably smaller than daylight or the intensity of light required for photosynthesis. Arguments for the latter mechanism are supported by the spectral power distribution of incident light whose peaks were in the red and far red spectrum (Osram Sylvania, 2000).

2.5.2 Temporal Variation of Senescence Onset

It is suggested that the time-course of this effective change in electrophysiology is associated with the 3rd week of measurement. However, we must be particularly vigilant on the identification of this temporal phenomenon as the change in the local environmental variables (change in season) peaked around this time. One particular argument in support of an actual change in physiology associated with the gradual change in the environment is supported by the results obtained from our discriminant analysis. The homogeneity of values obtained from the discriminant function for Weeks 2 and 3 are in good approximation of each other. Taking into consideration both the results obtained from the multiple regression and discriminant analyses, the likely temporal evolution of senescence demonstrates a gradual alteration in the electrophysiological parameters of the plant which peaks around Week 3 and whose changes are evident in Week 4 measures with respect to this particular experiment.

2.5.3 Quantitative Support for Electrophysiological Alterations

We have suggested in this document that chlorophyll is not necessarily responsible for the onset of senescence nor does it have to directly contribute to the underlying changes in electrophysiology of the plant. It is possible to demonstrate measurable changes in electrical potential of plants even though their chlorophyllic content has been compromised. We have suggested that perhaps other biological agents such as structural or enzymatic proteins may be responsible for the generation of voltage-associated changes in whole plant physiology. However, an alternative hypothesis suggests that the observed changes in electrical potential may arise from physical sources related to, or generated by, changes in the inherent electric and magnetic properties of the plant in response to light (electromagnetic radiation).

The electric field can be calculated by dividing the voltage by a distance. Here, if we assume that the change in voltage is in the order of millivolts over a linear distance of 20 cm (the distance between measuring sensors), the resultant electric field would be in the order of 10^{-2}V·m^{-1}. Using Maxwell's equation for the scalar field component ($\nabla \cdot E = \rho/\varepsilon$) where ρ is the charge density, ε is the permittivity of free space, E is the electric field and ∇ is a vector, and assuming that the magnitude of the scalar component is maximized (∇ = 1) and radiates isotropically, we can re-arrange the equation to find the charge density (ρ) which would yield a solution whose value would approach $8.85 \cdot 10^{-14}$ As·m^{-2}. If we multiply the charge density $8.85 \cdot 10^{-14}$ As·m^{-2} by a frequency (s^{-1}), we would get a current density J (A·m^{-2}). In this case we will assume that 10 Hz as a fundamental frequency for plant cell activity, derived from the range of conduction velocities (a mean between 1 and 100 Hz) from Masi *et al*. (2009) and Fell and Zimmerman (2007), the resultant value would be in the order of $8.85 \cdot 10^{-13}$A·m^{-2}.

Now, if we take Maxwell's magnetic field equation $\nabla x\, B = \mu(J + \varepsilon \frac{\delta E}{\delta t})$ and substitute the values of current density (J = $8.85 \cdot 10^{-13}$A·m^{-2}), μ ($1.26 \cdot 10^{-6}$ N·A^{-2}) the permeability of free space, ε ($8.85 \cdot 10^{-12}$ C^2·N^{-1}m^{-2}) the permittivity of free space and the value of $1.0 \cdot 10^{-2}$V/m for E. Over a period of 30 sec and would approach $1.12 \cdot 10^{-18}$ kg·A^{-1}s-^{2}, where 30 sec was chosen based off of conduction velocity parameters ranges (seconds to minutes) and reflects a mean value for this distribution. Furthermore, the onset of voltage changes, as measured in this experiment, demonstrate a 30 sec delay of onset before these changes were qualitatively different in raw recordings. We assume, as well, that the maximum intensities derived from this calculation is approximated when the operator,∇, is set to unity (1). We also consider that due to the changing nature of these fields these maxima occur transiently but contribute to the dynamic nature of observed plant potentials.

If we multiply the intensity of the magnetic field by the product of the magnetic diffusivity and the current density we would yield a $kg \cdot s^{-3}$. Here the magnetic diffusivity is the result of $1/\mu\sigma$, where $\mu = 1.26 \cdot 10^{-6}\ N \cdot A^{-2}$ and the conductivity (σ) is $5.0 \cdot 10^{-3}\ kg^{-1} \cdot m^{-3} \cdot s^{3} \cdot A^{2}$ for plants (Simpson and TenWolde, 1999), ranging between $1.08 \cdot 10^{-5}$ to $1.14 \cdot 10^{-2}\ kg^{-1} \cdot m^{-3} \cdot s^{3} \cdot A^{2}$ depending on the tissue and plant type (Stiles and Jörgensen, 1914), resulting in a value of $1.59 \cdot 10^{8} m^{2} s^{-1}$. The product of the current density ($8.85 \cdot 10^{-13} A \cdot m^{-2}$) and the magnetic diffusivity ($1.59 \cdot 10^{8} m^{2} s^{-1}$) results in a value of $1.41 \cdot 10^{-4} As^{-1}$. If we multiply this value by the magnetic field strength $1.12 \cdot 10^{-18}\ kg \cdot A^{-1} s^{-2}$ we would get a value of $1.58 \cdot 10^{-22} kg \cdot s^{-3}$. Assuming the lower limit of time necessary for a plant to demonstrate a change in voltage, which would approximate a duration in the order of a second (1 second) as derived from conduction velocities, the result would be $1.58 \cdot 10^{-22} J \cdot m^{-2}$. If we divide the energy density by $2.0 \cdot 10^{-20} J$ we would get a value of $1.274 \cdot 10^{2} m^{2}$. Given that plant cells have a surface area of $1.0 \cdot 10^{-8} m^{2}$, the total number of cells that would be affected by this millivolt equivalent depolarization would be in the order of 10^{10}.

Now, if we examine the static electric field component where $\nabla \times E = -\frac{\delta B}{\delta t}$ of a given plant operating at -300 mV to 500 mV (daily observations) over 20 cm, the resultant electric field strength would be 1.5 to 2.5 $kg \cdot A^{-1} s^{-3}$, assuming that ∇ is set to 1. If we take the charge density of $8.85 \cdot 10^{-14}\ As \cdot m^{-2}$ and multiply by $1.59 \cdot 10^{8} m^{2} s^{-1}$ we would produce a current of $1.41 \cdot 10^{-5} A$. The product of the changing magnetic field 1.5 $kg \cdot A^{-1} s^{-3}$ and the current $1.41 \cdot 10^{-5} A$ results in a value of $2.12 \cdot 10^{-5}\ Wm^{-2}$. Assuming again that this change occurs over a period of 1 second, defined by the lower limit of the time component for the onset of voltage changes based on conduction velocities, the value would equal $2.12 \cdot 10^{-5}\ Jm^{-2}$, where dividing this value by the fundamental quantum value of $10^{-20} J$ gives you a value of $10^{-15}\ m^{2}$, whose equivalent linear distance would be in the order of $3.16 \cdot 10^{-8} m$, or the approximated value of the thickness of the

cell membrane (Hine, 1989). Regardless of the change in the magnitude of the static potential difference, be it either ± 300 to ± 500 mV (daily observations), the only change would be found in the coefficients and not the magnitude of the relationship. It should be noted that the polarity of the static electric field component only changes the direction of the magnetic field.

We can further relate the electric field strength to a change in the polarity along this axis. Consequently the change in energy can be calculated as the product of the change in potential and the fundamental unit charge ($1.6 \cdot 10^{-19}$ As), for which a millivolt change is equivalent to $1.6 \cdot 10^{-22}$ J. What is interesting however is that there is usually a change in polarity (dipole moment) with the application of light (data presented as daily observations). Here the change in the dipole moment (Ams) can be calculated as the change in energy divided by the change in electric field strength (J / V·m^{-1}). The change in dipole moment derived from a change in energy of $1.6 \cdot 10^{-22}$ J and a change in electric field strength of $1.0 \cdot 10^{-2}$ V·m^{-1} is in the order of $1.6 \cdot 10^{-20}$Ams. The equivalence of a change of dipole moment whose magnitude is 10^{-20} Ams is essentially the distribution of one charge over the distance between sensors. The change in dipole moment, equivalent to a single charge along the 20 cm separation between sensors, may suggest one of two things: 1) a change in dipole moment equivalent to the movement of a single charge may be considered as the same as the movement of electrons traveling through a conducting material at drift velocity, and 2) the change in dipole moment may reflect a threshold of a number of cells that are required to elicit a generalized response. In order to examine the nature of the latter idea we investigate the relative change in magnetic moment that accompanies our millivolt depolarization.

The magnetic moment is related to the change in electric field strength by resistivity and conductivity, the latter of which is the reciprocal of the former. To calculate resistivity, and

consequently the conductivity, we must first calculate the net charge per area. If we take the threshold of stimulation to be 25 lux or the equivalent of $3.75 \cdot 10^{-2}$ $W \cdot m^{-2}$ and the net change in potential difference to be $1.0 \cdot 10^{-3}$V, the reciprocal of the charge per area would be the quotient of the voltage and the power density whose resultant value is in the order of $2.67 \cdot 10^{-2}$ $m^2 \cdot A^{-1}$. To calculate the resistivity we would simply multiply the electric field strength ($1.0 \cdot 10^{-2}$ $V \cdot m^{-1}$) and the reciprocal of the charge per area $2.67 \cdot 10^{-2}$ $m^2 \cdot A^{-1}$ whose value would approach $2.67 \cdot 10^{-4} \Omega \cdot m$. This resistivity, or its reciprocal conductivity, can be inserted in to the equation for magnetic diffusivity which is defined as $\eta = 1/(\sigma \cdot \mu)$, where η is the magnetic diffusivity, μ is the permeability of free space ($1.256 \cdot 10^{-6}$ $N \cdot A^{-2}$) and σ is the conductivity ($3.75 \cdot 10^{3}$ $A^2 s^3 \cdot kg^{-1} m^{-2}$). The resultant magnetic diffusivity would be $2.126 \cdot 10^{2} m^2 s^{-1}$. The magnetic moment can then be calculated through the operation of multiplying the unit charge ($1.602 \cdot 10^{-19}$As) and the magnetic diffusivity ($2.126 \cdot 10^{2} m^2 s^{-1}$) which approaches $3.40 \cdot 10^{-17}$ $A \cdot m^2$. We can calculate the total number of charges associated with the calculated change in magnetic moment by dividing the calculated change in magnetic moment by the magnetic moment of an electron ($9.28476 \cdot 10^{-24}$ $A \cdot m^2$). The total number of charges that can be affected by this change in magnetic moment would be approximately $3.67 \cdot 10^{6}$ charges, which converge on the number of charges required to generate the resting membrane potential in cells (Persinger, 2014). This may lend credence to the idea that the entire system is reflected in the sum of its parts and that a single component can affect the whole (Mach, 1887, Persinger, 2012).

From our results, it is suggested that there exists a finite limit of incident radiation which can preferentially alter the electrodynamic properties of sedge plants undergoing senescence in response to light. Here we describe the finite limit for the elicitation of voltage changes to be in the range of ~20 lux. A potential explanation for this limit is explored as the necessary threshold

to attain quantum-cell equivalence. The incident radiation of ~20 lux would have a corresponding power density in the order of $3.0 \cdot 10^{-2}$ W/m^2. In order to convert a power density to an energy density we would simply have to multiply by a time, or conversely divide by a frequency. Assuming that temporal component of the emitted light is $3.0 \cdot 10^{12}$ Hz (the frequency equivalent of $2.0 \cdot 10^{-20}$J) the energy density would be in the order of 10^{-10}J/m^2. If we use $E = mc^2$, where E is the energy, c is the speed of light and m is the rest mass of the photon (10^{-52}kg), the energy equivalent would be in the order of 10^{-36}J and we would be able to extract the number of photon equivalents of this process. The resultant quotient of the energy density of 10^{-10}J/m^2 and the energy of a rest mass photon (10^{-36}J) would be in order 10^{26} photons/m^2. Assuming that the photon equivalent of 10^{-20}J is roughly 10^{16} photons, then the number of quantum units that can be affected by 20 lux is in the order of 10^{10} quanta/m^2. If we were to apply this energy over the surface area of a cell (10^{-10}m^2) we would end up getting 1 quantum/cell. Alternatively, the energy equivalent or information equivalent, if applied over 1 m^2, would be enough to activate 10^{10} cells. This may represent the threshold necessary to re-activate plant photosystems or be the required energy to depolarize the cell and initiate the necessary physiological responses. It is suggested that anything below this threshold would not generate the necessary quanta-cell equivalence.

To further our exploration of the convergence of effects found in the electrophysiological properties of plants let us examine the capacitance associated with light stimulation. Capacitance can be calculated as the quotient of a unit charge divided by a voltage. Given that the unit charge is $1.602 \cdot 10^{-19}$ As and the change in potential difference is $1.0 \cdot 10^{-3}$ kg·m^2·A^{-1}·s^{-3} the resultant capacitance would be in the order of $1.602 \cdot 10^{-16}$ A^2·s^4·kg^{-1}·m-^{2}. If we postulate that the integrity of the resting membrane potential is maintained by 10^6 ions then the total capacitance would be

$8.01 \cdot 10^{-10}$ $A^2 \cdot s^4 \cdot kg^{-1} \cdot m\text{-}^2$. Capacitance is related to energy by the relationship of $E = ½ CV^2$ where E is the energy in Joules, C is the capacitance and V is the voltage. The resultant energy would be $8.01 \cdot 10^{-17}$ J given that the change in voltage is 1.0 mV and the capacitance is $8.01 \cdot 10^{-17}$ $A^2 \cdot s^4 \cdot kg^{-1} \cdot m^{-2}$.

Using the energy calculated in the previous section we can approximate a given wavelength equivalent of a stimulus using the relationship of $E = h \cdot c/\lambda$ where h is Planck's constant ($6.62 \cdot 10^{-34}$ $kg \cdot m^2 \cdot s^{-1}$), c is the speed of light ($3.0 \cdot 10^8 m \cdot s^{-1}$) and λ is the wavelength in meters. Solving for this equation using an energy of $8.01 \cdot 10^{-17}$J provides a wavelength equivalent of $2.50 \cdot 10^{-9}$m. The value of $2.50 \cdot 10^{-9}$m is the equivalent length of approximately 10 water and 10 hydronium ions, converging on the total possible number of water molecules that can be present in an aquaporin channel at a given time (Agre, 2006). The electrophysiological properties of whole plant senescence reflect the microstructural alterations at the level of the cell membrane and the dynamic alteration of the osmotic characteristics at this level. Furthermore, we postulate a cell-quantum equivalent of 1 photon that may be necessary to re-initiate cellular activity and displace the plant's senesced state.

2.6 References :

Agre P. The Aquaporin Water Channels. *Proceedings of the American Thoracic Society*. 2006;3(1):5-13. doi:10.1513/pats.200510-109JH.

Bond, B. J. (2000). Age-related changes in photosynthesis of woody plants. *Trends in plant science*, 5(8), 349-353.

Bleecker AB, Patterson SE. Last exit: senescence, abscission, and meristem arrest in Arabidopsis. *The Plant Cell*. 1997;9(7):1169-1179.

Buchanan-Wollaston, V., Earl, S., Harrison, E., Mathas, E., Navabpour, S., Page, T. and Pink, D. (2003), The molecular analysis of leaf senescence: a genomics approach. *Plant Biotechnology Journal*, 1: 3-22. doi: 10.1046/j.1467-7652.2003.00004.x

Davies, Eric. (2004). New Functions for electrical signals in plants. *New Phytologist* 161:607-610

Dickinson CD, Altabella T, Chrispeels MJ (1991) Slow-growth phenotype of transgenic tomato expressing apoplastic invertase. *Plant Physiol* 95: 420-425.

Ding B, Haudenshield JS, Willmitzer L, Lucas WJ (1993) Correlation between arrested secondary plasmodesmal development and onset of accelerated leaf senescence in yeast acid invertase transgenic tobacco plants. *Plant J* 4: 179-189.

Felle, H. H., & Zimmermann, M. R. (2007). Systemic signalling in barley through action potentials. *Planta*, *226*(1), 203-214.

Fensom, D. S. (1957). The bio-electric potentials of plants and their functional significance: I. An electrokinetic theory of transport. *Canadian Journal of Botany*, *35*(4), 573-582.

Fromm, J., & Lautner, S. (2007). Electrical signals and their physiological significance in plants. *Plant, Cell & Environment*, *30*(3), 249-257.

Gan S, Amasino RM. Making Sense of Senescence (Molecular Genetic Regulation and Manipulation of Leaf Senescence). *Plant Physiology*. 1997; 113(2):313-319.

Gan, S. (2003). Mitotic and postmitotic senescence in plants. *Science's SAGE KE*, 2003(38), 7.

Gurovich, L. A., & Hermosilla, P. (2009). Electric signalling in fruit trees in response to water applications and light–darkness conditions. *Journal of plant physiology*, *166*(3), 290-300.

Havel, L. and Durzan, D.J. (1996), Apoptosis in Plants. *Botanica Acta*, 109: 268- 277. doi: 10.1111/j.1438-8677.1996.tb00573.x

Hensel, L. L., Nelson, M. A., Richmond, T. A., & Bleecker, A. B. (1994). The fate of inflorescence meristems is controlled by developing fruits in Arabidopsis. *Plant Physiology*, *106*(3), 863-876.

Hine, Robert. "Membrane." *The Facts on File Dictionary of Biology. 3rd ed.* New York: Checkmark, 1999:198.

Kircher, S., Bauer, D., Schäfer, E., & Nagy, F. (2012). Intramolecular uncoupling of chromophore photoconversion from structural signaling determinants drive mutant phytochrome B photoreceptor to far-red light perception. *Plant signaling & behavior*, *7*(8), 904-906.

Krol, Elzbieta and Trebacz, Kazimirez. (2000). Ways of Ion Channel Gating in Plant Cells. *Annals of Botany*, 86: 449-469.

Lautner, S., Grams, T. E. E., Matyssek, R., & Fromm, J. (2005). Characteristics of electrical signals in poplar and responses in photosynthesis. *Plant Physiology*, *138*(4), 2200-2209.

Leopold, A. C., Niedergang-Kamien, E., & Janick, J. (1959). Experimental Modification of Plant Senescence. *Plant Physiology*, *34*(5), 570.

Lim, P. O., Kim, H. J., & Gil Nam, H. (2007). Leaf senescence. *Annu. Rev. Plant Biol*., 58, 115-136.

Mach, E. (1887). Mach's Principle. Mach's archive, Deutches Museum, Munich.

Masi, E., Ciszak, M., Stefano, G., Renna, L., Azzarello, E., Pandolfi, C.,... & Mancuso, S. (2009). Spatiotemporal dynamics of the electrical network activity in the root apex. *Proceedings of the National Academy of Sciences*, *106*(10), 4048-4053.

Newman, I. A., & Briggs, W. R. (1972). Phytochrome-mediated electric potential changes in oat seedlings. *Plant physiology*, *50*(6), 687-693.

Osram Sylvania. (2000). Technical Information Bulletin: Light and Plants Standard and wide spectrum SYLVANIA GRO-LUX fluorescent lamps. Danvers, MA. Osram Sylvania

Pfannschmidt, T. (2010). Plastidial retrograde signalling–a true "plastid factor" or just metabolite signatures?. *Trends in plant science*, *15*(8), 427-435.

Persinger, M.A., Lavalee, C.L. (2012) The Σn = n concept and the quantitative support for the cerebral-holographic and electromagnetic configurations of consciousness. *J Conscious Studies* 19:128–153

Persinger, M. A. (2014). Astronomical, chemical, and biological implications of 10-20 joules as a fundamental quantum unit of information for neurofunction. *Archives of Neuroscience*, *1*(3).

Pogson, B. J., Woo, N. S., Förster, B., & Small, I. D. (2008). Plastid signalling to the nucleus and beyond. *Trends in plant science*, *13*(11), 602-609.

Rolland, F., Baena-Gonzalez, E., & Sheen, J. (2006). Sugar sensing and signaling in plants: conserved and novel mechanisms. *Annu. Rev. Plant Biol.*, 57, 675-709.

Ryser, P., & Kamminga, A. T. (2009). Root survival of six cool-temperate wetland graminoids in autumn and early winter. *Plant Ecology & Diversity*, *2*(1), 27-35.

Simpson, W., & TenWolde, A. (1999). Physical properties and moisture relations of wood.

Stiles, W., & Jörgensen, I. (1914). The Measurement of electrical conductivity as a method of investigation in plant physiology. *New Phytologist*, *13*(6-7), 226-242.

Szechyńska-Hebda, M., Kruk, J., Górecka, M., Karpińska, B., & Karpiński, S. (2010). Evidence for light wavelength-specific photoelectrophysiological signaling and memory of excess light episodes in Arabidopsis. *The Plant Cell*, *22*(7), 2201-2218.

Szechyńska-Hebda, M., & Karpiński, S. (2013). Light intensity-dependent retrograde signalling in higher plants. *Journal of plant physiology*, *170*(17), 1501-1516.

Thomas, H. and Donnison, I. (2000) Back from the brink: plant senescence and its reversibility. In: Programmed Cell Death in Animals and Plants (Bryant, J.A., Hughes, S.G. and Garland, J.M., eds), pp. 149-162. Oxford: Bios.

Whitmarsh, J. (2004). Photosynthetic energy transduction. In A. S. Raghavendra (Ed.), *Photosynthesis: a comprehensive treatise*. Cambridge University Press Cambridge.

Yanovsky, M., Casal, J., & Luppi, J. (1997). The VLF loci, polymorphic between ecotypes landsberg erecta and Columbia, dissect two branches of phytochrome A signal transduction that correspond to very-low-fluence and high-irradiance responses. *The Plant Journal*, *12*(3), 659-667.

Zavaleta-Mancera, H.A., Thomas, B.J., Thomas, H. and Scott, I.M. (1999) Regreening of senescent Nicotiana leaves. II. Redifferentiation of plastids. *J. Exp. Bot.* 50, 1683-1689.

Zimmermann, M. R., Maischak, H., Mithöfer, A., Boland, W., & Felle, H. H. (2009). System potentials, a novel electrical long-distance apoplastic signal in plants, induced by wounding. *Plant Physiology*, *149*(3), 1593-1600.

Chapter 3

3 Experimental Trans-Species Excess Correlation

3.1 Abstract

Experimental evidence of entanglement and entanglement-like phenomena has been increasing steadily in the last decade. One example of entanglement phenomena is referred to as excess correlation (XSC), where there is a relative increase in the strength of a relationship between two spatially isolated locations. The Dotta-Persinger method for eliciting XSC employs identical electromagnetic field (EMF) applications at both local and non-local sites to homogenize the spaces, and timed injections of hydrogen peroxide at the local site. We observed the responses in electrical potential from two different species – *Glycine max* and *Escherichia coli* – with each species alternatively acting as both local and non-local sources. Using EMFs with 3 msec point durations led to an enhancement of the correlation strength compared to controls, but reversed the direction of the correlations. 1 msec point durations also enhanced the correlation strengths but without the directional change. The strength of the correlation also differed dependent on which species received the peroxide injections (local site). Taken together, these results suggest that XSC phenomena can occur between two different species, and is further confirmation that the application of identical electromagnetic fields at two spatially isolated spaces essentially unifies the locations.

3.2 Introduction

The superposition of space-time frames upon separate systems can result in the generation of spooky events that are not necessarily reflective of the causal nature of temporal relationships.

This "spooky action at a distance" was first coined by Einstein, and is expressed as the phenomenon of entanglement (Einstein *et al*., 1935). The nature of this effect can be likened to the simultaneous application of a stimulus at two locations, but where only one location actually receives any stimuli. However, the spatial separation between sites implies that the spaces be treated as a unitary location (same space) (Persinger and Dotta, 2011). Consequently, a change in the behaviour of one site results in a net change of opposite polarity and exact magnitude in the other site (Hoffman *et al*., 2012; Hill and Wooters, 1997). Under the appropriate application of rotating magnetic fields, it is possible to demonstrate a simultaneous doubling in photon emission from spatially separated chemical reactions (Dotta and Persinger, 2012). The result of increased spatio-temporal coherence, as measured by changes in the degree of photon emission, can be inferred as a measure of the degree of relatedness between systems. This entanglement-like process has been coined "excess correlation", the term arising from the relative increase in the strength of the relationship between spatially isolated sites (Bennet and DiVincenzio, 2000).

To date, several experiments have studied the operational extent of excess correlation, through examining changes in the amount of photon emissions (Dotta and Persinger, 2012), the degree of shared alterations in pH measures (Dotta *et al*., 2013; Rouleau and Carniello, 2014) and shared quantitative measures of the brain's electrical activity (Dotta *et al*. 2009; Dotta *et al*., 2011; Burke *et al*. 2011). Corroborated findings from all of these experiments determined an effective temporal window for maximizing the effects of excess correlation. Tandem exposure to effective bulk decelerating, immediately followed by accelerating, electromagnetic field configurations demonstrated an enhancement in the correlation between spatially isolated systems. The effective temporal window for maximizing the excess correlation, denoted as the enhancement of correlation strengths between spatially isolated systems, occurs between 7 and 8

min after the initiation of the accelerating (second) field. Thus, the effective temporal dispersion between 7 and 8 min will be examined extensively in this experiment.

However, these experiments have been predicated on the structural homology of the separated systems. A current knowledge limitation persists regarding the potential applications of excess correlation, as the functional extent is entirely based upon the shared geometry of the interacting centers. That is, one can only influence X-matter when X-matter is present at both local and non-local centers, where the terms local and non-local refer to areas receiving direct stimulation (local) or no stimulation (non-local). Ergo, the presupposition of entanglement-like phenomena relies on substance or spatial organization.

Structure - at least the aspect of ordered, discrete units - is strictly related to the occupancy of matter. Matter results in substance, a tangible construction of geometries, and a form of structure resulting in spatial organization. Conversely, structure can exhibit time-like qualities that do not change drastically from one measure to the next resulting in a process. Processes form a temporal pseudo-structure that is the transient organization of underlying activity. Transient organization of any process creates a fluid order that does not necessarily, directly or indirectly, result in a change in the overall spatial structure of the substance. Thus *temporal structure* can be defined as a process by which a measurable change can be elicited in a material without the decomposition of the original spatial organization.

If a requirement of excess correlation is structure, then temporal structure common to both distinct spatial organizations (material, species, *etc*.) should be an equal candidate for this type of investigation. The purpose of this experiment was to examine whether differences in structure can still appreciably demonstrate excess correlation between spatially separated systems. We

have utilized two unique species (plants and bacteria) in order to investigate whether structure is a requirement for excess correlation.

For our application the most probable process to be considered as a candidate for the application and generation of temporal homogeneity is the reaction of plants and bacteria to hydrogen peroxide. Hydrogen peroxide undergoes a radical cleavage to form the radical version of hydroxide ions (Inoue and Kawanishi, 1987; Floyd and Lewis, 1983). The increase in available free radicals can accrue large amounts of damage to DNA, mitochondria, cellular pathways and cell integrity (Yakes, and Van Houten, 1997; Richter *et al*., 1988). Furthermore, sufficient DNA damage can elicit SOS mechanisms and ultimately, given the appropriate concentrations, may result in apoptosis and/or necrosis (Slater *et al*., 1996; Gallucci and Matzinger, 2001). These processes are common to both plants and bacteria (Levine *et al*., 1994; Hassett *et al*., 1987) resulting in a homogenous source of variance. The homogeneity of processes between these two species should allow for the transient elicitation of the excess correlation effect.

3.3 Methods

3.3.1 Specimen:

Bacterial cultures of *Escherichia coli* (11303) were obtained from the American Type Culture Collection (ATCC), Manassas, VA, USA. Bacteria were sub-cultured from a stock plate and inoculated in 10 mL of nutrient broth media (Oxoid CM00001) for 24 h at 37ºC to a final cellular concentration of 10^8 to 10^9 cells/mL. Plant species consisted of *Glycine max* (soybean) seeds that were imbibed on moistened filter paper for approximately 3-5 d before testing. All seedlings were subjected to 14 f of continuous light stimulation and provided with 1-2 mL of

water per day. All plant specimens were purchased from Stokes Seeds Canada and were not genetically modified.

3.3.2 Measurement and Sensor Placement:

Measurements of DC (direct current) potential differences were simultaneously recorded from both *G. max* samples and *E. coli* cultures. DC potential difference was recorded by two separate digital multimeter units (Victor 70C) that sampled once every 5 sec with an uncertainty of ± 0.1 mV. Data from the mulimeters were recorded with two laptops: a Lenovo ThinkPad Y580 and a Samsung Notebook model NP550P5C. The combination of computers and their associated multimeters did not differ between trials. The individual multimeters possess internal time-keeping functions that are synchronized and any delays subject to the individual port times of the laptops are negligible.

Sensor placement for plant specimens consisted of small circuit connectors implanted directly into the seedlings. The free ends of the circuit connectors were connected to alligator clips on the anode and cathode of the multimeter. The implanted sensors were placed at the distal end (apex) of the seedling and was considered the reference (negative) lead. The measuring sensor (positive lead) was implanted into the initial germinative site of the root (the root protrusion). The seedlings were suspended in 6 mL of distilled water and placed in a 10 cm cell culture dish. A volume of 6 mL of distilled water was selected as the minimum required volume to accommodate complete coverage of the bottom of the culture dish.

Bacterial broth cultures (10 mL nutrient broth) were similarly suspended in 10 cm culture dishes where bacterial sensors were constructed by stripping approximately 2.5 cm off of the ends of 10 gauge insulated electrical wire. One end of electrical wire was submerged into the culture dish whilst the other end was attached to the positive and negative leads of the digital

multimeter. The separation between the two sensors in the culture solution was approximately 2 cm. Composition of the insulated wire was non-braided (solid), double stranded copper.

3.3.3 Elicitation of Excess Correlation:

Both *G. max* and *E.coli* were subjected to a specific application geometry of angular accelerating or decelerating fields with fixed point durations. The selected point durations were 3 and 1 msec points in accordance with previous research (Rouleau *et al*., 2014). The modulation of the angular component was accommodated by changing the duration of the inter-stimulus delay. Decelerating angular velocity was modulated by serially increasing the duration of the inter-stimulus delay by 2 msec from an initial duration of 20 msec to a final duration of 32 msec. Conversely, the accommodation of accelerating angular velocity was produced by serially decreasing the inter-stimulus delay by 2 msec from an initial duration of 20 msec to a final inter-stimulus delay of 8 msec. Both accelerating and decelerating angular velocities were continuously looped for their entire exposure duration (Rouleau *et al*., 2014). A visual representation of the order of the fields, their associated point durations and the constructs of the local and non-local sources are presented in Table 3.1.

Table 3.1: The identification of the experimental parameters with appropriate point durations and accelerating/decelerating rotating magnetic field configurations.

Local Species	Orientation	Point Duration (msec)	Field 1	Field 2
***E.coli* (bacteria)**	SHAM		----------	----------
***G. max* (plant)**			----------	----------
***E.coli* (bacteria)**	Forward	1 and 3	Decelerating	Accelerating
***G. max* (plant)**		1 and 3	Angular Velocity	Angular Velocity
***E.coli* (bacteria)**	Reversal	1 and 3	Accelerating	Decelerating
***G. max* (plant)**		1 and 3	Angular Velocity	Angular Velocity

An Arduino Uno microcontroller was utilized for the generation of angular accelerating and decelerating fields. The microcontroller altered the voltage supplied through two toroids, constructed using 14 gauge single stranded insulated stereo wire, to produce the electromagnetic field. The wire was wrapped 216 times around a plastic 10 inch crochet hoop purchased from a local crafts store. The Arduino microcontroller was attached to a circuit board which interfaced with the toroids and all field parameters were written in the associated Arduino programming software. Presence of field applications were verified using an AC milliGauss meter (model UHS, AlphaLabs, Inc USA) measuring tri-axial fluctuations in applied field intensities. When either the accelerating or decelerating angular velocity fields were presented there was a shift in background intensities of 3 nT. Specimens were placed in the center of the toroid in all conditions. A visual representation of the experimental set-up is presented in Figure 3.1.

All specimens were exposed to three conditions: Sham, Forward, and Reversal. Sham conditions consisted of the experimental paradigm being run as outlined, with the exception that the equipment was kept off for both specimens. Forward field presentations consisted of 6 min of

the decelerating angular velocity field followed immediately by 12 min of the accelerating angular velocity field. Conversely, the reverse field presentations consisted of 6 min of an accelerating angular velocity field followed immediately by 12 min of the decelerating angular field. Furthermore, 2 min pre-field exposure measures were also taken in all application geometries for a total experiment duration of 20 min. Sham, Forward and Reversed field presentations were presented for both 3 and 1 msec point durations which were selected as they overlap with calculated values associated with proton and electron dynamics (Persinger and Koren, 2007).

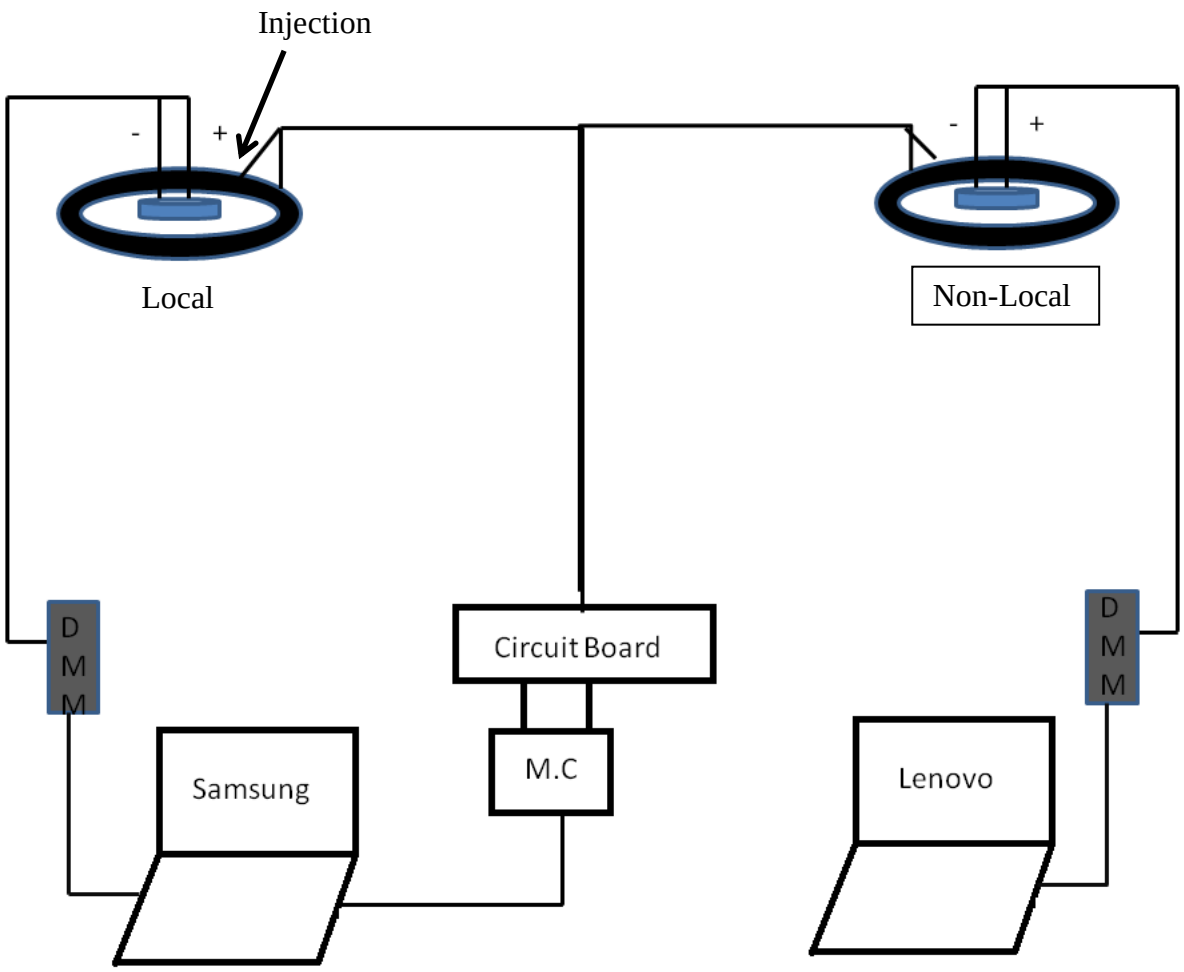

Figure 3.1: A diagrammatic representation of the experimental apparatus. Abbreviations are as follows DMM: digital multimeter, M.C: microcontroller.

In accordance with past evaluations of the excess correlation phenomenon, the introduction of a *process* was utilized in order to demonstrate dynamic alterations in DC profiles of the separate species. Here the process was the direct injection of 50 μL of 3% hydrogen peroxide purchased from a local pharmacy. Injections occurred at min 4, 7 and every min until min 15 into the initiation of the applied fields. Selection of hydrogen peroxide was based on the shared reactive oxygen species (ROS) response mechanisms of the distinct species and the notion of electron movement associated with the classical mechanics of electrical potential difference. The injection site, which consisted of one species, was considered the local site whilst the site and species that did not receive a direct injection of 3% hydrogen peroxide was considered the non-local site. In this design both plant and bacterial species served as alternating local and non-local sites. Rotations of the local and non-local species were conducted in order to identify the directionality of the efficacy of the elicitation of excess correlation.

3.3.4 Statistical Methods:

All data was collected using the software associated with the digital multimeter measuring devices and exported into SPSS v.17 statistical software for analysis. Data was subjected to a series of linear and non-linear curve fitting equations of which the cubic regression demonstrated the best fit for all cases (adj. R^2 =.146$\leq$ X $\leq$1.00, p<.05). From these analyses all data were cubically detrended to reduce the variability associated with time and the residuals were saved. Subsequent to detrending, residuals were standardized before further analyses were conducted. The resultant standardized residuals were used to compute Stouffer's composite Z-scores using Equation 3.1 to assess overall group effects between point durations and field presentation parameters over successive trials. That is to say the composite Z-score was

computed in order to determine net field effects irrespective of the potential influences of the local species.

$$\text{Equation 3.1: } Z_c = \sum Z/\sqrt{n}$$

Where Z_c is the cumulative/composite Z-score, Z is the Z-score for the individual trial and n is the number of trials.

Data were subdivided into four specific time bins (with their duration in brackets) and are identified as baseline (2 min), Field 1 (6 min after initiation of the first field presentation), Field 2A (the first 8 min of the second field) and Field 2B (the last 4 min of the second field). Construction of these temporal windows was used to identify specific instances in the excess correlation design where the effects were generally demonstrable. Partial correlation coefficients between local and non-local sites controlling for time were employed to examine the effects of the field presentations. Furthermore, standard error measures for each of the specific time bins were estimated for all composite scores by applying Wquation 3.2.

$$\text{Equation 3.2: } SE = \sqrt{\left((1 - r^2)/(n - 2)\right)}$$

Where r is the correlation coefficient and n is the number of points in the distribution being assessed.

3.3.5 Geomagnetic Data Extraction:

The weak intensities of the applied fields in these experiments show marked overlap with background fluctuations in the strength of the geomagnetic field. Thus, we examined the potential synergistic nature of the combination of planetary geomagnetic perturbations on local applied magnetic fields. Data for planetary magnetic field measures were extracted from the Space Weather Prediction Center's online database (ftp://ftp.swpc.noaa.gov/pub/indices/old_indices/) for the day of testing as well as three days before and after a particular experiment. All data were entered into SPSS for further parametric

and non-parametric testing. Data for the magnitude of the correlation coefficient for the first 8 min of the second field were computed for each individual trial.

3.4 Results:

3.4.1 Electrophysiology of Excess Correlation:

An example of the raw electrical potential dynamics between bacteria and plants has been presented in Figure 3.2. This demonstrates a conspicuous association between the changes in electrical potential of both the local and non-local sites. Examining the non-specific effects of the applied magnetic fields on the inter-relatedness between local and non-local sites reveals an overall effective trend associated with the combination of 3 msec point durations in the forward geometry ($z = 12.51$, $p < .001$, Figure 3.3). All other values demonstrated significantly ($p < .05$) weaker partial correlation coefficients when compared to controls.

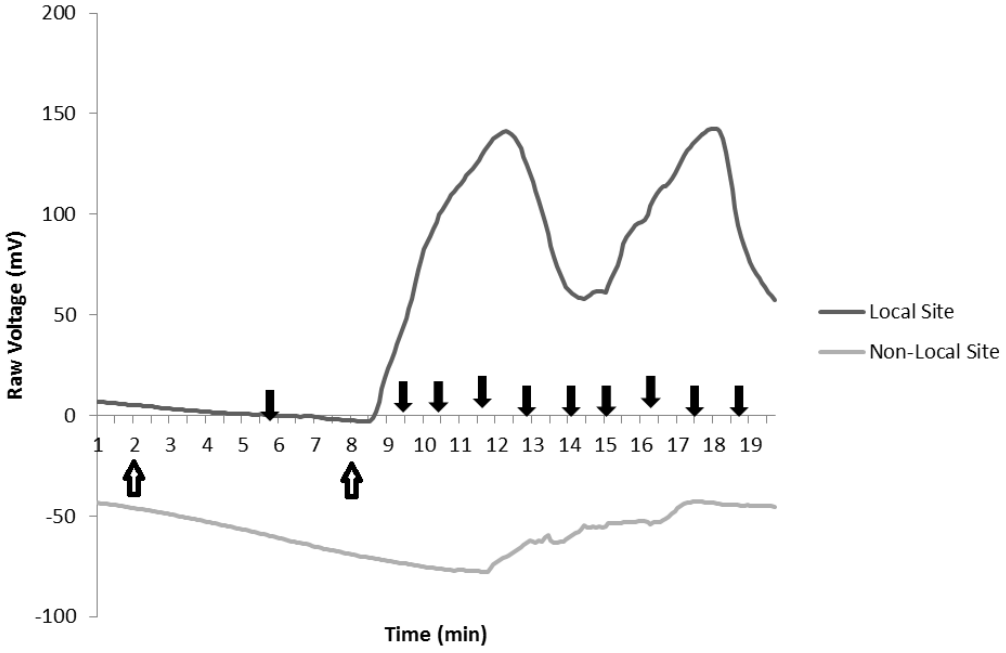

Figure 3.2: An example of the raw electrophysiological profile of local and non-local interactions. Downward arrows demonstrate when injections were made, and upward facing arrows denote when the fields were applied.

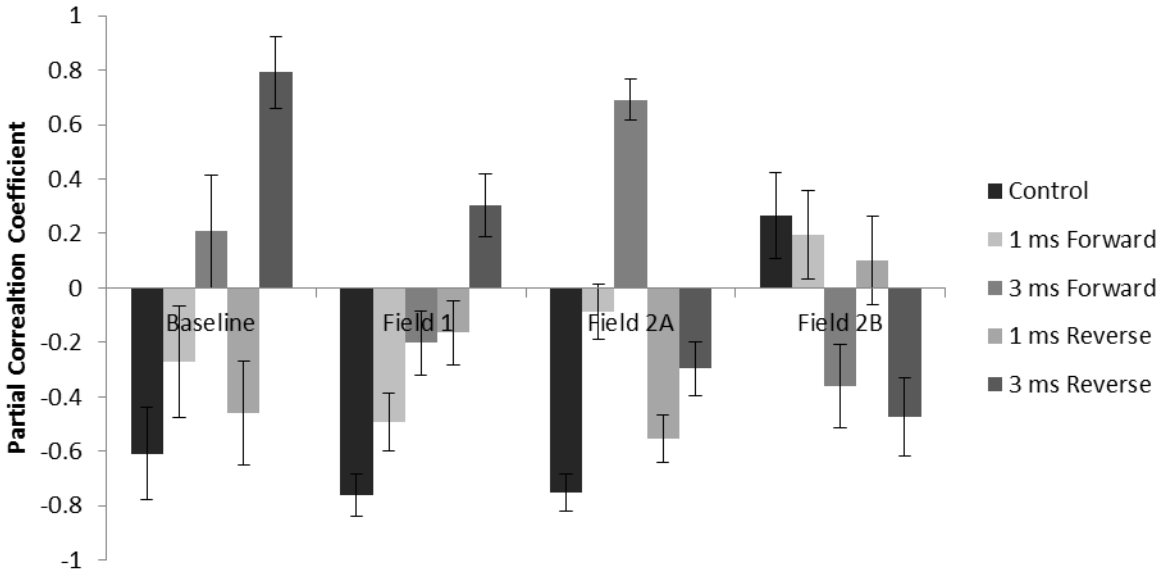

Figure 3.3: The non-specific effects of the applied magnetic field conditions on the degree of correlation between local and non-local sites. Error bars represent calculated standard error measures.

Further analysis of group effects were conducted in order to effectively assess the influence of local species type on the efficacy for eliciting excess correlation. The resultant Stouffer's composite Z-scores produced values for the orientation of the local and non-local species. Pearson correlation coefficients were computed for local and non-local sites during baseline, Field 1, Field 2A and Field 2B conditions. All resulting correlation coefficients were used to estimate the standard error of the relationship during the predefined temporal windows using Equation 3.2.

In order to demonstrate excess correlation effects between species, comparisons between the different fields of matched local species were conducted; i.e. control cases where bacteria had received an injection in the absence of magnetic fields were compared to cases where bacteria had received an injection of hydrogen peroxide in the presence of fields. A comparison between bacteria as the local source (i.e. receiving a series of injections of 3% hydrogen peroxide) subjected to the application of 3 and 1 msec point durations with the forward and reverse field

geometries is presented in Figure 3.4. Similarly, the comparisons between plants as the local source and the direction of field application (forward and reversed) and point durations (1 and 3 msec) are presented in Figure 3.5. These were the only conditions which demonstrated a conspicuous excess correlation-type phenomenon.

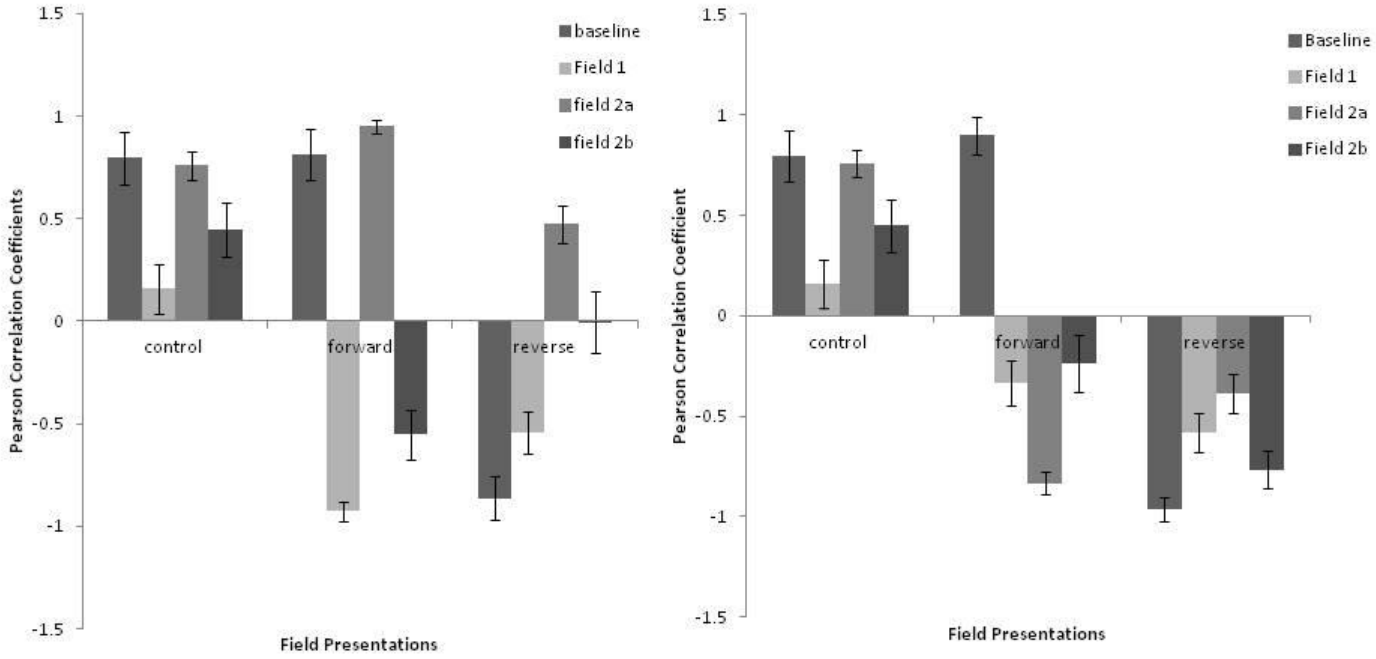

Figure 3.4: The nature of the effects on bacteria as a local source is demonstrated in the left (A) and right (B) graphs. The general trends represent the application of the different field geometries for both 1 (A) and 3 (B) msec respectively. Error bars represent the estimated standard error of the correlation.

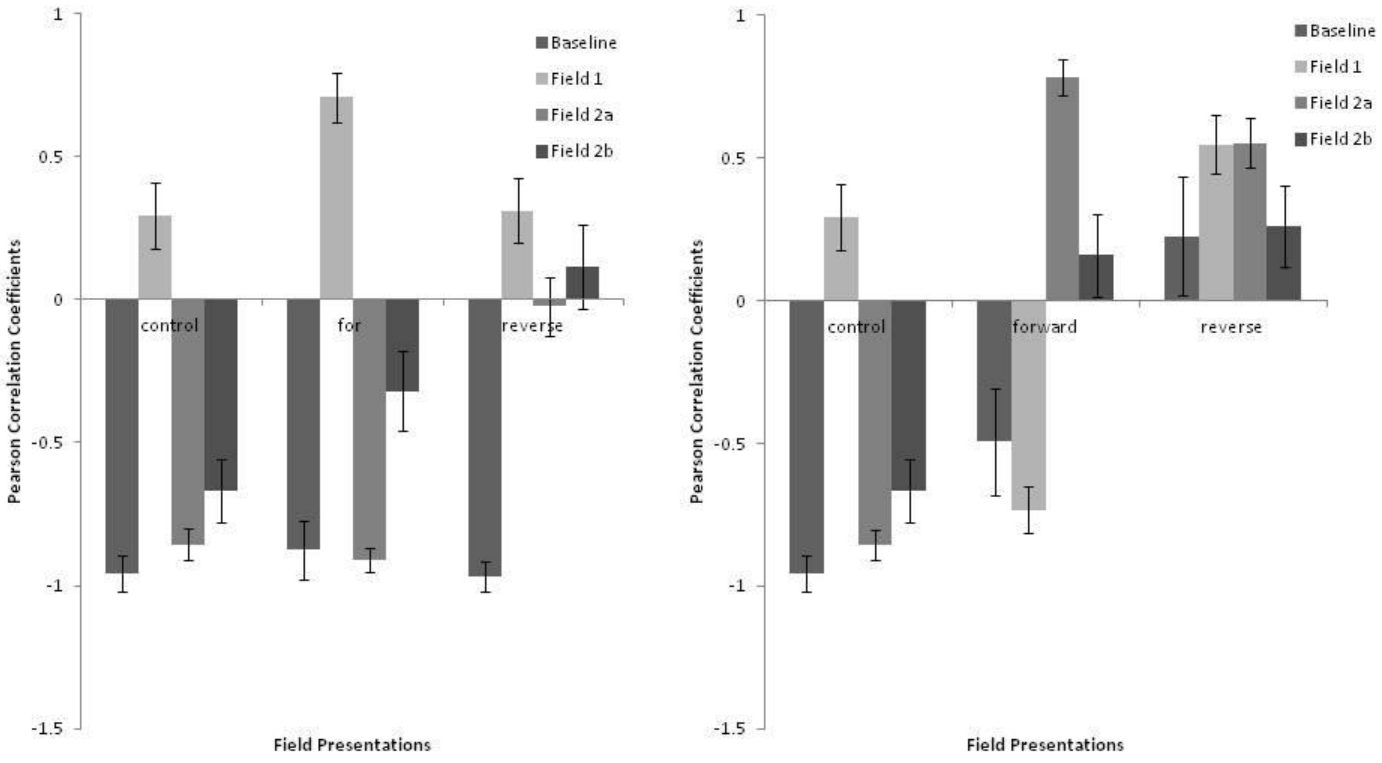

Figure 3.5: : The nature of the effects on PLANTS as a local source is demonstrated in the left (A) and right (B) graphs. The general trends represent the application of the different field geometries for both 1 (A) and 3 (B) msec respectively. Error bars represent the estimated standard error of the correlation.

Comparisons for the first 8 min of the second field application were conducted between each of the different combinations of species, point durations and field application order. Significant differences in the strength of correlations between controls and field exposed groups were assessed using Fisher's r-to-z transformation (Equation 3.3) and subsequent Z-score comparisons. For simplicity all statistical results are presented in Table 3.2.

$$\text{Equation 3.3: } Z = 0.5 \cdot \ln(1+r/1-r)$$

Where *Z* is the Fisher's Z-score value and *r* is the correlation coefficient you are converting.

Table 3.2: Presentation of the differences in the magnitude of the correlation coefficients as a function of species, field presentation and point duration. All values presented here are compared to controls of the same species during the first 8 minutes of the second field. The sign of the z statistic denotes the direction of the interaction as the computation performed was as such that the value of the field exposed groups were subtracted from the values obtained in sham conditions.

Local Species	**Field Presentation**	**Point Duration**	**Pearson r**	**Z statistic**	**p**
***E. coli* (bacteria)**		3 msec	-.835	-15.05	<.001
	Excess	1 msec	.949	5.69	<.001
***G. max* (plant)**	Correlation	3 msec	.784	-16	<.001
		1msec	-.912	-1.79	.074
***E. coli* (bacteria)**		3 msec	-.387	-9.6	<.001
	Reversal /	1 msec	.474	-3.37	<.01
***G. max* (plant)**	Inverted	3 msec	.553	4.49	<.001
		1 msec	-.024	8.6	<.001

3.4.2 Relationship between geomagnetic fluctuations and Excess Correlation:

Results of parametric and non-parametric correlational analyses demonstrated no relationship between the magnitude of the correlation coefficient for either excess correlation or reversed field presentations. This null relationship remained even when one accommodated for point duration of effective and non-effective fields. However, strong positive relationships between sham conditions and geomagnetic activity 2 ($r = .875$, $p < .05$, rho $= .829$, $p < .05$) and 3 ($r = .938$, $p < .01$, rho $= .899$, $p < .05$) days before testing were identified. This may suggest the possibility of excess correlation like results (i.e. strong relationships) on days where there was no field presented.

3.5 Discussion:

Of primary concern is the heightened strength of the association with respect to the control conditions. One hypothesis posits that the effects demonstrated may be the result of a unique resonant feature with geomagnetic fluctuations. Our analyses support this claim by demonstrating strong associations between the magnitude of parametric and nonparametric correlation coefficients of control conditions and planetary geomagnetic activity 2 and 3 days before testing. However, while examining the effective relationship between planetary geomagnetic activity and days in which fields were applied no significant correlations were found, similar to previous results with respect to psi and haunt phenomenon (Krippner, 1996; Persinger, 1985; Persigner *et al*., 2002; Roll and Persinger, 2001). This implies the possibility that the geomagnetic field proper may in fact contribute to spurious excess correlation events that cannot be accounted for given the temporal latency between heightened geomagnetic activity and the observation a given event.

We have successfully demonstrated that under the appropriate conditions the modulation of the electrodynamic properties (i.e. the dynamic alteration in potential difference as a function of time) of a given species can affect another species even though they are separated in both space and phylogenetic progression. Visual inspection of the graphs reveals a general trend associated with the effective 3 and 1 msec point durations for both plant and bacteria. Specifically, the 1 msec point durations fields resulted in an enhancement in magnitude of the correlation coefficient without a reversal in direction whereas the 3 msec point durations resulted in a magnitude enhancement and a reversal in direction. These effects are consistent with previous research using both similar (Rouleau and Carniello, 2014) and different (Dotta *et al*.,

2013) equipment with identical point durations and identical bulk acceleration and deceleration parameters.

Although the application of the reversed field parameters produced a net change in both the magnitude and direction of the correlation coefficients, the effects produced by the application of the appropriate excess correlation fields produced even greater effects. The net result suggests a gradient of excess correlation when specimens are presented with bulk angular accelerating and decelerating fields. These effects were not demonstrable using a different apparatus producing complex accelerating and decelerating components of bulk and phase velocities (Dotta and Persinger, 2012). These findings may suggest a unique property associated with bulk angular velocities that are not present when phase velocities are included.

Utilizing Table 3.2 we can identify the strongest coupling between local and non-local species. The results are suggestive that bacteria acting as the local mediator for energy transfer between the spatially separated sites is most effective for 1 msec point durations. Although the effects can be accommodated by both species, this slight skew towards a unique source is intriguing. It suggests, at least from the perspective of the working model, that there might be increased coherence between the bacteria (*E. coli*) and the properties of the applied electromagnetic field which might reflect interactions at the level of the electron (Persigner, 2013; Persinger and Koren, 2007).

Consider the resting membrane potential of *E. coli* to be in the order of -140 to -240 mV (Bot and Prodan, 2010). If a single charge is responsible for the generation and maintenance of this potential difference then the net energy can be calculated. If we take the product of the upper limit of the resting membrane potential ($1.40 \cdot 10^{-1}$ $kg \cdot m^2 \cdot A^{-1} \cdot s^{-3}$) and the unit charge ($1.6 \cdot 10^{-19} A \cdot s$) the resultant energy would be in the order of $2.24 \cdot 10^{-20}$ J ($kg \cdot m^2 \cdot s^{-2}$). This value converges on the

energy associated with the action potential and that energy required to maintain the separation between charges along the membrane of animal cells (Persinger, 2010).

If the linear dimension of the *E. coli* cell is approximately 1 μm ($1.0 \cdot 10^{-6}$ m) (Nanninga and Woldrich, 1985) then the volume a single *E. coli* cell occupies would be $1.0 \cdot 10^{-18} m^3$. Given that the concentration of *E. coli* is approximately 10^8 to 10^9 cells/mL and our solution had a final volume of 10 mL, the total number of cells would be in the range of 10^9 to 10^{10}. The net volumetric occupancy of all the cells would then be approximately 10^{-8} to 10^{-9} m^3. Taking the net energy associated with a single cell ($2.24 \cdot 10^{-20}$ J) and dividing this value by the total volume occupied by the cells ($10^{-8} m^3$) yields an energy density of $2.24 \cdot 10^{-12}$ $J \cdot m^{-3} (kg \cdot m^{-1} \cdot s^{-2})$. It is possible to calculate the energy density resulting in the application of a magnetic field using Equation 3.4:

$$\text{Equation 3.4 : } J \cdot m^{-3} = B^2/2\mu$$

where *B* is the strength of the magnetic field in Tesla ($kg \cdot A^{-1} s^{-2}$) and μ is the permeability of free space ($1.256 \cdot 10^{-6}$ $kg \cdot m \cdot A^{-2} s^{-2}$). Rearranging to isolate for the necessary field strength producing an energy density equal to $2.24 \cdot 10^{-12}$ $J \cdot m^{-3}$ results in an intensity of $2.23 \cdot 10^{-9}$ T. This approaches the value associated with the intensity of the applied electromagnetic fields employed in this study.

We may further describe phenomena associated with magnetic fields as they affect the rate of change of their complimentary electric field. This dynamic interaction can be modeled using Maxwell's equation for Faraday induction represented in equation 3.5:

$$\text{Equation 3.5: } \nabla \times B = \mu \left(J + \varepsilon \frac{\delta E}{\delta t}\right)$$

where $\nabla \times$ is the curl operator, B is the strength of the magnetic field, μ is permeability of free space, ε is the permittivity of free space, $\delta E/\delta t$ is the rate of change in the electric field and J is the charge density.

If we assume that the curl operator represents a unitary value and that the magnitude of J is negligible the expression reduces itself such that the strength of the field is related to the product of the permeability, permittivity and the changing electric field. Re-arranging Equation 3.5, we can solve for the intensity of the electric field. Given that the permeability is $1.256 \cdot 10^{-6}$ $N \cdot A^{-2}$, the permittivity is $8.85 \cdot 10^{-12}$ $C^2 \cdot N^{-1} m^{-2}$, the strength of the applied field is $3.0 \cdot 10^{-9}$T and the temporal application duration is in the order of milliseconds (10^{-3} sec) the net magnitude of the electric field would be $2.7 \cdot 10^5$ $V \cdot m^{-1}$ ($kg \cdot m \cdot A^{-1} s^{-3}$). Conversely, if we take the magnitude of the resting membrane potential of *E. coli* to be in the order of 10^{-1} V, the diameter of the cell to be 1 μm (10^{-6}m) the resultant electric field would be in the order of $10^5 V \cdot m^{-1}$. This implies a convergence of the applied magnetic fields on the operational basis of the cell, with respect to energies and electric field strengths that may demonstrate a functional mechanism associated with excess correlation.

3.6 References :

C. H. Bennett and D. P. DiVincenzo, *Nature* 404,247(2000).

Bot, C. T., & Prodan, C. (2010). Quantifying the membrane potential during E. coli growth stages. *Biophysical chemistry*, 146(2), 133-137.

Burke, R. C., Gauthier, M. Y., Rouleau, N., & Persinger, M. A. (2013). Experimental demonstration of potential entanglement of brain activity over 300 Km for pairs of subjects sharing the same circular rotating, angular accelerating Magnetic fields: verification by s_LORETA, QEEG measurements. *Journal of Consciousness Exploration & Research*, 4(1).

Dotta, B. T., Mulligan, B. P., Hunter, M. D., & Persinger, M. A. (2009). Evidence of macroscopic quantum entanglement during double quantitative electroencephalographic measurements of friends vs. strangers. *NeuroQuantology*, 7(4), 548-551.

Dotta, B. T., Buckner, C. A., Lafrenie, R. M., & Persinger, M. A. (2011). Photon emissions from human brain and cell culture exposed to distally rotating magnetic fields shared by separate light-stimulated brains and cells. *Brain research*, 1388, 77-88.

Dotta, B. T., & Persinger, M. A. (2012). "Doubling" of local photon emissions when two simultaneous, spatially-separated, chemiluminescent reactions share the same magnetic field configurations. *Journal of Biophysical Chemistry*, 3(01), 72.

Dotta, B. T., Murugan, N. J., Karbowski, L. M., & Persinger, M. A. (2013). Excessive correlated shifts in pH within distal solutions sharing phase-uncoupled angular accelerating magnetic fields: Macro-entanglement and information transfer. *Int J Phys Sci*, 8, 1783-1787.

Floyd, R. A., & Lewis, C. A. (1983). Hydroxyl free radical formation from hydrogen peroxide by ferrous iron-nucleotide complexes. *Biochemistry*, 22(11), 2645-2649.

Gallucci, S., & Matzinger, P. (2001). Danger signals: SOS to the immune system. *Current opinion in immunology*, 13(1), 114-119.

Hassett, D. J., Britigan, B. E., Svendsen, T., Rosen, G. M., & Cohen, M. S. (1987). Bacteria form intracellular free radicals in response to paraquat and streptonigrin. Demonstration of the potency of hydroxyl radical. *Journal of Biological Chemistry*, 262(28), 13404-13408.

Hill, S., & Wootters, W. K. (1997). Entanglement of a pair of quantum bits. *Physical review letters*, 78(26), 5022.

Hoffmann, J., Krug, M., Ortegel, N., et al. (2012) Heralded Entanglement between Widely Separated Atoms. *Science*, 337, 72-75. http://dx.doi.org/10.1126/science.1221856

Inoue, S., & Kawanishi, S. (1987). Hydroxyl radical production and human DNA damage induced by ferric nitrilotriacetate and hydrogen peroxide. *Cancer research*, 47(24 Part 1), 6522-6527.

Krippner, S. T. A. N. L. E. Y., & Persinger, M. I. C. H. A. E. L. (1996). Evidence for enhanced congruence between dreams and distant target material during periods of decreased geomagnetic activity. *Journal of Scientific Exploration*, *10*(4), 487-493.

Levine, A., Tenhaken, R., Dixon, R., & Lamb, C. (1994). H 2 O 2 from the oxidative burst orchestrates the plant hypersensitive disease resistance response. *Cell*, 79(4), 583-593.

Nanninga, N., and Woldringh, C.L. (1985). Cell growth, genome duplication, and cell division. In Molecular Cytology of Escherichia coli, N. Nanninga, ed. (London: Academic Press), pp. 259-318. p.261 figure 1

Persinger, M. A. (1985). Geophysical variables and behavior: XXII. The tectonogenic strain continuum of unusual events. *Perceptual and Motor Skills*, *60*(1), 59-65.

Persinger, M. A., Cook, C. M., & Tiller, S. G. (2002). Enhancement of images of possible memories of others during exposure to circumcerebral magnetic fields: correlations with ambient geomagnetic activity. *Perceptual and Motor Skills*, *95*(2), 531-543.

Persinger, M. A., & Koren, S. A. (2007). A theory of neurophysics and quantum neuroscience: implications for brain function and the limits of consciousness. *International Journal of Neuroscience*, 117(2), 157-175.

Persinger, M. A. (2010). 10-20 Joules as a neuromolecular quantum in medicinal chemistry: an alternative approach to myriad molecular pathways?. *Current Medicinal Chemistry*, *17*(27), 3094-3098.

Persinger, M. A. (2013). Support for Eddington's Number and his approach to astronomy: recent developments in the physics and chemistry of the human brain. *International Letters of Chemistry, Physics and Astronomy*, 8.

Richter, C., Park, J. W., & Ames, B. N. (1988). Normal oxidative damage to mitochondrial and nuclear DNA is extensive. *Proceedings of the National Academy of Sciences*, 85(17), 6465-6467.

Roll, W.G. (2003) Poltergeists amd haunts. In J. Houran & R. Lange (Eds.), *Hauntings and Poltergeists: Multidisciplinary perspectives* (pp. 123-163). Jefferson, NC: McFarland & Company.

Rouleau, N., Carniello, T. N., & Persinger, M. A. (2014). Non-local pH shifts and shared changing angular velocity magnetic fields: Discrete energies and the importance of point durations. *Journal of Biophysical Chemistry*, 2014.

Slater A.F.G., Stefan C., Nobel I., Van Den Dobblesteen D.J., Orrenius S. (1996) Intracellular redox changes during apoptosis. *Cell Death Differ*. 3,57–62.

Yakes, F. M., & Van Houten, B. (1997). Mitochondrial DNA damage is more extensive and persists longer than nuclear DNA damage in human cells following oxidative stress. *Proceedings of the National Academy of Sciences*, 94(2), 514-519.

Chapter 4

4 Passive Excess-Correlation in Water

4.1 Abstract

Experimental examination of effective excess correlation can be demonstrated in a passive manner. Spatially isolated beakers of spring water were subjected to the application of identically counter-clockwise rotating magnetic fields exhibiting bulk accelerating and decelerating angular velocities with 3 and 1 msec point durations. Simultaneous measures of direct current (DC) voltage demonstrate shared voltage deviations between the isolated systems even when these systems were not presented with a stimulus. Data suggest that the appropriate application of electromagnetic fields with specific application geometries remains a contingency of eliciting the excess correlation phenomenon. Of all the possible combinations of fields presented only two geometries were identified as being effective in eliciting passive excess correlation in separated sources of water. It was determined that 3 msec point durations produced the strongest effect when applied in a decelerating-accelerating pattern whilst similar results were identified using 1 msec points in an accelerating-decelerating pattern. However, similarities between the present research and the established model evidently diverge when 1 msec stimulus point durations are utilized. Possible mechanisms involving the expansion of interfacial water are suggested as the origin of passive excess correlation.

4.2 Introduction

The process in which the physical attributes of two separate particles, such as quantum spin, can be synchronized over vast distances can be attributed to the quantum mechanical nature of entanglement (Hoffman *et al*., 2012; Hill and Wootters, 1997). Effectively, entangled particles operate in a manner such that a change in one of the paired particles results in a proportional, yet opposite, change in the other. The complementary change that is exhibited by the entangled particles is generally conceived of as occurring instantaneously. Conceptualizing the effect of entanglement would be akin to having both particles sharing similar spaces.

The theoretical application of entanglement is often limited to the scope of fundamental particles such as electrons and protons. However, experimental evidence suggests that under the appropriate application of time-varying electromagnetic fields macromolecules interact in ways that mimic an entanglement type phenomenon (Persinger *et al*., 2007). The application of accelerating and decelerating bulk angular velocities, in combination with phase modulated decelerating and accelerating components, has been shown to elicit excess correlation between spatially separated locations (Dotta and Persigner, 2012; Dotta *et al*., 2009).

In the Dotta-Persinger studies, excess correlation was inferred through photon emission spectra resultant from the reaction of hydrogen peroxide and sodium hypochlorite, which showed a marked correlation (or doubling effect) between 7 and 8 min after the onset of the second field (Dotta and Persinger, 2012). Similar effects were demonstrated when spatially separated samples of water were subjected to injections of acetic acid and shared the same configuration of complex magnetic fields (Dotta *et al*., 2013). Exposure to the same combination of magnetic fields demonstrated a marked coherence between cell culture emission spectra (Dotta *et al*., 2011) and human quantitative electroencephalographic measures even when the separation

between sources was vast (Burke *et al*., 2013). Spatially separated water samples subjected to serial injections of 5% acetic acid (a proton donor) that share bulk decelerating and accelerating magnetic fields generated from different equipment than the Dotta-Persinger studies replicated and corroborated their findings (Rouleau and Carniello, 2014).

The net effect of this excess correlation phenomenon is a conspicuous alteration in the relationship between the sources exposed to the fields, which is made apparent by a relative increase in the strength of correlations between spatially separated systems, however the direction of the correlation is opposite with respect to each source. That is to say, if source A is positively correlated with source B, then source B shows a negative correlation with source A. Thus far, specific parameters for generating the magnetic fields also appear to be contingent upon eliciting the excess correlation effect. Systematically changing point durations of the field pattern around 1 and 3 msec leads to a change in correlation coefficients, i.e. the strength of the excess correlation effect. It is hypothesized that specific point durations are a requirement for maximizing the effect based on observations in previous studies (Rouleau and Carniello, 2014; Persinger and Koren, 2007; Persinger, 2014a; Persinger, 2014b).

The selection of 3 and 1 msec point durations was based upon the marked convergence of the physical properties of the proton and electron, respectively (Persinger and Koren, 2013). Theoretically, the combination of an external force (a reaction) coupled with the presentation of bulk accelerating and decelerating angular velocity fields comprised of discrete 3 and 1 msec point durations are considered the requirements to elicit excess correlation. As such, the limits to eliciting excess correlation have only been examined with respect to the configurations of the applied electromagnetic fields. It should be noted that in this design there was no exogenous application of a process (local injections) which has been a staple of the Dotta-Persinger excess

correlation method. The purpose of the present study was to investigate whether two spatially isolated sites could demonstrate excess correlations in two homeostatic systems; i.e. passively entangling the locations. For the purposes of this study, “passive correlation” refers specifically to employing a modified Dotta-Persinger methodology, utilizing the electromagnetic field applications but not the injections of hydrogen peroxide or acetic acid.

4.3 Methods

4.3.1 Measurement Apparatus:

The experimental design consisted of passively monitoring the direct current (DC) electrical potential of President’s Choice Brand spring water under the appropriate application geometry of angular accelerating and decelerating counter-clockwise rotating magnetic fields. Water was sampled from either a communal 4 L container or individual 500 mL bottles in order to examine possible differences between the sources. 25 mL samples of room temperature spring water were placed in open beakers while simultaneous measures of DC potential were recorded. The potential difference of the water samples was measured using a Victor 70C digital multimeter. Sampling occurred at 5 sec intervals with an uncertainty of ±0.1 mV. Recorded values were contingent upon the internal clock mechanism of the digital multimeters and thus delays associated with the respective computer port times are negligible.

Silver-chloride disc sensors modified from a Grass P79 electroencephalographic (EEG) recording device were employed to record potential difference. Two sensors were fixed with electrical tape to separate phallic, carbon-graphite rods, attached to a central rod in order to maintain a constant distance between disc surfaces. The heights of the sensors were as such that the entire surface of the discs were submerged below the surface of the water. However, the sensors were affixed in such a way so as to completely eliminate contact between the suspended

carbon-graphite rods and the surface of the liquid (Figure 4.1). The local (L) and non-local (NL) source beakers had their multimeter data actively recorded on two separate laptop computers, a Samsung NP550P5C and a Lenovo ThinkPad E531, respectively. The laptop-multimeter combinations remained the same for the duration of the experiment. The selections of these terms are arbitrary with respect to the design presented here.

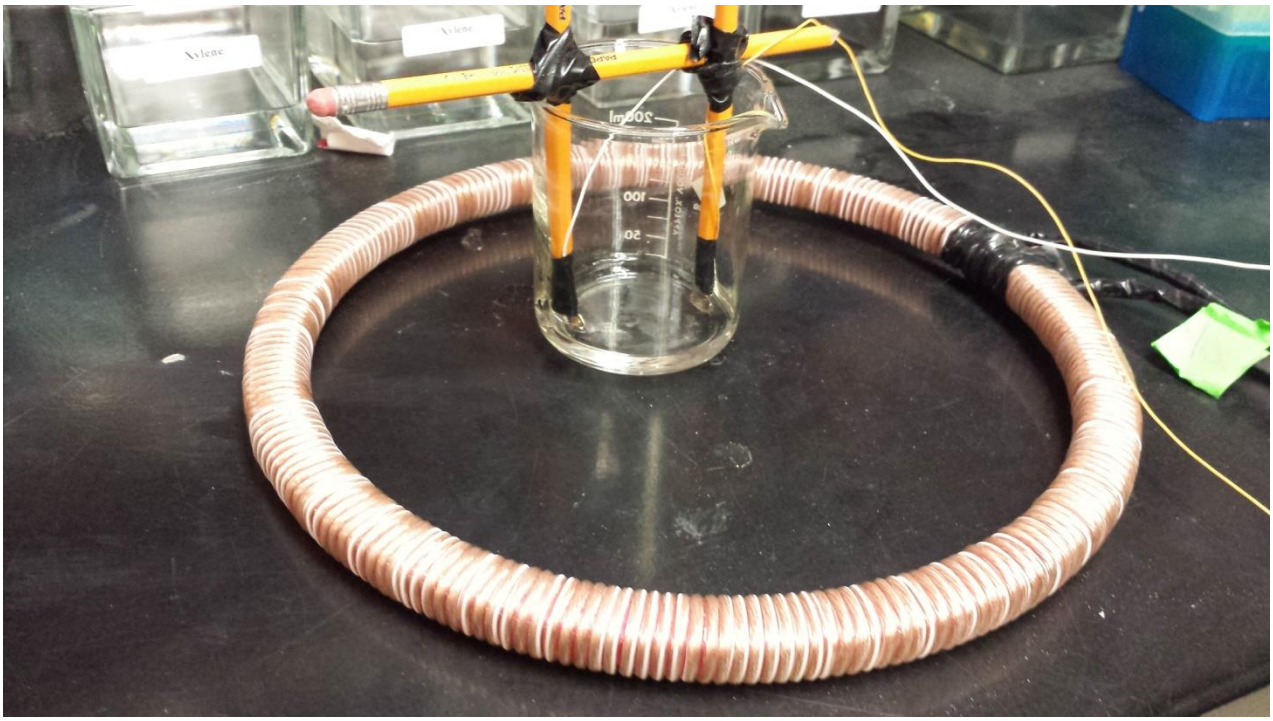

Figure 4.1: Photograph of the sensor configuration and accompanying toroid.

4.3.2 Magnetic Field Configurations:

Water samples were subjected to a combination of angular accelerating or decelerating counter-clockwise rotating electromagnetic fields with fixed point durations. A point duration is the length of time in which a current is transmitted through the magnetic field coil from the microcontroller. The point durations selected for this experiment were 1 and 3 msec which converge upon theoretical and practical applications. Production of the accelerating or decelerating angular velocities for the counter-clockwise rotation was accomplished by serially

modulating the inter-stimulus delay. The inter-stimulus delay is the amount of time when no current is being transmitted through the coil. A serial reduction of the inter-stimulus delay by 2 msec from an initial value of 20 msec to a final 8 msec constituted the accelerating angular velocity field. Conversely, serially increasing the inter-stimulus delay by 2 msec from an initial value of 20 msec to a final 32 msec constituted the parameters of the decelerating angular velocity. Electromagnetic fields were continuously generated for the entire duration of their respective exposures.

The electromagnetic fields were generated using an Arduino Uno microcontroller and simultaneously presented through two matched toroids that interfaced at a circuit board generated from the L-laptop (Figure 4.2). Toroids are electromagnetic field coils constructed by wrapping 14 gauge insulated copper wire around a plastic hoop. Systematic measurements of the strength of the accelerating and decelerating rotating angular velocity fields were taken using an AC milliGauss meter (model UHS, AlphaLabs, Inc USA), which showed 0.03 mG oscillations in electromagnetic field intensities. These 0.03 mG, or 3 nT, perturbations were not present when the fields were removed nor were they present in sham conditions.

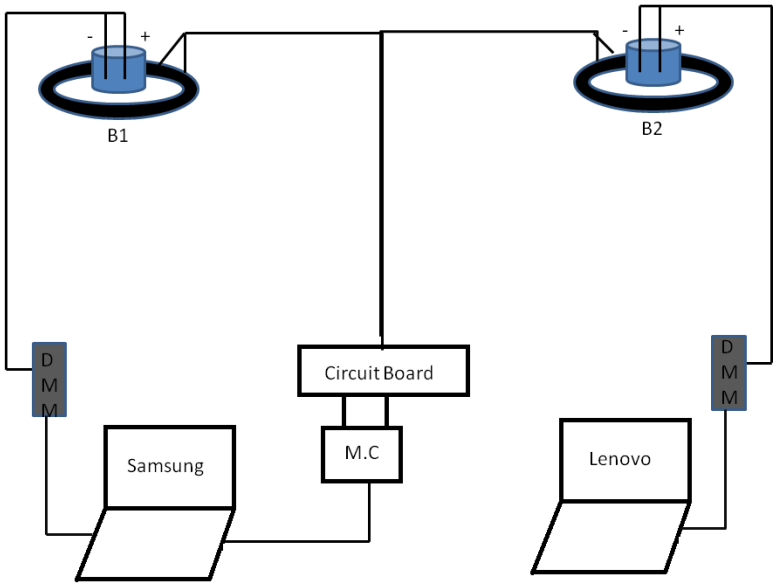

Figure 4.2: The representation of the experimental set-up. Here the abbreviations are as follows B1; beaker 1, B2: beaker 2, M.C; microcontroller, DMM: digital multimeter.

Water samples were placed in the center of the toroid-coils and exposed to either the sham, forward, or reverse field paradigms. For the magnetic field conditions both 1 and 3 msec point durations were used in separate trials. The exposure paradigm for both field conditions begins with a pre-exposure 2-min baseline recording. After the baseline, the first magnetic field pattern is presented for 6-min, followed by the second field for 12-min. Finally, a post-exposure baseline measure is recorded for 2-min. The total duration of the paradigm is 22 min (Table 4.2).

Table 4.1: Representation of the field application series and associated point durations

Designation	Point duration	Field 1	Field 2
Sham	----------	----------	----------
Forward	3 1	Decelerating	Accelerating

Reversal	3 1	Accelerating	Decelerating

4.3.3 Excess Correlation Selection Criteria:

To determine whether specific application geometries elicited a comparable trend as in previous research critical criteria had to be met. Here the criteria applied to this phenomenon are: 1) transition between the application of the first field and the first 8 min of the second field must result in significant differences in the magnitude of correlation coefficients, and 2) the magnitude of the correlation coefficients during the application of the second field of a given geometry of interest must be significantly different from controls. Differences in the strength of correlation coefficients were computed using Fisher's r-to-z method.

4.3.4 Statistical Methods:

A raw time series data sample before any statistical transformations but demonstrating the excess correlation effect is provided in Figure 4.3. Subsequent to visual data inspection raw data for all trials were imported into Microsoft Excel 2007 and IBM SPSS 17 for further analysis. Due to large discrepancies between measures of electrical potential between trials all data was within-subject Z-scored to reduce the influence of different initial conditions. Pearson correlations were computed for all Z-standardized data for min by min analysis. Further statistical explorations examined relevant time-periods within the excess correlation design and are specified in Table 4.2 below. Mean standardized Pearson correlation coefficients were computed between the independent and communal sources of water for analysis between sample sources. Distribution of data into appropriate temporal bins was constructed in accordance with

the divisions of Table 4.2 and is demonstrated in all subsequent and relative graphical representations and their respective statistical analyses.

Table 4.2: A representation of the time-course of the experiment and the associated identification of appropriate time bins. All values associated with labeled bins represent time during experiment in minutes. Only those field combinations which have met the pre-defined criteria are represented in this table along with sham condition. This table is complimentary to figure 4.1.

Field Parameters		**Bin Labels and Time of experiment**				
Designation	Point Duration	Pre-BL	Field 1	Field 2a	Field 2b	Post-BL
Sham	----------					
Forward	3	1-2	2-8	8-16	16-20	20-22
Reversal	1					

4.4 Results

4.4.1 Raw Time Series Data:

An example of the raw voltage output simultaneously recorded from both local and nonlocal beakers is presented in Figure 4.3. Minute fluctuations in the non-local sample's activity demonstrate a weak positive change in voltage which is associated with the decline in voltage of the local beaker beginning at approximately min 8 of the experiment. Although this is merely an example of one trial of one effective field application all other relationships for the effective fields demonstrated a similar trend.

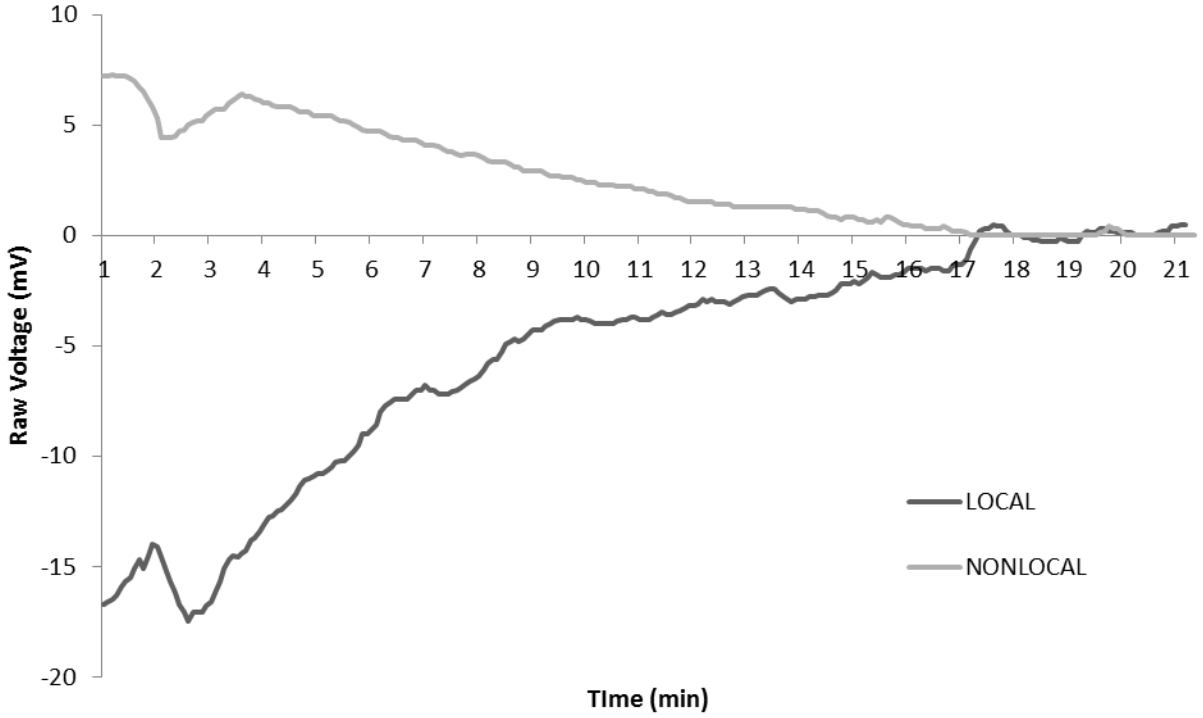

Figure 4.3: Raw outputs of the DC potential of local and nonlocal sources. The example above is one that represents the 3 msec forward field presentation.

Analyses of variance (ANOVAs) were conducted on the computed mean standardized Pearson correlation coefficients and revealed no differences in the strength (magnitude) of the correlation coefficients between independent (isolated bottles) and communal (4L container) water sources. Additional analyses revealed no interactions between water sources (i.e. isolated and communal bottles) and point durations (1 and 3 msec) with respect to correlation coefficients.

Of all the examined combinations of fields only two met the criteria for excess correlation as outlined in our Methods. The two identified application geometries to elicit excess correlation were the decelerating-accelerating pattern employing 3 msec point durations, and the accelerating-decelerating pattern employing 1 msec point durations. A visual representation of the mean over trials of the within-subjects Z-scored data is presented in Figure 4.4A thru C.

Large discrepancies in the initial onset of the measurement can be attributed to one of two things: 1) that each beaker displayed an inverted polarity with respect to the spatially separated beaker and thus would be reflected in the magnitude and direction of the Z-scored data, and 2) that there is a temporal latency that is associated with the measurement equipment favouring higher values at the beginning of the experiment gradually reducing its magnitude throughout the course of the recording. Even when we accommodate such large discrepancies by within subject transformations the data remained normally distributed and passed all other statistical assumptions. Visual comparison of the effective fields to control conditions revealed a conspicuous discrepancy at the point of intersection between conditions. Figures 4A thru 4C show that the region of intersection of the DC activity between local and non-local sources in control conditions occurs at approximately measure 128 which corresponds to a real time of 10 min and 40 sec into the trial. Conversely, the intersection between the effective excess correlation fields occurs at measure 130. When converted to real time values, this suggests an effective field homogeny at around min 11, or 3 min into the presentation of the second field.

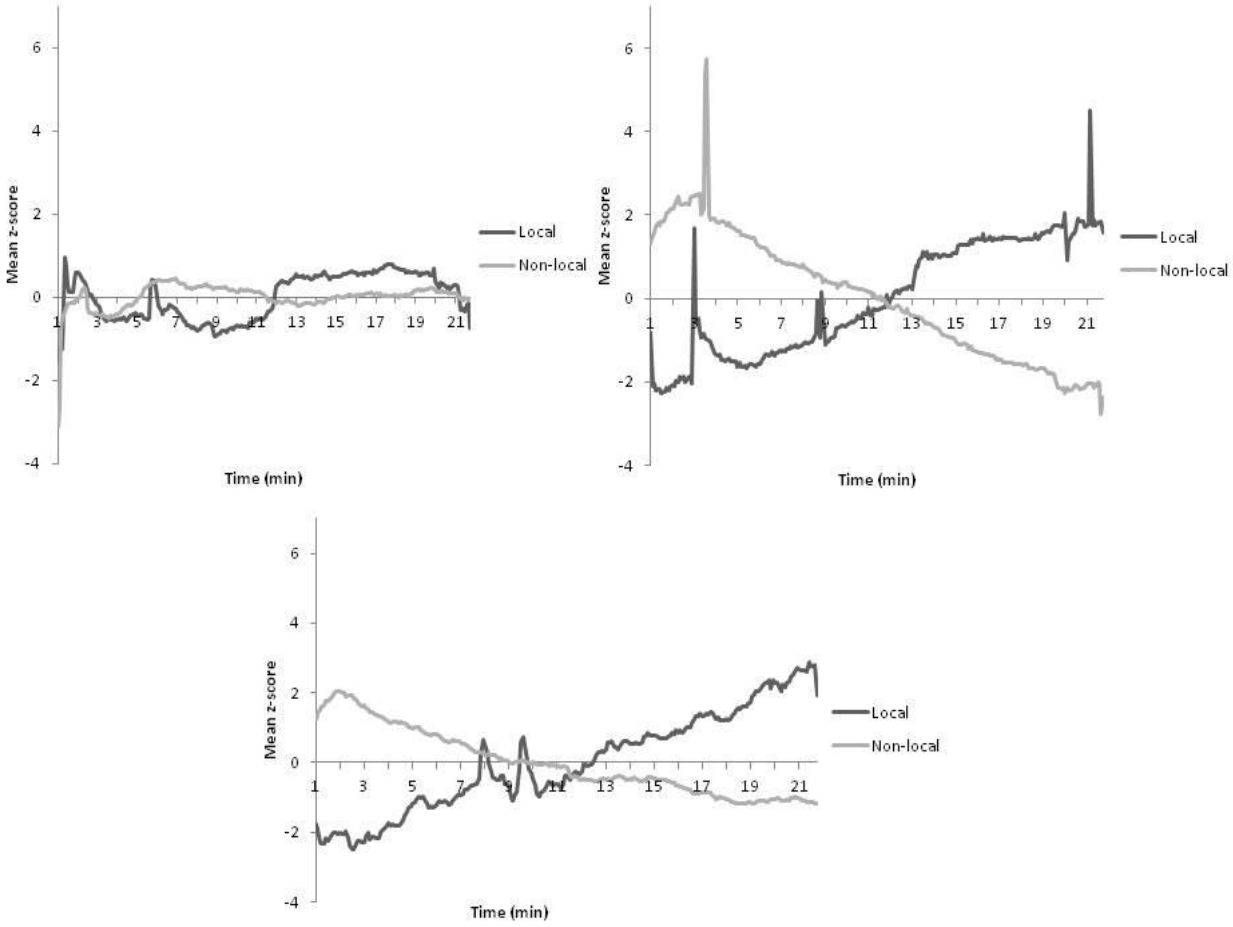

Figure 4.4 a-c : Top left hand graph represents the 3 msec field presentation, top right hand graph represents the 1 msec field presentation series whilst the central bottom figure represents the control conditions. All values presented in the graphs above consist of mean Z-score values within each condition.

A systematic examination of the critical time periods (Table 4.2) associated with the onset of the different fields was conducted. Results demonstrate an inversion and enhancement of the Pearson correlation coefficients for the 3 msec decelerating-accelerating and 1 msec accelerating-decelerating which are classified as the effective field configurations from this experiment (Figure 4.5). The reversal and enhancement in the magnitude of the Pearson correlation coefficients persist until approximately min 16 or, consequently, the first 8 min of the second field application.

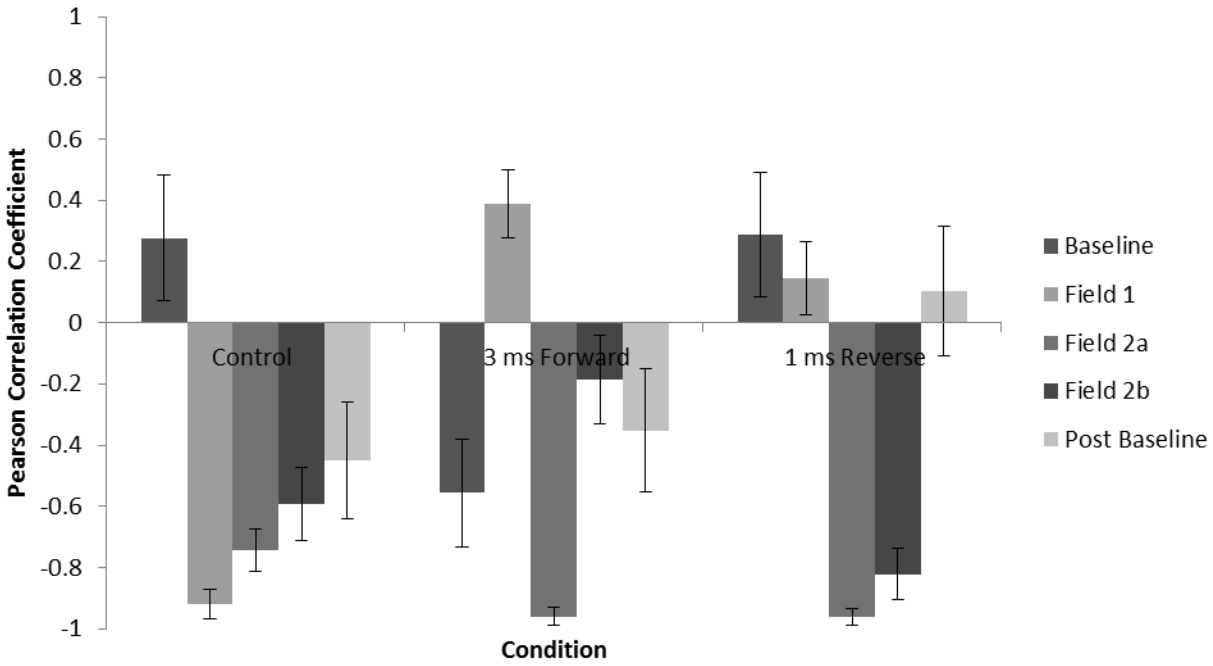

Figure 4.5: Demonstration of the effective application geometries as compared to control conditions. Error bars reflect calculated standard error measures.

To further identify the temporal window of this phenomenon, min by min investigations were conducted on the mean Z-score data. Min by min analysis of the two effective application geometries are presented in Figure 4.6. In this particular instance the duration of the separation of the correlation coefficients occurs at approximately min 8 and persists to min 12. The 8 to 12 min window corresponds to the first four min of the second field application.

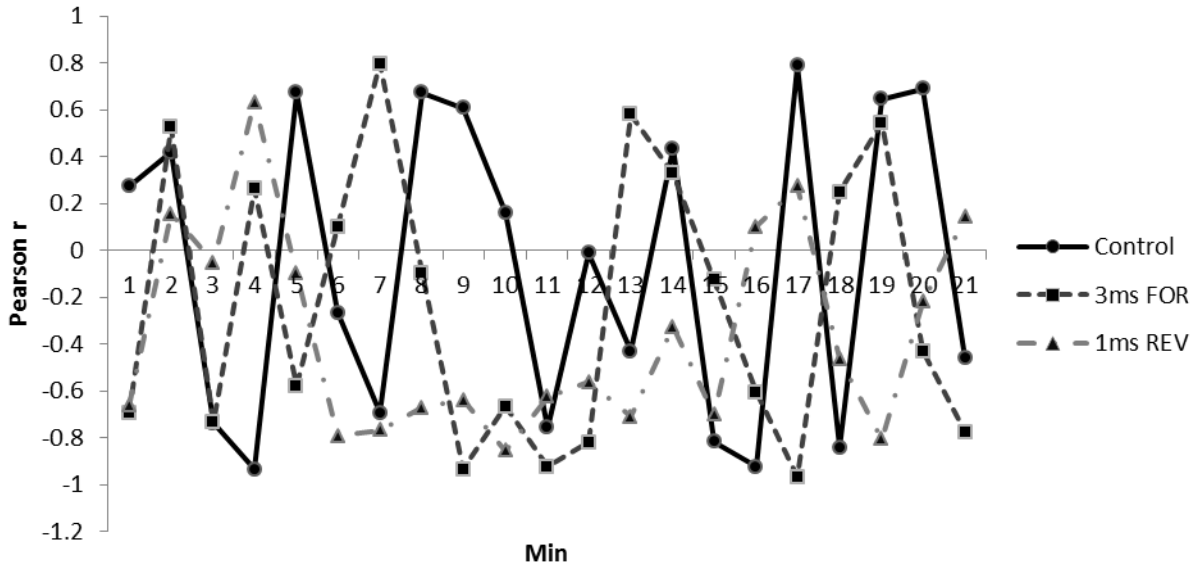

Figure 4.6: Representation of minute by minute trends in Pearson correlation coefficients with respect of differential application geometry.

4.5 Discussion

4.5.1 Differences between sources:

These results suggest that despite the samples of water being taken from distinct sources (separate bottles of water) or were extracted from the same source (4L container of water) there were no differences identified in the degree of excess correlation. The lack of differences suggests a level of homogeneity which was exhibited between the spatially separated samples. Given that both samples were chemically identical, but sampled from different sources (i.e. containers) they should demonstrate predictable responses to the same applied magnetic fields.

4.5.2 Experimental Phase-shift of DC voltage Inflection:

If one calculates the cycle duration (temporal component of the exposure) of both the 3 msec and 1 msec point durations in their appropriate accelerating or decelerating angular velocity fields, one can determine the number of elapsed cycles between the initiation of the

second field and min 3. The calculated ratio between the number of cycles elapsed of the distinct 3 and 1 msec fields is within the error of $1/2\pi$. The ratio of the number of elapsed cycles between the distinct point durations may demonstrate an underlying geometry driving the nature of excess correlation that has yet to be fully investigated. The geometrical relevance of a $1/2\pi$ relationship may correspond to a phase-shift in the temporal duration of the excess correlation effect reducing the longevity of the excess correlation window.

If one compares the presented results to previous research in the same field one will notice a temporal phase-shift with respect to the window associated with the peak of excess correlation. Quantitative support of the excess correlation paradigm suggests that the peak, where the correlation strength between local and non-local sites is maximized, should occur immediately after the onset of the accelerating field and persist for 7 to 8 min (Persinger and Koren, 2015). In contrast to these findings, the duration of the excess correlation window was determined to be only 4 min in this experiment. It would seem as if the temporal window was phase shifted, resulting in a temporal delay only lasting 4 min. We posit that the phase relationship of $1/2\ \pi$, demonstrable as the time of intersection of DC profiles of local and non-local sources, modulates the field by 4 min.

In order for this hypothesis to hold true then the nature of excess correlation must follow a sinusoidal pattern. By this we suggest that the observed window of 7 to 8 min constitutes the real portion of a sine wave, which is mathematically described by positive integers between 0 and π radians. The imaginary portion of the wave, that which is mathematically described as the negative integers between π and 2π, would constitute an unseen portion of the excess correlation phenomenon. Thus a displacement of $1/2\pi$ would necessarily represent a phase-shift in the sinusoidal nature of excess correlation elongating the imaginary portion of the wave. It would

then be theoretically possible to extend and shorten the effective transfer phase (real observable portion of the excess correlation wave) through direct manipulation. The phase-shift postulate adheres to the common theories of wave propagation which suggest a phase delay of ¼ wavelength could accommodate for the brevity of the excess correlation window, whilst the nature of the imaginary portion of the excess correlation wave may represent some form of storage of the transferred energy or information.

4.5.3 Water Dynamics:

At any interface water demonstrates a more organized structure resulting in an emergent property capable of excluding a number of solutes within 200 μm of the (Pollack *et al*., 2009). The emergence of these solute free regions, termed exclusion zones (EZ), results in a characteristic alteration of the fundamental properties of water such as electrical potential, viscosity and pH (Pollack *et al*., 2009). For instance, the potential difference of water demonstrates a 100 to 200 mV gradient separating interfacial water from bulk water (Pollack *et al*., 2008). Assuming that the electrical potential gradient separating bulk water from interfacial water is maintained by a single charge, and given that a charge has a value of $1.602 \cdot 10^{-19}$ A·s, then the energy required to maintain the gradient between bulk and interfacial water would be the product of the unit charge and the potential difference, which results in a value of $2.4 \cdot 10^{-20}$ Joules ($kg \cdot m^2 \cdot s^{-2}$). Energy in the order of 10^{-20} Joules converge upon the fundamental operational energy of the cell (Persinger, 2014c).

Another physical property of interfacial water is its relatively low pH and the ability for protons to move across the electrical potential gradient. The movement of protons from the EZ can influence the pH of the surrounding bulk water so long as the EZ builds or expands. The process of building the EZ is influenced by the intensity and exposure length of external energy

(Chai *et al*., 2009). Thus the application of electromagnetic fields provides energy to the system and induces a change in the electric field of the material. A consequence of this alteration in the electric field is a change in the magnitude of the electrical potential gradient allowing for the expansion of the EZ and increasing the movement of protons from EZs to bulk water. The application of the appropriate time-varying magnetic fields liberates contained hydronium ions, altering the pH of the solution. Although we did not directly measure the pH of the solution, we may be able to infer the pH from the electrical potential (Alberts *et al*., 2002). A general hypothesis for the duration of the 4 min may be accommodated by the expansion of the EZ. The terminal velocity of expansion resulting in the formation of an extended EZ may reduce the temporal window for excess correlation. Modulation of the EZ has been accomplished by Chai *et al*. (2010) by applying 3.4 μm wavelength light (infrared) for 10 min. The effects of the light stimulation resulted in a net increase of the water's temperature by 1℃ and increased the boundary of the EZ by a factor of 4 in a volume of 5 mL.

Given that the specific heat of water in its liquid form is 4.184 $J \cdot g^{-1}K^{-1}$ the total amount of energy donated to the system was approximately 20.92 J. Given that the energy required to grow theEZ is 20.92 Joules and that 5 mL of water contains $1.67 \cdot 10^{23}$ molecules, the net energy per molecule is $1.19 \cdot 10^{-22}$ J/molecule. The amount of energy provided to the system through the application of the time-varying magnetic fields can be calculated using the equation:

$$\text{Equation 4.1: } J = \frac{B^2}{2\mu} \cdot V$$

where *J* is the energy in Joules, *B* is the strength of the applied magnetic field in Tesla ($kg \cdot A^{-1} \cdot s^{-2}$), *V* is the volume of space affected and 2μ is the permeability of free space. In our experiment, the application of a 3 nT field in the volume of a 25.4 cm diameter toroid results in an energy of $1.79 \cdot 10^{-16}$ J. If we take the total energy impacting the system and the energy associated with the

expansion of the EZ ($1.19 \cdot 10^{-22}$ J/molecule) the total number of water molecules affected was approximately $1.50 \cdot 10^{6}$ molecules.

The baseline formation of the EZ extends approximately 200 μm, and when subjected to a 4 fold increase in size (to 800 μm) the resultant change in the size of the EZ is approximately 600 μm per 10 min. If we consider the change in the size of the EZ to occur isotropically in all directions, we can then calculate the diffusion velocity for the expansion. Here if the change in size of the exclusion zone is 600 μm over 10 min the diffusion velocity would be in the order of $6.0 \cdot 10^{-10} m^2 \cdot s^{-1}$. Given that our window of excess correlation is 4 min in duration then the degree of linear expansion would be approximately $3.79 \cdot 10^{-4}$m. If the intramolecular separation between an H-atom and an O-atom in water is $0.0978 \cdot 10^{-9}$ m (Bieze *et al*., 1993), then the approximate length of the entire molecule would be $1.96 \cdot 10^{-10}$ m. The total number of molecules which are recruited to the EZ through its expansion would be the quotient of the distance expanded and the linear distance of a water molecule, resulting in $3.06 \cdot 10^{6}$ molecules. These results converge at the same magnitude and mimic the number of ions responsible for maintaining the electrical potential of the cell membrane (Persinger, 2014c).

4.5.4 Further Quantitative Support:

The results obtained in this experiment corroborate other findings suggesting that applied magnetic fields can elicit excess correlation (Dotta and Persigner, 2012; Dotta *et al.*, 2009; Burke *et al.*, 2013; Dotta *et al.*, 2013; Rouleau and Carniello, 2014). However, it has introduced an occult variable that has otherwise gone unnoticed. The overlap between the appropriate order of decelerating and accelerating angular velocity magnetic fields with 3 msec point durations may reflect the discrete fluctuations of hydronium dynamics. The generation of interfacial EZs is theoretically sufficient at elucidating the demonstrated effects. Identifying the basic

characteristics of an inverted field presentation with 1 msec point durations as an effective field geometry does not resonate with current hypotheses of mechanism. Indeed the structure of the presentation has altered but the effect remains the same suggesting that the destabilization of bulk group velocity as a theoretical mechanism may still apply

Brushci and colleagues (2014) proposed an experiment whereby the manipulation of the acceleration of entangled particles may enhance or degrade the phenomenon. The alteration of physical acceleration can be considered a disruption in local gravitational effects. Although the proposed experiment relies on the physical acceleration of the system to elicit said effects, one may apply appropriate magnetic fields to elicit similar results. It has been proposed that in higher dimensions of space-time interactions between electromagnetic fields and gravitational fields occur, suggesting that this interaction between gravity and electromagnetism can be observed in Minkowski space-time (Kaluza, 1921).

Consider gravitational effects to be described as an accelerated frame and that the effects of electromagnetism on gravitational alterations can be measured in local space-time. Treating gravity as an acceleration we can then relate the gravitational force to the electromagnetic force via the relationship of:

$$\text{Equation 4.2: } m \cdot a = \frac{B^2}{4\pi\mu} \cdot A$$

where m is the mass, a is the acceleration, B is the intensity of the magnetic fields, μ is the permeability of free space and A is the area the field occupies.

The acceleration component of the magnetic fields can be calculated as described by the equation:

$$\text{Equation 4.3: } a = \frac{\Delta v}{\Delta t}$$

where a is the acceleration, Δv is the change in velocity and Δt is the change in time. However the velocity around a circle is calculated as $2\pi r/T$, where r is the radius of the circle and T is the period. For our applied magnetic fields the acceleration around a 25.4 cm diameter with a change in time of 2 msec approaches $10^4 m \cdot s^{-2}$. Rearranging Equation 4.1 to solve for the intensity of the field required to elicit responses in protons with a mass of $1.6 \cdot 10^{-27}$ kg and electrons with a mass of $9.11 \cdot 10^{-31}$ kg solves to a required intensity range of 10^{-28} to 10^{-34} T. Given that the intensities of the applied fields were ~0.03 mG (or the equivalent of $3.0 \cdot 10^{-9}$ T) and if we assume that the limit of 10^{-28} to 10^{-34} T represents the necessary field required to disturb a single particle, then the total number of particles that can be affected range from 10^{19} to 10^{25} particles. These values represent the possible number of protons and electrons which may be respectively involved in this process. Furthermore, if one utilizes the calculation for coherence between the time of weakly dissipative systems (Bush and Parentani, 2013) in Equation 4.4 one can calculate the mass associated with the 8 min window of the excess correlation effect:

$$\text{Equation 4.4: } t = \hbar/(mc^2)$$

where t is the coherence time, $\hbar$ is reduced Planck's constant, m is the mass and c is the speed of light. When one isolates the effective mass component of Equation 4.3 and solves for its value, given that the approximated temporal relationship of the excess correlation design is in the order of 10^2 sec, the value of the mass is effectively 10^{-52} kg. This value represents the upper limit of the rest mass of the photon as determined by Tu and colleagues (Tu et al, 2005).

If the absolute duration of the excess correlation phenomenon is contingent upon photon and electron activity then this may indirectly support the notion of a coupling *between* the electron and the photon. Conceptually we can envision the positron as being a composite of the superposition of both an electron and photon and thus can be described, with respect to the

principles of quantum electrodynamics, as an electron traveling backwards in time (Feynman, 1949). Considering this definition of electron-photon coupling it could be argued that the reverse presentation of differential accelerating and decelerating angular velocity fields could elicit this effect through positrons. This argument can be justified in the sense that the calculated effective values for the electron are retained even if the electron is assumed to be a positron. Furthermore, the addition of any external force or stimulus would fix the linearity of causality and allow for the elicitation of effects via the classical electron model rather than through the activity of a positron node.

Based on the criteria established in this document it can be demonstrated that the application of an accelerating angular velocity field followed by a decelerating angular velocity field containing 1 msec point durations can elicit the excess correlation effect without the presumed necessary application of an exogenous stimulus. Similar results can are demonstrated with the application of decelerating angular velocity field followed by the application of an accelerating angular velocity field only when using 3 msec point durations as demonstrated in Figures 4.5 and 4.6. The conspicuous nature of these results show that an external stimulus is not required to elicit excess correlation. We have demonstrated the possibility of passive excess correlation between spatially separated samples water that share specific magnetic field configurations, however the mechanism by which these alterations in electrical potential occur has not been determined. We suggest that the dynamics of water at an interface may contribute to the overall phenomenon of excess correlation with or without the application of an exogenous proton donor.

4.6 References:

Alberts B, Johnson A, Lewis J, et al. Molecular Biology of the Cell. 4th edition. New York: Garland Science; 2002.

M.C. Arnesen, S. Bose, V. Vedral Natural thermal and magnetic entanglement in the 1D Heisenberg model *Phys. Rev. Lett*., 87 (2001) 017901(1)-4.

Bieze, T. W. N., van der Maarel, J. R. C., & Leyte, J. C. (1993). The intramolecular OH bond length of water in a concentrated poly (ethyleneoxide) solution. An NMR relaxation study. *Chemical physics letters*,*216*(1), 56-62.

Burke, R. C., Gauthier, M. Y., Rouleau, N., & Persinger, M. A. (2013). Experimental demonstration of potential entanglement of brain activity over 300 Km for pairs of subjects sharing the same circular rotating, angular accelerating Magnetic fields: verification by s_LORETA, QEEG measurements. *Journal of Consciousness Exploration & Research*, 4(1).

Busch, X. and Parentani, R. *Phys. Rev. D* 88, 045023 (2013).

Bruschi, D. E., Sabín, C., White, A., Baccetti, V., Oi, D. K., & Fuentes, I. (2014). Testing the effects of gravity and motion on quantum entanglement in space-based experiments. *New Journal of Physics*, 16(5), 053041.

Chai, B., Yoo, H., & Pollack, G. H. (2009). Effect of radiant energy on near-surface water. *The Journal of Physical Chemistry B*, *113*(42), 13953-13958.

Dotta, B. T., Mulligan, B. P., Hunter, M. D., & Persinger, M. A. (2009). Evidence of macroscopic quantum entanglement during double quantitative electroencephalographic measurements of friends vs. strangers. *NeuroQuantology*, 7(4), 548-551.

Dotta, B. T., Buckner, C. A., Lafrenie, R. M., & Persinger, M. A. (2011). Photon emissions from human brain and cell culture exposed to distally rotating magnetic fields shared by separate light-stimulated brains and cells. *Brain research*, 1388, 77-88.

Dotta, B. T., & Persinger, M. A. (2012). "Doubling" of local photon emissions when two simultaneous, spatially-separated, chemiluminescent reactions share the same magnetic field configurations. *Journal of Biophysical Chemistry*, 3(01), 72.

Dotta, B. T., Koren, S. A., & Persinger, M. A. (2013). Demonstration of entanglement of "pure" photon emissions at two locations that share specific configurations of magnetic fields: implications for translocation of consciousness. *Journal of Consciousness Exploration & Research*, 4(1).

Dotta, B. T., Murugan, N. J., Karbowski, L. M., & Persinger, M. A. (2013). Excessive correlated shifts in pH within distal solutions sharing phase-uncoupled angular accelerating

magnetic fields: Macro-entanglement and information transfer. *Int J Phys Sci*, 8, 1783-1787.

Feynman, R. P. 1949a. "The Theory of Positrons."*Phys. Rev.* 76, pp. 749-759.

Hill, S., & Wootters, W. K. (1997). Entanglement of a pair of quantum bits. *Physical review letters*, 78(26), 5022.

Hoffmann, J., Krug, M., Ortegel, N., et al. (2012) Heralded Entanglement between Widely Separated Atoms. *Science*, 337, 72-75. http://dx.doi.org/10.1126/science.1221856

Kaluza, Theodor (1921). "Zum Unitätsproblem in der Physik". *Sitzungsber. Preuss. Akad. Wiss. Berlin. (Math. Phys.)*: 966–972.

Persinger, M. A., & Koren, S. A. (2007). A theory of neurophysics and quantum neuroscience: implications for brain function and the limits of consciousness. *International Journal of Neuroscience*, 117(2), 157-175.

Persinger, M. A., Tsang, E. W., Booth, J. N., & Koren, S. A. (2007). Enhanced Power within a Predicted Narrow Band of Theta Activity During Stimulation of Another By Circumcerebral Weak Magnetic Fields After Weekly Spatial Proximity: Evidence for Macroscopic Quantum Entanglement?. *NeuroQuantology*, 6(1).

Persinger, M. A. (2013). Support for Eddington's Number and his approach to astronomy: recent developments in the physics and chemistry of the human brain. *International Letters of Chemistry, Physics and Astronomy*, 8.

Persinger, M. A., & Koren, S. A. (2013). Dimensional analyses of geometric products and the boundary conditions of the universe: implications for a quantitative value for the la-teensy to display entanglement. *Open Astronomy Journal*, 6, 10-13.

Persinger, M.A. (2014). Discrepancies between predicted and observed intergalactic magnetic field strengths from the universe's total energy: is it contained within submatter spatial geometry? *International Letters of Chemistry, Physics and Astronomy*, 11, 18-23.

Persinger, M. A. (2014b). Quantitative convergence between physical-chemical constants of the proton and the properties of water: *Implications for sequestered magnetic fields and a universal quantity. Physics* and Astronomy, 2, 1-10.

Persinger, M. A. (2014c). Astronomical, chemical, and biological implications of 10-20 joules as a fundamental quantum unit of information for neurofunction. *Archives of Neuroscience*, *1*(3).

Persinger, M. A., & Koren, S. A. (2015). Potential role of the entanglement velocity of 10^{23} m· s^{-1} to accommodate recent measurements of large scale structures of the Universe. *International Letters of Chemistry, Physics and Astronomy*, *3*, 106.

Pollack, GH; Clegg, J. Unsuspected Linkage Between Unstirred Layers, Exclusion Zones and Water. Phase Transitions in Cell Biology; Pollack, GH, Chin, WC, Eds.; Springer: New York, USA, 2008; p. 183.

Pollack, G. H., Figueroa, X., & Zhao, Q. (2009). Molecules, water, and radiant energy: new clues for the origin of life. *International journal of molecular sciences*, *10*(4), 1419-1429.

Rouleau, N., Carniello, T. N., & Persinger, M. A. (2014). Non-local pH shifts and shared changing angular velocity magnetic fields: Discrete energies and the importance of point durations. *Journal of Biophysical Chemistry*, 2014.

Tu, L. C.; Luo, J.; Gilles, G. T.(2005).The mass of the photon. *Rep.Prog. Phys*. 68, 77-130.

Chapter 5

5 Interaction of Bulk Angular Velocity Electromagnetic Fields and Temperature Variations on the Latency of pH shifts

5.1 Abstract

We investigated the potential interaction between temperature variations and bulk accelerating or decelerating electromagnetic fields on temporally delayed, decreased magnitude shifts in pH in response to weak acids. The appropriate combination of near 0^0C temperatures and an accelerating bulk angular velocity electromagnetic field with 1 msec point durations maximized the reduction in absolute shifts of pH in response to the injection of weak acids in a local beaker. However, the application of near 40^oC temperatures exacerbated the delayed response of water to serial injections of weak acids which had been exposed to a 3 msec decelerating bulk angular velocity electromagnetic field configuration. The latter configuration of applied electromagnetic fields has been successful in reducing the degree of pH shifts in the past. The gravitational-electromagnetic equivalence across the temporal duration of the Universe is explored as a potential mechanism for the observed effect.

5.2 Introduction

Water has the distinct characteristic of altering its physical properties at an interface. The resultant differentiation into two distinct physical entities has been termed bulk and interfacial water, respectively (Fenn *et al*., 2009). Invariably, properties such as viscosity, proton dynamics and even electrical potential are enhanced by the influence of uncharged, polar surfaces (Chen *et al*., 2007; Zheng *et al*., 2006; Henderson, 2002; Thiel *et al*., 1987; Chai *et al*., 2012).

Furthermore, an enhancement of the physical properties of water at an interface creates a zone at which solutes, including some ions, are excluded from interfacial water (Yoo *et al*., 2011). These exclusionary properties, also termed the exclusion zones of water, have been remarkably implicated with the intricacies of the formation of primordial membranes (Trevors and Pollack, 2012).

Recall that the ultimate function of the cell membrane, the primary constituent of all living organisms, is its ability to selectively filter required molecules and ions for the generation and maintenance of the electrical equilibrium responsible for maintaining the integrity of the cell. The exclusion zone and associated its interfacial water have been metaphorically approached as a static equilibrium and has been presented as such in the academic literatures. However, liquid water is not a static solution, as the molecules are in a constant state of flux. Furthering this claim, water has the unique ability to temporarily form hydronium ions which demonstrate a relatively short existence (on the picosecond scale, Persinger, 2014). In corroboration with these presented ideas Chai and Pollack demonstrated the potential of expanding the influence of the exclusion zone via irradiation with 3.4 μm wavelength light (Chai and Pollack, 2010). This may lend credence to the notion that the exclusion zone of water is not actually static and demonstrates its dynamic potential to be influenced by physical manipulation. Thus the potential then arises for one to examine this dynamic nature of the interfacial aspects of water and its associated exclusion zone in further detail. Chai and Pollack have identified that the effects of incident radiation resulted in a differential increase of the measured temperature of the solution by 1^{o}C. The alteration in the ambient temperature of the solution was accompanied by an expansion of the exclusion zone (Chai and Pollack, 2009). In this manner the practical

investigation would be to examine the influence of temperature on a potential dynamic measure of the exclusion zone or its associated processes.

Here we suggest that the simple observation of alterations in pH measurements should suffice as an approximate measure of the dynamic nature of the exclusion zone. Intuitively, if one injects a solution with an acid (a proton donor) the pH of the solution should acidify, however in an area which is surrounded by interfacial water deviation in pH recordings should reflect a marked delay in response to the stimulus or an overall reduction in the magnitude of the shift. Holding effects in pH are transient events that present as a reduction, or temporal dilation, in the absolute magnitude of the recorded pH as has been demonstrated by Murugan and colleagues (Murugan *et al*., 2015). In the Murugan *et al*. (2015) studies, water which was exposed to patterned electromagnetic fields demonstrated a conspicuous slowing of the onset of pH shifts when injected with a proton donor. In this particular context, the mechanism was akin to the strengthening of the exclusion zone of water. The combination of the appropriate electromagnetic fields could thus enhance the expansion of the exclusion zone to a point which would also expand the temporal window of reduction in pHs shifts. The net temporal delay in the onset of deviations in pH would be akin to increasing the effective range of the exclusion zone and should be investigated in greater detail. To define the causal relationship between the potential holding properties of water and the degree of reduction in absolute pH shifts or the onset of said shifts, its interaction with applied electromagnetic fields and temperature variations must be investigated to understand the potential mechanistic formation of primordial substrates similar to our now-defined cell matrices.

5.3 Materials and Methods

Open 250 mL beakers containing 25 mL of PC Brand Spring Water (Gray County Ontario) were subjected to a series of injections of 50 μL of 5% v/v acetic acid. 9 min of continuous data were sampled at 1 Hz increments using a Dr. DAQ pH recording device and associated pH sensor probe, while simultaneous measures of temperature were monitored each min using a mercury thermometer (range - 20^{o}C to 100^{o}C). Of the 9 min continuous data set the first 2 min segment was designated as a pre-exposure baseline measure, followed by 5 min of weak intensity bulk accelerating and decelerating angular velocity fields with 50 μL injections of 5% acetic acid. Injections occurred once every min for the duration of the 5 min field exposure. The final 2 min of the recording was followed by the immediate cessation of the field but not the removal of the sample from the exposure apparatus and constituted post-exposure measures.

5.3.1 Field Parameters and Exposure Apparatus:

The field exposure apparatus consisted of a single toroid constructed out of a 25.4 cm diameter plastic hoop, which was wrapped 216 times with 22 gauge insulated copper wire. Field exposure parameters consisted of either an accelerating bulk angular velocity field or a decelerating bulk angular velocity field. Each respective accelerating and decelerating field consisted of either 1 or 3 msec point durations, respectively. In this particular instance the concept of point durations is the specified length of time that a current will be passed into the exposure apparatus resulting in the production of transient (time-varying) electromagnetic fields. The accelerating and decelerating component of the resultant magnetic fields were generated by serially modulating the delay between point durations and is referred to as the inter-stimulus delay. For the accelerating bulk angular velocity field the initial inter-stimulus delay was set to 20 msec and was serially decreased by 2 msec from its initial value to a final value of 8 msec. Similarly, the decelerating angular velocity field had an initial inter-stimulus delay of 20 msec

which was serially increased by 2 msec to a final value of 32 msec. Each iteration of the appropriate increase or decrease in inter-stimulus delay was followed by the appropriate 1 or 3 msec point durations. Both the accelerating and decelerating bulk angular velocity fields were continuously looped for the entire 5 min exposure duration. Here, the modulation of both the inter-stimulus delays and point durations were accommodated by an Arduino Uno microcontroller and associated software. Intensities of the resultant electromagnetic fields were 0.03 mG (3.0 nT) which were verified using an AC milliGauss meter (model UHS, AlphaLabs, Inc USA).

5.3.2 Modulation of Temperature Variables:

For this experiment there were three different temperature conditions (Room Temperature, Cold and Hot) which were subjected to three field conditions (Sham, Accelerating and Decelerating) consisting of two different point durations (1 and 3 msec points), with time as a within subjects measure. The Sham field condition comprised the same experimental procedure (i.e. placing the open beaker in the toroid and monitoring the pH and temperature variations over the course of 9 min) without the fields being turned on. For the room temperature condition the water samples never exceeded the ambient temperature of the testing room (23 ± 1^0C).Cold and hot conditions were accommodated by placing the 250 mL open beaker into a 1 L (containing 300 mL of water or ice water) ice bath or double boiler and hot plate until a temperature of 8^0C and 35^0C were reached in each respective condition. In these cases the 1 L beaker was removed from the hot plate, or cooling location, and placed inside the toroid. All hot and cold conditions did not deviate more than $\pm 6^0$C of their starting temperatures of 35^0 and 8^0C respectively.

5.3.3 Statistical Methods:

All raw recorded data was imported into SPSS 17 statistical software for transformations and subsequent data analysis. The arithmetic means from the raw records of all trials sampled at 1 Hz increments were aggregated into 1 min bins. A relative change in pH from the computed mean values of the 1 min bin was calculated over the course of the experiment. The resultant computed relative changes in pH were subsequently within subjects Z-scored within the time domain before being subjected to further statistical analyses.

5.4 Results

A repeated measures analysis of variance (ANOVA) was conducted with time of injection as a within-subjects factor and revealed a significant 3-way within-subjects interaction of field by temperature by time [$F_{(56,217)} = 1.68$, $p<.01$, partial $\eta^2 = 0.30$] which are displayed in Figures 1 thru 3.

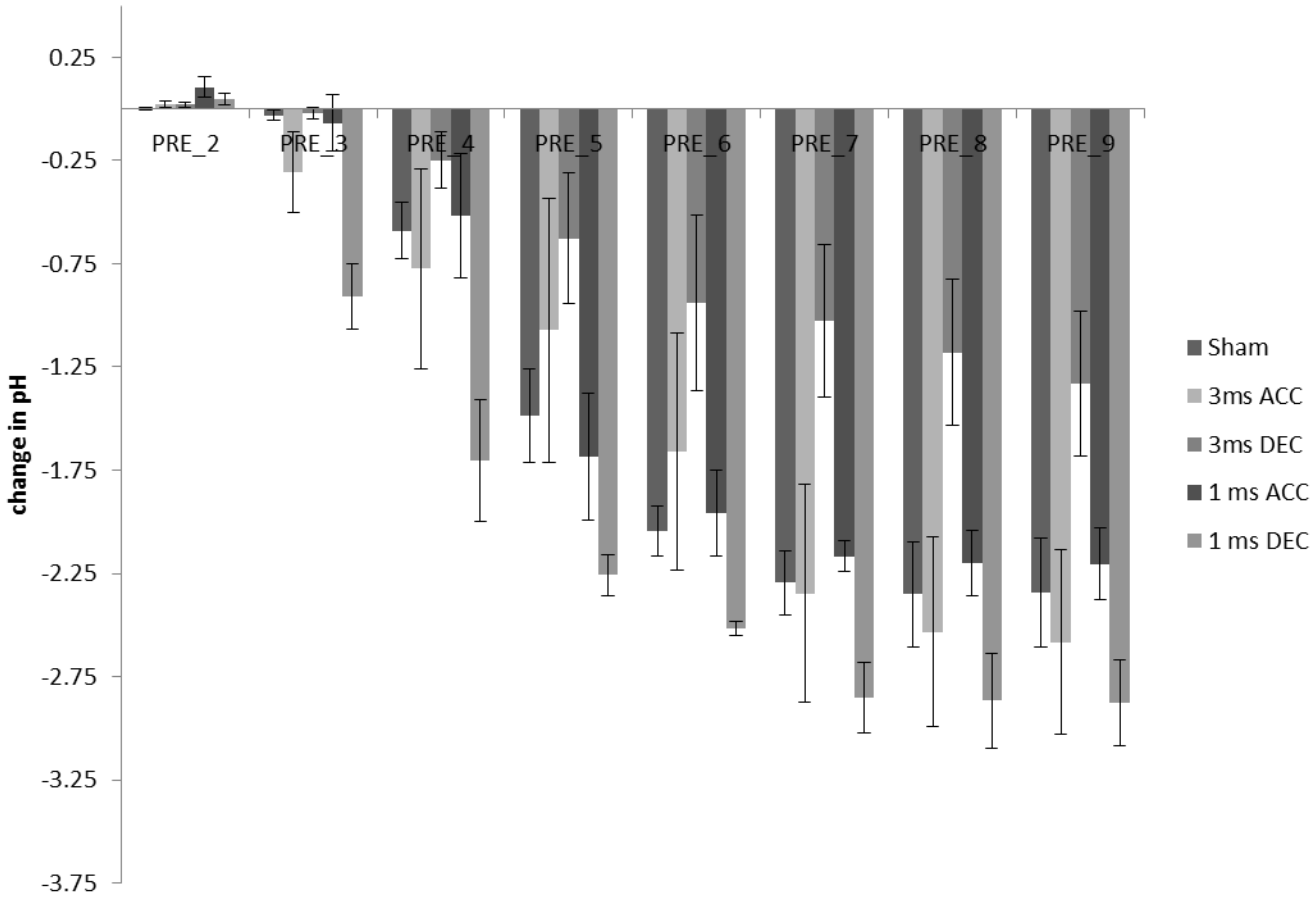

Figure 5.1: Room temperature events. In this condition the effects of 3 msec decelerating field was most effective to hold pH over time while 1 msec accelerating field reduced overall shifts in pH after 9 minutes. Error bars are measures of SEM. ACC denotes accelerating field parameters whilst DEC represents the decelerating field parameters.

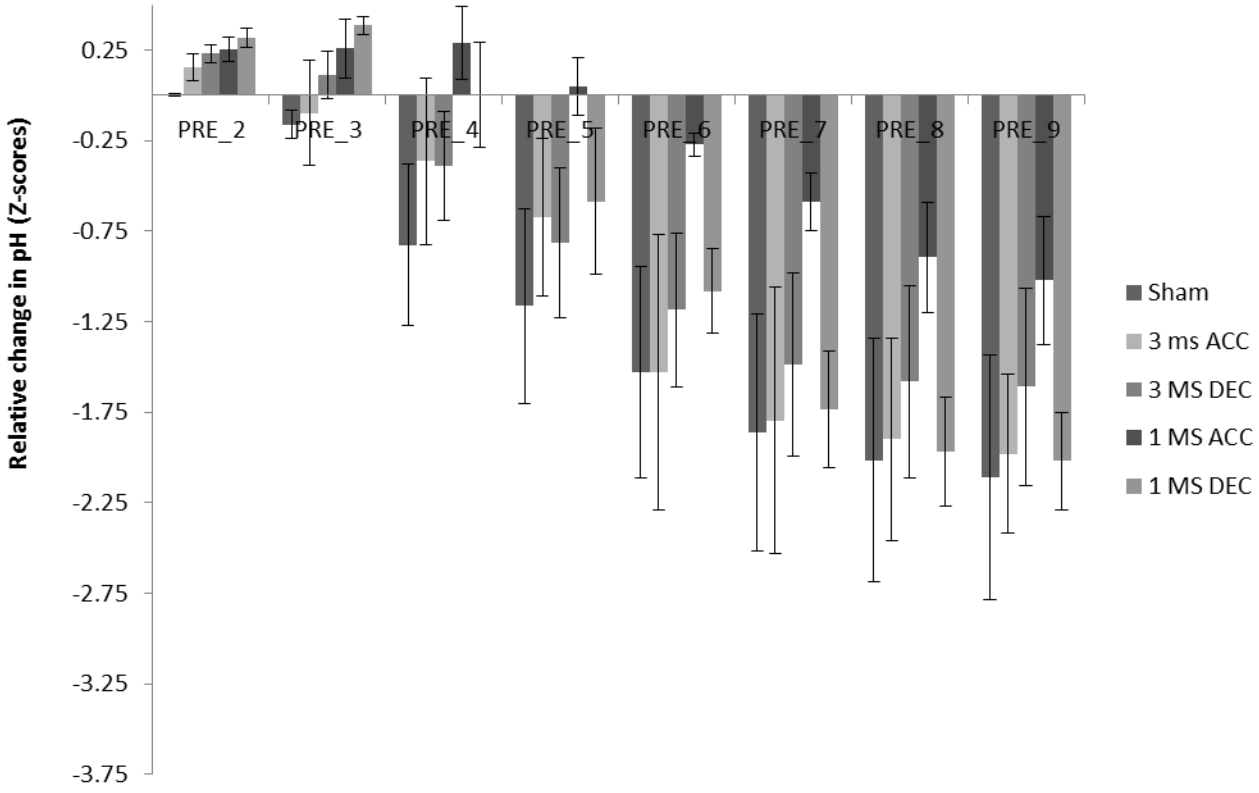

Figure 5.2: Cold condition, approximately 0^0C, demonstrative that 1 msec accelerating field reduces the overall change in pH over time. Error bars are measures of SEM. ACC denotes accelerating field parameters whilst DEC represents the decelerating field parameters.

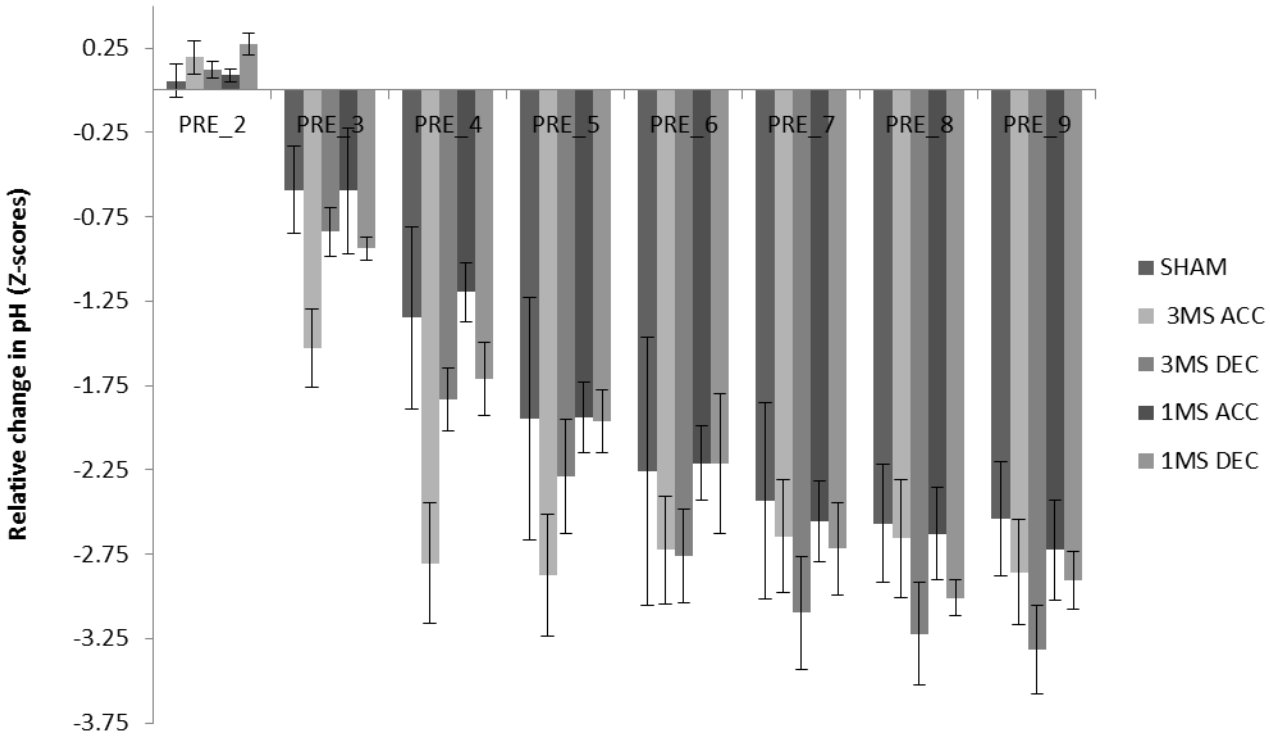

Figure 5.3: : Hot condition, 1 msec accelerating field effects are reduced and holding occurs for only 2 minutes. Error bars are measures of SEM. ACC denotes accelerating field parameters whilst DEC represents the decelerating field parameters.

Supplementary *post-hoc* ANOVAs were conducted in order to discern the net driving factor behind the 3-way interaction. The within subject standardized relative shift in pH during min 2 for room temperature sham, room temperature 3 msec decelerating, and room temperature accelerating field presentations as well as sham field exposure during cold conditions did not differ amongst themselves however were all were significantly different from 1 msec decelerating cold parameters which had a less significant (towards alkalinity) shift. Min 3 differences were accommodated by a greater drop in the within-subjects standardized relative pH for 3 msec accelerating bulk angular velocity field at high temperatures as compared to the 1 msec decelerating cold temperature condition. This trend continued into min 4 however the 1 msec accelerating field condition in the cold temperatures was not different from the 1 msec decelerating cold condition. In min 5 the only significantly different changes in pH were between

the 3 msec accelerating high temperature condition and the 1 msec accelerating cold condition. The latter of which produced a reduction in the within subjects standardized relative shift in pH (less acidic) whilst the former enhanced the change in pH towards acidity. Min 6 showed that the 3 msec accelerating high temperature, 3 msec decelerating high temperature and 1 msec decelerating room temperature conditions did not differ in the degree of the magnitude of the within-subjects standardized relative pH but however they were significantly different from the 1 msec accelerating cold condition which displayed a reduction in the within-subjects relative change in pH. The same trend which was identified in min 6 of the experiment was also identified in min 7 of the experiment. The final 2 min shared the same driving factors which identified the 3 msec hot decelerating condition as having a much lower pH (greater negative shift in the within-subjects standardized relative change in pH) as compared to cold water samples which were exposed to 1 msec accelerating bulk angular velocity fields.

5.5 Discussion

Here we have presented a myriad of data supporting a complex interaction between electromagnetic fields and temperature on standardized relative changes in the pH of water subjected to injections of a proton donor. This interaction can be labeled as a pH "holding" effect which our lab has previously identified as being associated with the application of weak intensity magnetic fields consisting of 3 msec point durations (Murugan *et al*., 2015 and unreported results). We have also demonstrated that varying the temperature of the immediate environment without the appropriate application of magnetic fields does not have an effect on the change in pH as measured by our equipment. Thus the direct implication of temperature as a moderator of the organization and expansion of the exclusion zone cannot, under these conditions, explain the dynamic processes associated with the pH holding effect and suggests an alternative mechanism

to this expansion as denoted by Chai and Pollack (2010). Of note, however, is the reduction in the efficacy of the pH holding effect at approximately 40^{o}C when exposed to a 3 msec decelerating field at which had otherwise produced a reduction in the relative change in pH.

Our most conspicuous effects presented in this report were the marked reduction in the relative change in pH at low temperatures (cold) while exposed to 1 msec accelerating bulk angular velocity fields. Remarkably, the reduction in the relative change in pH in this particular condition was greater than any other condition investigated. A possible explanation for the observed effect is akin to the strengthening of the organization of the water molecules within the exclusion zone. Thus, we endeavour to mathematically verify the potential of a 1 msec accelerating bulk velocity field at approximately 0^{o}C to affect the underlying structure of the water molecules in 25 mL of spring water. One assumption of this mathematical interpretation is centered on the notion that structured organization of any substance is directly related to the underlying space-time geometry which the matter influences.

In this instance, the curvature (geometry) of space-time is not solely affected by gravity but is also influenced by the magnetic properties of the contained matter. Thus, the geometric representation of the influence of water on space-time is represented by the Einstein-Maxwell relationship:

$$\text{Equation 5.1: } R = \frac{8\pi G}{c^4 \mu}\left[\frac{1}{2}\varepsilon E^2 + \frac{1}{\mu} B^2\right]$$

where R is the curvature (m^{-2}), G is the gravitational constant ($6.67 \cdot 10^{-11}$ $m^3 \cdot kg^{-1} \cdot s^{-2}$), ε is the permittivity of free space $8.85 \cdot 10^{-12}$ $A^2 \cdot s^4 \cdot kg^{-1} \cdot m^{-1}$), μ is the permeability of free space ($1.256 \cdot 10^{-6}$ $kg \cdot m \cdot A^2 \cdot s^2$), E is the electric field ($kg \cdot m \cdot A^{-1} \cdot s^{-3}$) and B is the magnetic field ($kg \cdot A^{-1} \cdot s^{-2}$). For water at 0^{o}C, the thermodynamic energy (entropy/structured energy) is 75.97 $J \cdot mol^{-1}K^{-1}$. Therefore, 25 mL of water (1.39 moles) would have a thermodynamic equivalent energy of

$2.88 \cdot 10^4$ J ($kg \cdot m^2 \cdot s^{-2}$) at 0^oC. Given the total number of water molecules stored in 25 mL of water is $8.37 \cdot 10^{23}$ molecules and the electric dipole moment of water is $6.16 \cdot 10^{-30}$ As·m (Clough *et al*., 1973) the total electric dipole of the solution would be $51.55 \cdot 10^{-7}$As·m. Dividing the thermodynamic energy of all the water molecules stored within the solution by the net dipole moment of all the water molecules would yield an electric field strength of $5.58 \cdot 10^9$ $kg \cdot m \cdot A^{-1} \cdot s^{-3}$ (V/m).

Equivalently, the squared magnetic field strength of water can be approximated by using the equation $B^2 = [J \cdot 2\ u]/V$, where *V* is the volume of water (25 mL = $2.5 \cdot 10^{-5}$ m^3) in cubic meters. The resultant squared magnetic field strength would be $2.88 \cdot 10^3$ $kg^2 \cdot A\text{-}^2 \cdot s\text{-}^4$ (T^2). Inserting the value of the squared magnetic field strength and the electric field into the Einstein-Maxwell equation yields a value of $1.27 \cdot 10^{-27} m^{-2}$, the inverse of which is $7.87 \cdot 10^{26} m^2$. From here we can calculate a time component associated with the structure of 0^oC water using a magnetic diffusivity constant. Given that the average conductivity of water is $1.75uS \cdot cm^{-1}$ and that the magnetic diffusivity is calculated using the relationship $1/\mu\sigma$, where μ is the permeability of free space and σ is the conductivity of water, the value approaches $10^9 m^2 \cdot s^{-1}$. Dividing the inverse of the Einstein-Maxwell geometry by the magnetic diffusivity of water results in a value of 10^{17} sec. This suggests that the structure of water at 0^oC converges at the level of the age of the Universe in regards to the magnetic diffusivity. That is, the time it would take for that magnetic equivalent of water to diffusive across the inverse of its own curvature is the age of the universe. This implies that the 1 msec effects of an accelerating field may homogenize the structure of water such that the proton diffusion is smeared across space-time and supports the theories of (Wheeler, 1946).

Conversely, if one divides the value of obtained from the Einstein-Maxwell equation ($1.27 \cdot 10^{-27} m^{-2}$) by the magnetic diffusivity of water ($4.57 \cdot 10^{9} m^{2} \cdot s^{-1}$), the resultant temporal duration would be in the order of $2.77 \cdot 10^{-37}$ sec or the equivalent of $3.60 \cdot 10^{36}$ Hz. Given that the energy of this frequency can be calculated using Planck's relationship E = hv, where E is the energy, h is Planck's constant $6.626 \cdot 10^{-34}$ $kg \cdot m^{2} \cdot s^{-1}$, it yields an energy in the order of $2.38 \cdot 10^{3}$ $kg \cdot m^{2} \cdot s^{-2}$. Dividing this resultant energy by the total number of available water molecules results in an energy of $2.85 \cdot 10^{-21}$ $kg \cdot m^{2} \cdot s^{-2}$ per molecule. When one calculates the Landauer limit for $0^{o}C$ water using the relationship $S = k_{b} T \ln 2$, where k_{b} is Bolztmann's constant ($1.28 \cdot 10^{-23}$ $kg \cdot m^{2} \cdot s^{-2} \cdot K$) and T is the temperature in degrees Kelvin, the value obtained approaches $2.6 \cdot 10^{-21}$ $kg \cdot m^{2} \cdot s^{-2}$. That is to say that the energy equivalent of the magnetic diffusivity of water at $0^{o}C$ is within the error of limit of energy required to transform one bit of information.

Furthermore, a theoretical inference of the efficacy of the presentation of the accelerating field parameters may be an induction of the stretching and compression of the hydrogen bonds and other associated molecular bonds of water. As water is cooled to $4^{o}C$, the density of the aqueous state is increased, thus resulting in a decrease in the separation of the bonds. However, as the liquid state approaches the limit of $0^{o}C$ on its transition to a solid state the density is reduced. A reduction in the density of liquid water upon its transition from $4^{o}C$ to $0^{o}C$ increases the bond length between the atoms alongside the reduction in the hydrogen bonding potential. The net effect upon transitioning into these lower temperatures is a condition that is similar to an initial compression and stretching of the molecules. In this instance the resultant stretch after the transition between $4^{o}C$ and $0^{o}C$ is akin to the tangential effects of a centripetal acceleration whereby a tethered mass is displaced outwardly. The tangential displacement of the molecules that underlie the structure of water synchronize with the applied accelerating field resulting in a

form of resonance. The homogeneity driven by the accelerated frame not only results in the appropriate enhancement of the pH holding effects, but also agrees with the architecture of general relativity which suggests gravity can be modeled as an accelerated frame (Einstein, 1952; Einstein, 1921). Furthermore, the presented theory is corroborated by the interaction of the electron comprises the molecular bonds of the solution and the convergence of its activity in the 1 msec temporal window which has been presented elsewhere (Persinger and Koren, 2007).

5.6 References :

Chai, B., Yoo, H., & Pollack, G. H. (2009). Effect of radiant energy on near-surface water. The *Journal of Physical Chemistry B*, 113(42), 13953-13958.

Chai, B., & Pollack, G. H. (2010). Solute-free interfacial zones in polar liquids. *The Journal of Physical Chemistry B*, *114*(16), 5371-5375.

Chai, B., Mahtani, A. G., & Pollack, G. H. (2012). Unexpected presence of solute-free zones at metal-water interfaces. *Contemporary materials*, 3(1), 1.

Chen, X., Yang, T., Kataoka, S., & Cremer, P. S. (2007). Specific ion effects on interfacial water structure near macromolecules. *Journal of the American Chemical Society*, 129(40), 12272-12279.

Clough, S. A., Beers, Y., Klein, G. P., & Rothman, L. S. (1973). Dipole moment of water from Stark measurements of H2O, HDO, and D2O. *The Journal of Chemical Physics*, 59(5), 2254-2259.

Einstein, A. (1921). A brief outline of the development of the theory of relativity. *Nature*, *106*(2677), 782-784.

Einstein, A. (1952). The foundation of the general theory of relativity. *The Principle of Relativity*. Dover Books on Physics. June 1, 1952. 240 pages. 0486600815, p. 109-164, 1, 109-164.

Fenn, E. E., Wong, D. B., & Fayer, M. D. (2009). Water dynamics at neutral and ionic interfaces. *Proceedings of the National Academy of Sciences of the United States of America*, 106(36), 15243–15248. doi:10.1073/pnas.0907875106

Henderson, M. A. (2002). The interaction of water with solid surfaces: fundamental aspects revisited. *Surface Science Reports*, 46(1), 1-308.

Murugan, N. J., Karbowski, L. M., Dotta, B. T., & Persinger, M. A. (2015). Delayed shifts in pH responses to weak acids in spring water exposed to circular rotating magnetic fields: A narrow band intensity-dependence. *International Research Journal of Pure and Applied Chemistry*, 5(2), 131.

Persinger, M. A., & Koren, S. A. (2007). A theory of neurophysics and quantum neuroscience: implications for brain function and the limits of consciousness. *International journal of neuroscience*, *117*(2), 157-175.

Persinger, M. A. (2014). Quantitative convergence between physical-chemical constants of the proton and the properties of water: Implications for sequestered magnetic fields and a universal quantity. *International Letters of Chemistry, Physics and Astronomy*, 2, 1-10.

Thiel, P. A., & Madey, T. E. (1987). The interaction of water with solid surfaces: fundamental aspects. *Surface Science Reports*, 7(6), 211-385.

Trevors, J. T., & Pollack, G. H. (2012). Origin of microbial life hypothesis: A gel cytoplasm lacking a bilayer membrane, with infrared radiation producing exclusion zone (EZ) water, hydrogen as an energy source and thermosynthesis for bioenergetics. *Biochimie*, 94(1), 258-262.

Wheeler, J. A. (1946). Problems and prospects in elementary particle research. *Proceedings of the American Philosophical Society*, 36-47.

Yoo, H., Paranji, R., & Pollack, G. H. (2011). Impact of hydrophilic surfaces on interfacial water dynamics probed with NMR spectroscopy. *The journal of physical chemistry letters*, 2(6), 532-536.

Zheng, J. M., Chin, W. C., Khijniak, E., & Pollack, G. H. (2006). Surfaces and interfacial water: evidence that hydrophilic surfaces have long-range impact. *Advances in colloid and interface science*, 127(1), 19-27.

Chapter 6

6 Quantitative Support for Water as the Conduit of Interaction between the Immaterial (Energy) and Matter: The Necessary Contingencies for Universal Equivalence

We have successfully demonstrated the potential role of water in the onset of senescence and the excess correlation between two spatially isolated and phylogenically isolated species. Furthermore, we have directly investigated the electrodynamic properties of excessively correlated water and the dynamic nature of the exclusion zone. In Burr's original hypothesis the *Blueprint for Immortality* was stored within the electric fields of the organisms which he investigated. Recall the supposition that energy is transient and fluid in nature with a level of fragility that accompanies its structure. Energy requires a necessary structural analog in order for it to persist over a larger temporal span. However, the structure must also be malleable in order for modifications and additions to be effectively represented in the long term. Structure without energy or a driving process is static and does not allow for the propagation of the system over an extended period of time. It is the interaction between matter and energy that reflects the indeterminate longevity of the unit (organism). The more complex the unit becomes, the more specialized the structure, the less the longevity. The rigidity of the inherent, correlated structure must not exceed a certain threshold in order for it to pervade large expanses of time. Here we do not exclude the thesis of Burr but aim to synthesize structure and process. The physical properties of water reflect a necessary conduit for the generation of complex electrodynamic processes reflective of the dynamic nature of the structure from which it is formed.

We have implicated water as a central moderator for the interactions of plants and bacteria and have also implied a photon-water mechanism for the effective elicitation of passive excess

correlation. In the latter example the water does not require the influence of an external stimuli allowing for the potential exchange of information over vast distances. Similarly, the influence of light on water, at least with respect to senescence, demonstrates an underlying property of the nature of the interaction of light with water. Although differences were obtained across time for each successive stage of senescence, generally plants did not respond in an intensity dependent manner to incident radiation. We hypothesized that a residual biological or non-biological agent may be mediating the observed alterations in electrical potential. Furthermore, the lack of intensity dependence in this particular instance could also suggest a photo-electric phenomenon whereby frequency, pattern and intensity are required in order to maximize the observed changes in electrical potential. It is suggested that optimal wavelengths associated with the activity of photosystems I and II be applied with peak wavelengths of water and 3.4 μm waves. The application of the aforementioned wavelengths of light would narrow the spectrum of observation and illuminate potential sources driving the observed effect. Finally interactions with the exclusion zone, as measured by changes in the latency and magnitude of pH shits, when exposed to the appropriate configuration of magnetic fields is of interest and has been discussed at length. The most probable common denominator of all the experiments lies within the realm of water and every experiment should reflect a continuity of the properties of water even in distinct levels of discourse. If water is the source of the Blueprint for Immortality and is the central moderator for the effects observed here, then its physical properties should be reflected not only across multiple levels of discourse but also precipitate as a central variable on the scale of the Universe.

Water has the ability to form clusters of various sizes which are reflective of microstructural organizations of a fluid medium that undergoes marked dynamic alterations (Pan *et al*., 2004).

These water clusters then, even in large bodies of water, would possess unique electrical properties reflective of the geometric organization of said cluster. The aggregate perspective would support the electrodynamic fingerprint of a given material proposed by Burr.

6.1 Basic Properties of Water

If altering the structure of a given medium can change its electrodynamic properties so too should altering the nature of water. Zheng and colleagues (2006) examined the exclusion zone of water corresponding to the alignment of molecules along a boundary, whose results suggest that the extent of the exclusion zone extended beyond 200 μm to 1 mm depending on the material which served as an interface. Most notably, non-zero potentials could be detected between 120 and (-) 160 mV and which were altered by the addition of various chloride salts. The addition of any salt to a solvent changes the solvation state (the degree of interaction of water molecules in order to reduce the net charge distribution in the medium) of the molecules resulting in the ultimate change in structure. Again, the causal change in structure is associated with a change in the electrical potential of the substance lends credit to Burr's hypothesis.

Further alterations in the physical properties of water reflecting changes in its electrical characteristics are presented by Teschke *et al.* (2001). Here, measures of the relative permittivity of bulk and interfacial water were conducted and suggest that the permittivity of bulk water decreased from 79 to 3.8 at the level of the interface (within 10 nm of the surface) between water and a mica surface. Relative permittivity is a measure of the potential for a medium to generate electric field flux. The greater the relative measure of permittivity, the greater the resistance for the formation of an electric field. Conversely, a low relative permittivity increases the net potential to generate an electrical field of flux within a medium.

Although not directly related to the electrical properties of water, changes in viscosity at an interface can infer structural arrangements and electrodynamic changes. Goertz *et al.* (2009) measured the viscosity of nanometer thick water films corresponding to interfacial water with effective alterations in viscosity approaching 10^6 times greater than bulk water. Alterations of the interacting media to a non-polar surface resulted in the absence of the enhancement of viscosity. Viscosity ($kg \cdot m^{-1} \cdot s^{-1}$) is related to electric field strength ($kg \cdot m \cdot A^{-1} \cdot s^{-3}$) by way of magnetic diffusivity ($m^2 \cdot s^{-1}$) and the inverse of charge (As^{-1}). If both the number of charges and the magnetic diffusivity remain constant, any change in the magnitude of viscosity would result in a proportional change in the electrical field strength of water. Consider the interface between water and the membrane (a polar molecule) which is undergoing rotation, flipping and precession. The resultant effect on the generated electric field would also respond to the dynamic nature of the membrane and in turn become itself dynamic or time-varying. This hypothesis is merely conjecture however all data supporting changes in the physical properties of water are conducted in static conditions. Recall that even the structure of water itself is dynamic and consists of the movement of charge amongst adjacent molecules.

The physical characteristics of hydronium dynamics were investigated by Lobaugh and Voth (1996) who determined the activation energy of the proton transfer to H_3O^+ is approximately 0.51 kcal/mol or 0.9 k_bT and is based on the geometric assemblage of the solvent. A charge in the concentration of available H_3O^+ invariably changes the dynamics of the system and should be reflected in the structural organization of the solvent. The latter structural re-organization in the presence of excess protons was investigated by Lobaugh and Voth (1996) which revealed a smaller O-O separation which approximates 2.5 Å and allows for the flipping of a proton between the pairs in a Grötthus-type mechanism. These inter-molecular O-O

distances corroborate the findings of Tuckerman *et al*. (1995) who also demonstrated that the temporal duration of the hydration shell associated with the hydronium ion complex remains intact (structured) for a duration of 2-3 picoseconds.

In order to maintain an equilibrium state hydronium ions must undergo a neutralization reaction with its diametric opposition, the hydroxide ion whose time constants should also reflect the same temporal duration as the generation of the hydronium ion itself. Mathematical verification was performed by Hassanali *et al*. (2011) on the recombination of H_3O^+ and OH^- suggesting that the neutralization reaction involved a collective compression of oxygen along the water wire corresponding to a time of 0.5 picoseconds and involved the simultaneous movement of 3 protons. The proposed movement along the water wire, although occurring over a relatively short duration, should express a relatively short distance of action. Hassanali *et al.* (2011) determined that within a distance of 6 Å, the hydrogen wires coordinating the movement of protons enhances the diffusion constant whilst outside this limit, diffusion constants are best modeled according to bulk water parameters.

If water demonstrates the properties of changing electric fields then it should also be affected by magnetic fields and thus can be modeled by Maxwell's relationships. Yamashita *et al*. (2003) determined that the application of 60 Hz AC magnetic fields (~100 mG) and DC magnetic fields (~1000 G) effected slow to large fluctuations in pH deviations and deviations on oxidation reduction potentials of 60 mV. Gang *et al*. (2012) exposed samples of spring water to a 0.16 T horseshoe magnetic and determined an increase in viscosity that was maximized after 5.9 h, 7.4 h and 8.6 h corresponding to 25, 50 and 100 mL samples, respectively. Water exposed to high intensity (14 T) magnetic fields intensities demonstrated a measurable change in peak wavelengths by 1 - 3 nm (Iwaska and Ueno, 1998). Application of 1 μT intensity,

physiologically patterned electromagnetic fields which to water in the dark for 18 d demonstrated a reliable 10 nm shift in peak fluorescence of water (Murugan *et al*., 2015) and reliably demonstrates the ability of water to respond weak intensity electromagnetic fields.

Here we have also demonstrated that isolated samples of water exposed to rotating electromagnetic fields (and temperature variations) reliably show a reduction in the net magnitude of pH shifts over time. Furthermore, spatially isolated samples (1 m distances) exposed to the appropriate configurations of rotating bulk angular velocity fields demonstrate transient epochs of excess correlation without the addition of an exogenous stimuli. If water, or at least the microstructural organization of water, denotes the conduit between the manifestation of complex biological organizations and the necessary energetic equivalents driving the processes responsible for the emergence of said organisms then the properties of water should demonstrate a convergence upon the physical parameters of the entire set of observable variables (the Universe) and the fundamental units which comprise the entire set (Planck scale). The synthesis of dynamism and materialism should be inherently linked to a fundamental organization of the Universe which reflects fundamental physical properties of the whole.

6.2 Casimir and Electromagnetic Interactions

When two parallel, non-conducting plates are brought into proximity with each other such that the separation between the plates is significantly less than the surface area of the plates, a negative force is generated between the plates (Plunien *et al*., 1986). The resultant force that is generated has been coined the Casimir Force and reflects the possibility of transforming virtual particles into real particles in the presence of a magnetic field. The force generated through a Casimir-type effect is modeled by Equation (6.1):

$$\text{Equation 6.1} \quad : F_c = \frac{-\hbar c \pi^2}{720 a^3} A$$

where $\hbar$ is reduced Planck's constant ($1.05 \cdot 10^{-34}$ kg·m^2·s^{-1}), a is the separation between the plates (meters) and A is the surface of the plates (m^2).

If we set the resultant Casimir force in the order of bond strengths (10^{-12} kg·m·s^{-2}) and if the distance between the parallel plates is set to the distance between adjacent oxygen atoms in a solution containing excess protons (2.5 Å or $2.5 \cdot 10^{-10}$m), the surface area required to generate forces in the order of bonds would be $3.62 \cdot 10^{-14}$m^2. The resultant surface area is in the order of the annulus surrounding a 1 μm axon. Taking the square root of the calculated surface area results in a linear equivalent distance of 190 nm, which is well within the distances occupied by the exclusion zone of water. Furthermore, if one treats the resultant linear equivalent of 190 nm as a wavelength of light, energy can be calculated using Equation (6.2):

$$\text{Equation 6.2:} \quad E = h\frac{c}{\lambda}$$

where E is the energy in Joules (kg·m^2·s^{-2}), h is Planck's constant ($6.626 \cdot 10^{-34}$ kg·m^2·s^{-1}), c is the speed of light ($3.0 \cdot 10^8$ m·s^{-1}) and λ is the wavelength of light in meters.

The resultant energy would be in the order of $1.05 \cdot 10^{-18}$ kg·m^2·s^{-2}. Furthermore, the temporal equivalent of this wavelength can be approached using Equation (6.3)

$$\text{Equation 6.3:} \quad t = d \cdot v^{-1}$$

where t is the time (seconds), d is the distance (meters) and v is the velocity (m·s^{-1}).

Assuming, again, that the distance displaced is a wavelength of light in the order of 173 nm, the relative speed of travel would the speed of light ($3.0 \cdot 10^8$m·s^{-1}) resulting in a temporal component in the order of $5.76 \cdot 10^{-16}$ sec. The calculated temporal duration of $6.33 \cdot 10^{-16}$ sec is within the limits of error for the duration of rotation of a Bohr electron and is complimented by the duration of time it takes light, at c, to traverse the thickness of a cell membrane. Finally, given that the

spatial extent of a molecule of oxygen is approximately $3.0 \cdot 10^{-10}$ m, $6.3 \cdot 10^{2}$ molecules would be required to accommodate a distance of 190 nm. This latter organization is reflective of 10-20 clusters of water (40-50 molecule aggregates at varying temperatures).

Furthering the idea that water is the necessary conduit for the interaction between the generation of structure (life) and the underlying processes that pre-determine the ultimate geometric organization of the organism (the Blueprint), values reflective of the inherent electric field generated by a single molecule should converge upon Universal constraints. Provided that the energy of a water molecule is contingent upon the generation of the hydronium complex, the energy associated with this process is ~ $2.0 \cdot 10^{-20}$ Joules (Persinger, 2010; Persinger, 2014). The electric field strength can be dimensionally approached as the quotient of energy and the electrical dipole moment of water (Equation 6.4).

$$\text{Equation 6.4: } E = \frac{J}{p}$$

where E is the electric field ($kg \cdot m \cdot A^{-1} \cdot s^{-3}$), J is the energy in Joules ($kg \cdot m^{2} \cdot s^{-2}$) and p is the electric dipole moment (Asm).

Given that the electric dipole moment of water is 1.85 Debye ($6.17 \cdot 10^{-30}$ Asm) and the energy associated with a water molecule is $2.0 \cdot 10^{-20}$ J, the solution produces an electric field strength in the order of $3.2 \cdot 10^{9}$ $kg \cdot m \cdot A^{-1} \cdot s^{-3}$. To relate the intensity of the electric field to the intensity of a magnetic field (B) measured in Tesla ($kg \cdot A^{-1} s^{-2}$) we would simply have to divide by a speed. If we wish to isolate a speed necessary to equate the inherent electric fields strength of water to the intergalactic magnetic field we can use Equation 6.5:

$$\text{Equation 6.5: } v = E/B$$

where E is the electric field strength, B is the intensity of the magnetic field and v is velocity ($m \cdot s^{-1}$).

Thus for the lower limit of the intensity of the intergalactic magnetic field (10^{-15}T), and the electric field strength of $3.2 \cdot 10^{9}$ kg·m·A^{-1}·s^{-3}, results in a speed in the order of ~10^{23} m·s^{-1} and reflects the theoretical limit of the entanglement velocity (Persinger and Koren, 2013).

The magnetic field strength squared can be dimensionally approached by the relationship (Equation 6.6)

$$\text{Equation 6.6: } B^2 = \frac{\sigma}{\varepsilon}$$

where B is the intensity of the magnetic field, σ is the density of the material (kg·m^{-3}) and ε is the relative permittivity of the material ($A^2s^4 \cdot kg^{-1}m^{-3}$).

For water the density of the material is 10^{3} kg·m^{-3} and the relative permittivity along the interfacial surface is $3.363 \cdot 10^{-11}$ $A^2s^4 \cdot kg^{-1}m^{-3}$, the squared magnetic field strength would be in the order of $2.97 \cdot 10^{13}$ T^2. However, the energy stored within the magnetic field can be described by the relationship (Equation 6.7):

$$\text{Equation 6.7: } E = \frac{B^2}{2 * \mu} \cdot V$$

where E is the energy of the magnetic field, B is the intensity of the magnetic field, μ is the permeability of free space ($1.256 \cdot 10^{-6}$ kgm·$A^{-2}s^{-2}$) and V is the volume (m^3).

Assuming that the resultant magnetic field strength squared of $2.97 \cdot 10^{13}$ T^2, had an energy equivalent of $2.0 \cdot 10^{-20}$ J, the resultant volume that is required to equate the two would be in the order of $1.69 \cdot 10^{-39}m^3$.

6.3 Gravitational Considerations

Similarly, the gravitational potential energy can be calculated using Equation (6.8):

$$\text{Equation 6.8: } E_g = G \cdot \frac{m^2}{r}$$

where E_g is the gravitational potential energy is Joules, G is the gravitational constant ($6.67 \cdot 10^{-11}$ $m^3 \cdot kg^{-1}s^{-2}$), m is mass (kg) and r is the separation between the masses.

Setting Equation 6.7 equal to 6.8 and isolating for a given separation between water molecules in order to accommodate the equivalence is represented in Equation 6.9:

$$\text{Equation 6.9: } r = \frac{2\mu * G * m^2}{B^2 * V}$$

Thus the separation between water molecules having mass $3.0 \cdot 10^{-26}$ kg, with approximately $6.3 \cdot 10^{2}$ molecules that occupy the exclusion zone, the distance must be $1.15 \cdot 10^{-36}$ m or within the error of a Planck's length ($1.616 \cdot 10^{-35}$ m). Consider the possibility that two water molecules approach the limit of separation in the order of Planck's length. The resultant energy associated with two non-conducting surfaces can be approached using a Casimir phenomenon and can be calculated using the equation (6.10).

$$\text{Equation 6.10: } E_c = \frac{-\hbar c \pi^2}{720 a^3} A$$

where a is the separation between the plates, A is the surface area of the plates, c is the speed of light and $\hbar$ is reduced Planck's constant.

Continuing with the hypothesis that two water molecules approach the limit of separation of a Planck's length, then the surface of the plates would be in the order of the molecular diameter of water which is $10^{-12}m^2$ and the separation between the molecules would be $1.15 \cdot 10^{-36}$ m. The calculated resultant Casimir energy would be in the order of 10^{69} J, reflecting the total energy stored within the Universe (Persinger, 2013; Persinger, 2014; Persinger 2015). Further support for the convergence of water as a mediator for the transition from Universal operational parameters and the potential for the generation of the organism would be contingent upon homogeneity between the photon and the graviton. One can calculate the change in magnetic moment of an object operating in a magnetic field with Equation 6.11.

$$\text{Equation 6.11: } \Delta m = \frac{e^2 r^2}{4me} B$$

where Δm is the change in magnetic moment ($kg \cdot A^{-1}s^{-2}$), e is the charge of the electron ($1.6 \cdot 10^{-19}As$), r is the distance between water molecules ($2.5 \cdot 10^{-10}m$) m_e is the mass of the electron ($9.11 \cdot 10^{-31}$ kg) and B is the applied magnetic field.

Dimensionally analyzing Equation 6.11 ultimately results in a magnetic moment (Am^2) which can be further digested as the aggregate of a Joule divided by a Tesla. In this instance in order to accommodate an energy we would simply have to modify Equation 6.11 producing Equation 6.12.

$$\text{Equation 6.12: } E = \frac{e^2 r^2}{4me} B^2$$

where E is the energy obtained in Joules and all other parameters are consistent with Equation 6.11.

When one simply inputs all variables except for a value for B, an approximate value of $1.74 \cdot 10^{-26}$ $A^2s^2m^2 \cdot kg^{-1}$. Setting an external field to a measure of 1 T would demonstrate a change in magnetic moment of water in the order of $1.74 \cdot 10^{-26}Am^2$ or effectively the difference in magnetic moment between the spin magnetic moment of the electron and the orbital magnetic moment of the electron. Now consider an applied magnetic field in the order of 10^{-13} T, or the intensity of the intergalactic magnetic field. In this instance the net energy that would result from Equation 6.12 would be in the order of 10^{-52} Joules. This may be an inherently small amount of energy however if we consider the mass equivalent of this energy at rest (when c is set to 1) then the mass, as derived by the Einstein-Eddington equation (6.13) would be in the order of 10^{-52} kg or the upper limit of the rest mass of the photon (Tu *et al*., 2005; Luo *et al*., 2033).

$$\text{Equation 6.13: } E = mc^2$$

Furthermore, consider the application of weak intensity magnetic fields in the order of 3.0 nT (values that were utilized in our experiments), the resultant energy calculated from Equation 6.12

would be in the order of 10^{-44} Joules. Again the mass equivalent of this energy, as calculated using the Einstein-Eddington Equation (6.13) would isolate a mass in the order of 10^{-60} to 10^{-61} kg. This range of mass is well within the order of magnitude of the graviton (Gershtein *et al*., 1997; Novello and Neves, 2002; Goldhaber and Nieto, 1974; Goldhaber and Nieto, 2010). Another parameter that can be extracted from the approach offered here is a temporal component of water operating in a nanoTesla strength field. Given that the energy obtained from the change in magnetic moment of water in a 3.0 nT field is in the order of 10^{-43} to 10^{-44} J a frequency can be calculated using Equation 6.14.

$$\text{Equation 6.14: } f = \frac{E}{h}$$

where f is the frequency (s^{-1}), E is the energy in Joules ($kgm^2 \cdot s^{-2}$) and h is Planck's constant ($6.626 \cdot 10^{-34}$ $kgm^2 \cdot s^{-1}$)

Given a mean value of $5.0 \cdot 10^{-43}$ Joules for water in a 3.0 nT field, the resultant frequency would be $7.55 \cdot 10^{-10}$ s^{-1}. The inverse of a frequency would be a time, thus the temporal equivalent of $7.55 \cdot 10^{-10}$ s^{-1} would be $1.325 \cdot 10^{9}$ sec which is within the order of the approximate lifetime of a human being. Could it be that the inherent construction of our being is strictly limited in its duration not by the complex activity of biochemical agents or cellular constituents, but by the innate nature of water and its interaction with weak intensity magnetic fields?

6.4 The Exclusion Zone

Stepping aside from Universal hybridization of water into other physical parameters we examine the physical nature of the exclusion zone. It is suggested that a net increase in the viscosity of the exclusion zone occurs such that the increase is within ~10^6 times larger than the normal viscosity of water. Here we endeavour to determine the effects that could mediate such an interaction using force as an intermediate. The general linear expansion of the exclusion zone suggests a relative mean occupancy in the order of 100 μm. Given that that the molecular

diameter of a water molecule is 3.0^{-10} m the total amount of water molecules that would occupy the linear equivalent of 100 μm would be approximately $3.0 \cdot 10^5$ molecules. Given that the bond strength of water is in the order of 10^{-12} N ($kgm \cdot s^{-2}$) the net force is calculated as the product of the force of a single bond and the total available molecules and would approach 10^{-6} to 10^{-7} N. Given the upper limit of force is 10^{-6} N we can approach the viscosity as the quotient of the force by a diffusion constant (Equation 6.15).

$$\text{Equation 6.15: } \eta = \frac{F}{\upsilon}$$

where F is force ($kgm \cdot s^{-2}$), υ is the diffusion constant ($m^2 \cdot s^{-1}$) and η is viscosity ($kg \cdot m^{-1} s^{-1}$).

Given that the force is in the order of 10^{-6} and the diffusion mobility constant of water to be in the order of $3.6 \cdot 10^{-7}$ $m^2 \cdot s^{-1}$, the viscosity would be in the order of 10^1. Comparatively, given the lower limit of force across the exclusion zone to be in the order of 10^{-7} N, and substituting the diffusion constant for that of water ($8.65 \cdot 10^{-9} m^2 \cdot s^{-1}$) the magnitude of the viscosity would approach 10^2 $kg \cdot m^{-1} s^{-1}$. Given that the viscosity of bulk water is $8.94 \cdot 10^{-4} kg \cdot m^{-1} s^{-1}$, these calculated values would be 10^5 to 10^6 times greater and reflects what Goertz *et al.* (2009) found in their experiments.

Extending the previous section we can find an energy equivalent of 10^{-7} N as energy is the product of force and distance. Provided that the force of the linear equivalent of the exclusion zone extends the length of the exclusion zone (10^{-4}m) the resultant energy would be in the order of 10^{-11} Joules. One can isolate a magnetic field strength associated with the energy of the magnetic field using the equation (6.16)

$$\text{Equation 6.16: } B = \sqrt{\frac{E * 2\mu}{V}}$$

where B is the intensity of the magnetic field ($kg \cdot A^{-1}s^{-2}$), E is the energy in Joules, μ is the permeability of free space and V is the volume.

If we assume that the volume of water is consistent with the volumes used in our experiments (25 mL) then the strength of the magnetic field would be in the order of 10^{-6} Tesla. This value is equivalent to the magnetic field generated by the firing of all the neurons in the brain. Similarly, if one substitutes the volume in Equation 6.16 with the approximate volume of the human brain ($10^{-3}m^3$) the resultant magnetic field strength would be in the order of 10^{-7} T, or the equivalent of 10^9 neurons firing or the equivalent of high intensity geomagnetic perturbations (Persinger, 1983).

6.5 Photon-Graviton Entanglement in Water

Given that the background radiant flux density of photons is in the order of $2.0 \cdot 10^{-12} W \cdot m^{-2}$ ($kg \cdot s^{-3}$) the convergence upon the level of water should be evident. Here if we assume that the flux density is related to the magnetic density an equivalence can be equated such that (equation 6.17):

$$\text{Equation 6.17: } B = \Phi \cdot I \cdot f$$

where B is the magnetic field, I is the current (A) f is frequency, and Φ is radiant flux density ($kg \cdot s^{-3}$)

Assuming that the effective intensity of an incident magnetic field is $\sim 10^{-9}$ T, to homogenize the structure of water with background parameters of the Universe, then the aggregate of current and frequency would represent a current per unit time ($A \cdot s^{-1}$). The necessary value to equate a magnetic field strength of 1 nT and background radiant flux density of 10^{-12} $kg \cdot s^{-3}$ would be in the order of $2\text{-}3 \cdot 10^{-3}$ $A \cdot s^{-1}$.

Consider that the Universe is composed of $1.58 \cdot 10^{79}$ particles, Eddington's number, and that each particle has a charge equivalent of $1.6 \cdot 10^{-19}$ As. The resultant net Universal charge

would be $2.53 \cdot 10^{60}$ As (Persinger, 2015b). Here if we take the quotient of the net Universal charge and a current of $2\text{-}3 \cdot 10^{-3}$ $A \cdot s^{-1}$ it results in a frequency squared of $1.14 \cdot 10^{-63} s^{-2}$, or frequency equivalent of $3.37 \cdot 10^{-32}$ s^{-1}. An energy equivalent of this latter frequency can be calculated by multiplying by Planck's constant ($6.626 \cdot 10^{-34}$ $kgm^2 \cdot s^{-1}$) and would be $2.24 \cdot 10^{-65}$ Joules. The rest mass equivalent (when c is set to 1) of an energy of $2.17 \cdot 10^{-65}$ Joules would be $2.24 \cdot 10^{-65}$ kg, or the upper limit of the rest mass of the graviton (Gershtein *et al*., 1997; Novello and Neves, 2002; Goldhaber and Nieto, 1974; Goldhaber and Nieto, 2010). Furthermore, if we take the product of the mass of $2.24 \cdot 10^{-65}$ kg and the square of the entanglement velocity ($10^{23} m \cdot s^{-1}$) the resultant energy would be in the order of 10^{-18} to 10^{-19} Joules converging on the approximate energy of 190 nm light which was determined to be inherently linked to water.

If Mach's principles of the eminence of the Universe (Mach, 1887) hold true then the convergence upon $2\text{-}3 \cdot 10^{-3}$ $A \cdot s^{-1}$ should also be present in the properties of water. Dimensionally, the inherent current per unit time can be calculated by the product of conductivity, electric field strength and a diffusion parameter and is represented in equation 6.18.

$$\text{Equation 6.18: } \frac{I}{t} = \sigma \cdot E \cdot \upsilon$$

where I/t is current per unit time ($A \cdot s^{-1}$), σ is the conductivity ($A^2 s^3 \cdot kg^{-1} m^{-3}$), E is the electric field ($kgm \cdot A^{-1} s^{-3}$) and υ is diffusion ($m^2 \cdot s^{-1}$).

Provided that the current is in the order of $2\text{-}3 \cdot 10^{-3}$ $A \cdot s^{-1}$, the average conductivity of water is $1.75 \cdot 10^{-4}$ $A^2 s^3 \cdot kg^{-1} m^{-3}$, and the inherent electric field of a given water molecule was calculated to be $3.2 \cdot 10^9$ $kgm \cdot A^{-1} s^{-3}$, the resultant diffusion constant would be in $4.46 \cdot 10^{-9} m^2 \cdot s^{-1}$ or within the error of the diffusion constant of water (Bett and Cappi, 1965). This suggests that the convergence between light, magnetic fields and the graviton is reflected or mediated by the simple diffusion of water over a given temporal span. The persistence of the homogeneity of

physical parameters converging at the level of water consistently reflects the possibility that water may act as a conduit for necessary for the interaction of the energetic equivalent of the Blueprint for Immortality to interact in our physical world.

6.6 References:

Bett KE, Cappi JB (1965). Effect of pressure on the viscosity of water. *Nature* **207:** 620-621.

Gang, N., St-Pierre, L. S., & Persinger, M. A. (2012). Water dynamics following treatment by one hour 0.16 tesla static magnetic fields depend on exposure. *Water, 3*, 122-131.

Gershtein, S. S., Logunov, A. A., & Mestvirishvili, M. A. (1997). The upper limit on the graviton mass. *arXiv preprint hep-th/9711147*.

Goertz, M. P., Houston, J. E., & Zhu, X. Y. (2007). Hydrophilicity and the viscosity of interfacial water. *Langmuir*, 23(10), 5491-5497.

Goldhaber, A. S., & Nieto, M. M. (1974). Mass of the graviton. *Physical Review D*, *9*(4), 1119.

Goldhaber, A. S., & Nieto, M. M. (2010). Photon and graviton mass limits. *Reviews of Modern Physics*, *82*(1), 939.

Hassanali, A., Prakash, M. K., Eshet, H., & Parrinello, M. (2011). On the recombination of hydronium and hydroxide ions in water. *Proceedings of the National Academy of Sciences*, 108(51), 20410-20415.

Iwasaka, M., & Ueno, S. (1998). Structure of water molecules under 14 T magnetic field. *Journal of applied physics*, 83(11), 6459-6461.

Lobaugh, J., & Voth, G. A. (1996). The quantum dynamics of an excess proton in water. The *Journal of chemical physics*, 104(5), 2056-2069.

Luo, J., Tu, L. C., Hu, Z. K., & Luan, E. J. (2003). New experimental limit on the photon rest mass with a rotating torsion balance. *Physical review letters*, 90(8), 081801.

Mach, E. (1887). Mach's Principle. *Mach's archive, Deutches Museum, Munich*.

Murugan, N. J., Karbowski, L. M., Lafrenie, R. M., & Persinger, M. A. (2015). Maintained exposure to spring water but not double distilled water in darkness and thixotropic conditions to weak (~ 1 μT) temporally patterned magnetic fields shift photon spectroscopic wavelengths: effects of different shielding materials. *Journal of Biophysical Chemistry*, 6(01), 14.

Novello, M., & Neves, R. P. (2002). The mass of the graviton and the cosmological constant. *arXiv preprint gr-qc/0210058*.

Pan J, Lorenzen LH, Carrillo F, Wu H, Zhou M, Wang ZY (2004). Clustered water and bio-signal networks. *Cybernetics and Intelligent Systems, 2004 IEEE Conference on,* **2**: 902-907.

Persinger, M.A. The effects of transient and intense geomagnetic or related global perturbations upon human group behavior. In J.B. Calhoun (Ed.), *Perspectives on adaptation, environment and population*. New York: Praeger, 1983. Pp. 28-30

Persinger, M. A. (2010). 10-20 Joules as a neuromolecular quantum in medicinal chemistry: an alternative approach to myriad molecular pathways?. *Current Medicinal Chemistry*, 17(27), 3094-3098.

Persinger, M. A. (2014). Astronomical, chemical, and biological implications of 10-20 Joules as a fundamental quantum unit of information for neurofunction. *Archives of Neuroscience*, 1(3).

Persinger, M. A., & Koren, S. A. (2013). Dimensional analyses of geometric products and the boundary conditions of the Universe: Implications for a quantitative value for the latency to display entanglement. *Open Astronomy Journal*, 6, 10-13.

Persinger, M. A. (2014). Discrepancies between predicted and observed intergalactic magnetic field strengths for the Universe's total energy: Is it contained within submatter spatial geometry?. *International Letters of Chemistry, Physics and Astronomy*, 11, 18-23.

Persinger, M. A. (2013). Support for Eddington's Number and his approach to astronomy: recent developments in the physics and chemistry of the human brain. *International Letters of Chemistry, Physics and Astronomy*, 8(1), 8-19.

Persinger, M. A. (2015a). Thixotropic phenomena in water: quantitative indicators of Casimir-Magnetic transformations from vacuum oscillations (virtual particles*). Entropy*, 17: 6200-6212.

Persinger, M. A. (2015b). The graviton: an emergent solution from the equivalence of universal magnetic field intensity and radiant flux density. *Journal of Advances of Physics*, 10: 2811-2815.

Plunien, G., Müller, B., & Greiner, W. (1986). The Casimir effect. *Physics Reports*, *134*(2), 87-193.

Teschke, O., Ceotto, G., & De Souza, E. F. (2001). Interfacial water dielectric-permittivity-profile measurements using atomic force microscopy. *Physical Review E*, 64(1), 011605.

Tu, L. C., Luo, J., & Gillies, G. T. (2005). The mass of the photon. *Reports on Progress in Physics*, 68(1), 77.

Tuckerman, M., Laasonen, K., Sprik, M., & Parrinello, M. (1995). Abinitio molecular dynamics simulation of the solvation and transport of hydronium and hydroxyl ions in water. *The Journal of chemical physics*, 103(1), 150-161.

Yamashita, M., Duffield, C., & Tiller, W. A. (2003). Direct current magnetic field and electromagnetic field effects on the pH and oxidation-reduction potential equilibration rates of water. 1. Purified water. *Langmuir*, 19(17), 6851-6856.

Zheng, J. M., Chin, W. C., Khijniak, E., & Pollack, G. H. (2006). Surfaces and interfacial water: evidence that hydrophilic surfaces have long-range impact. *Advances in colloid and interface science*, 127(1), 19-27.

Chapter 7

7 Conclusion

We have systematically examined three different geometric organizations (water, bacteria and plants) in order to identify a potential homogenous substrate that acts as a binding agent to conform to Burr's Blueprint hypothesis. Although we have not definitively identified a universal agent capable of binding distinct forms of information/energy resulting in complex aggregates, we have identified a convergent level of discourse that has allowed for the generation of distinct forms of life. It is suggested from both theoretical and experimental perspectives that water may be the essential conduit necessary to extract the relevant energy in order to structure, at least, the basic elements required for the generation of life.

We have successfully identified that whole plants (*Carex stricta*) demonstrate conspicuous alterations in electrodynamic profiles when they undergo changes in their ultrstructural organization (i.e. senescence). Furthermore, significant changes in electrical potential measures of these plants were modified by peak intensity light stimulation, reflecting a threshold that converges at the level of the cell (described as being a quantum-cell equivalent) driving the potential transition into and out of senescence. We proposed the complementarity between electric and magnetic fields whereby the alteration in one can ultimately affect the other.

In this particular experiment consider the essence of the incident light radiation which was distinctly capable of altering the electrodynamic profiles of plants. Light is a form of electromagnetic radiation and thus contains both electric and magnetic properties within its wave function. Theoretically, the incident electromagnetic radiation can interact with the material and

alter its electric field parameters alongside the addition of a discrete amount of energy which is essential for the appropriate operation of the organism. Outside interaction with material, that is the interaction between magnetic and electric fields in a vacuum, one assumes the direct implication of the interference between both the electric and the magnetic fields to occur simultaneously. However, if one component of the electromagnetic dichotomy must interact with a material intermediary, the process of alteration in one of the measured components would require a temporal latency. Effectively, the interaction of one component of the electromagnetic spectrum interacts with the material through the exchange of energy. This energy is then utilized by the material, in this case living plant tissue, in order to alter some component, or geometric assemblage, resulting in a change in the temporal electrodynamic properties of the organism. In our experiment a measurable change in the electric field of the organism was observed, however it was not instantaneous which suggests that the organism required time to respond to the stimulus and supports our presented hypothesis of a structural intermediary.

From our first experiment it was imperative to identify a relatively homogenous substrate for the interaction of electromagnetic fields that pervades multiple levels of discourse. Thus we examined the possibility of two distinct species (plant and bacteria) separated in space and exposed to rotating electromagnetic fields to share a process. When a germinating seedling is presented with a given stimulus and a sample of bacteria some distance away and not presented with a stimulus, and both these of samples are exposed to the same configurations of rotating electromagnetic fields, the response of the plant material can be represented in the bacterial sample. If both bacteria and plants demonstrate the same alteration in their electrodynamic profiles (that variable which is being measured) when subjected to the appropriate elicitation of

excess-correlation then it is not the structural dissimilarities which bind them but their similarities which allows them to reciprocally interact.

The results presented in our third chapter demonstrate the potential for spatially separated and phylogenically separated species exhibit the possibility to become excessively correlated with each other. In this sense we postulate that there exists candidate(s) for the potential to interact with the underlying material organization which is representative of the distinct species. The results of the this experimental design demonstrated two distinct geometries, consisting of discrete 1 and 3 msec point durations, which were successful at maximizing the convergence of temporally correlated activity in both species. We identified that the appropriate application of forward and reverse presentation parameters were successful at generating excess correlation between species and formed what was described as a gradation of appropriate application geometries necessary to elicit the excess correlation effect. The convergence upon the duration of the points (stimuli) exhibiting the potential to effectively elicit excess correlation overlaps with quantitative solutions reflecting the nature of the proton and electron, respectively. The idea of a gradation associated with the effective application of excess correlation eliciting fields and their reversed configurations leads to the postulate that the material of interaction may, most likely, be a common source between the species. We also postulate that the gradation of effectiveness is contingent upon the differences identified between the species and may reflect a conserved ultrastructural arrangement.

In the previous section we suggested and presented supporting evidence that there exists a common variable associated with the excess correlation between different species allowing for the interaction to persist. In light of this idea we have eliminated all other variables, i.e. similar and different structures that are associated with the organization of the respective bacterial and

plant organisms, and have strictly examined the nature of water as being the potential variable which binds the interaction between incident electromagnetic radiation and the resultant alteration in the electric field properties of the system. Chapter 4 devotes its essence to the application of 3 and 1 msec accelerating and decelerating field presentations and the possible effects on water. Two geometries were identified as capable of eliciting passive excess correlation in spatially separated sources of water which consisted of 3 msec point durations serially applied in a decelerating-accelerating pattern and 1 msec points in an accelerating-decelerating pattern were effective at eliciting the excess correlation effect.

The resultant interaction between water and electromagnetic fields provides us with two further insights into the nature of the Blueprint for Immortality. The first insight suggests that excess correlation does not require a driving force to initiate its processes provided that the material itself demonstrates the capacity of displaying transient processes. The second insight derived from this experiment implicates water as the most likely candidate driving the homogenization permitting the interaction between distinct entities. There exists a marked overlap in the applied electromagnetic field configurations which reflect the possibility of eliciting excess correlation in distinct species and those field configurations which effectively demonstrated correlated changes in the electrical potential of isolated water samples.

Seemingly, it is water that may be the most probable candidate for the maximized alterations associated with the proposed electromagnetic-material interaction. The electromagnetic-material interactions sub-serves the primary method by which energetic packets of information, consistent with the genesis of life, bind to structure. The biding of information to structure elicits the appropriate geometric alterations directing the aggregation of units into the assemblages of the basic units which contribute to the formation of life. With respect to water, the latency by which

a hydronium complex requires to form and the duration of its existence are equivalent. In this particular context, energy can interact with material or it can direct a process and the result of that process can interact with a material. Any alteration that occurs upon the transition from energetic equivalents to structural equivalents will be represented in the final product. In the case of a finite being such as a cell or a full scale organism, the application of discrete packets of information are held in place via the prolonged structural organization of the system. The biding to matter is essential to the formation of an organism as the resultant structural analogues do not change readily over time. However in the case of water, the exchange of information and its integration into structure occurs so quickly that any detrimental alteration that could possibly arise from its incorporation into the aggregate is dismissed. This dismissal is due to the latency of the formation of the intermediary complex into which information can be stored. It is here at the interface between the formation and persistence of structure with information which can be incorporated to direct the essential genesis of the complex organism. Ultimately the structure integration of all units is reflected in the electrodynamic profile of said organism. As we have identified, the transition between formation and structural retention in water proceeds on a time scale that would not allow for the genesis of ordered states let alone highly specialized cell types.

If water is the generative source for our existence there must have previously existed systematic alterations in exogenous variables which in turn invariably reduced the latency of the degradation of the formation of the hydronium complex allowing for the proliferation of more complex structures. The notion of a systematic alteration in the dynamics of water leading to the prolonged organization of aqueous domains is summarized in the final experiment of this document. The results from this experiment suggest that the combination of near $0^{o}C$ temperatures and accelerating bulk angular velocity field application with 1 msec point durations

maximizes the reduction in absolute magnitudinal shifts of pH in response to injection of weak acids and increases the latency of said alterations. The delay and reduction of the magnitude of the pH shift upon the addition of acetic acid suggests an extended organized domain of water which, in this instance, demonstrated the ability to exclude protons within a given expanse of water. These results suggest that temperature reductions and the appropriate magnetic field configurations can structure a dynamic system such that its physiological properties are altered and that the system essentially becomes a static organization. In this instance, we have provided a possible mechanism which would allow for the prolongation of structured domains of water. These domains produce an impermeable region and may reflect the necessary contingencies required to initiate the formation of prototypical cellular constructs. Taking all the presented information together, we suggest that water acts as the conduit for the formation of complex organizations of geometries resulting in the emergence of proto-typical parameters necessary for the genesis of life-forms whose directed organization is mediated by the fundamental interaction between matter and electromagnetic fields.